Full-Duplex Multi-Antenna Base-Stations with Reduced Complexity

Von der Fakultät für Ingenieurwissenschaften,
Abteilung Elektrotechnik und Informationstechnik
der Universität Duisburg-Essen

zur Erlangung des akademischen Grades

Doktor der Ingenieurwissenschaften (Dr.-Ing.)

genehmigte Dissertation

von

Nidal Zarifeh

aus

Damaskus, Syrien

Gutachter:

Prof. Dr.-Ing. Thomas Kaiser

Prof. Dr.-Ing. Iyad Dayoub

Tag der mündlichen Prüfung: 11.12.2019

DOI: 10.17185/duepublico/71452
URN: urn:nbn:de:hbz:464-20200401-083152-2

Fachgebiet Digitale Signalverarbeitung (DSV)
Universität Duisburg-Essen
Bismarckstrasse 81
47057 Duisburg
Germany
Tel.: +49 (203) 3 79-32 87
Fax : +49 (203) 3 78-34 98

Referent:	Prof. Dr.-Ing. Thomas Kaiser
Co-Referent:	Prof. Dr.-Ing Iyad Dayoub
Vorsitzende:	Prof. Dr.-Ing. Holger Vogt
Tag der Promotion:	11.12.2019

Acknowledgment

I would like to express my gratitude to my supervisor Prof. Dr.-Ing. Thomas Kaiser, who gave me the honor to work, and pursue my PhD, in the institute of Digital Signal Processing (DSV), in University of Duisburg-Essen. For me, he is not a supervisor but a mentor, he is not a boss but a leader, he presents no instructions but inspiration. I'm deeply grateful for his support, encouragement and understanding.

I would like, as well, to acknowledge my deep appreciations to Prof. Dr.-Ing. Iyad Dayoub, Université Polytechnique Hauts-de-France. I'm honored that he accepted to co-supervise my thesis, and in particular I'm thankful for the invaluable thoughts, the fruitful discussions, and the sincere support.

Also, my thanks go to Dipl.-Ing. Theo Kreul, who provided me with consistent support through the years, and a lot of creative ideas. His consistency and discipline at work inspired me and pushed me forward.

Many sincere thanks to Mrs. Sabine Jankowski. She always intends to spend her time and effort to support, and to solve any issue. I'll always be grateful for her kindness and caring.

In addition, deep gratitude to Dr. Maha Shadaydeh who opened the door of scientific research for me, and showed me with her dedication the true values of the academic devotion. Also big thanks to Dr. Hicham Aroudaki for his valuable discussions. With his exceptional wide vision, he showed me, in his lectures, the strong relation between the academic and the industry fields.

I would like to thank all my colleagues in DSV for creating an inspiring and friendly atmosphere for research. Special thanks to Mai Alissa, Maher Ahmed, and Yamen Zantah for the cooperation and support. Further thanks to Ahmed Elawamry, Abdelfattah Megahed, Marc Hoffmann, Mohammed El-Absi, and Fawad Sheikh. Many thanks go to previous colleagues,

who left DSV, but their kindness and nice memories are still around: Ammar Kabbani, Yuan Gao, Hanwen Cao, and Wei Jiang. Also, deep appreciation to Ramez Askar from Fraunhofer HHI institute for the collaboration work and the fruitful discussions.

Personally, I would like first to thank my parents, who did everything they could to see me in this place. My mother, who knew, for always how to raise me up and push me forward, sometimes with only few words, but behind them a whole life of dedication and sacrifice. My father and my favorite teacher, who not only taught me physics in his class, but also taught me to love science and believe in it.

My heartfelt gratitude to my caring sisters who made me believe that family is everything: Nibal, Manar, Nawar; and their families.

The deepest gratefulness is to my beloved and exceptional wife, Sumou, who supported me through ten years and inspired me a lot of ideas in my career. If it were fair enough, she would have her name right beside mine on the thesis cover, as she contributed to it with a lot of support, love, care, and tenderness.

Finally, this work, like every other work I do, is dedicated to my lovely boy Usseim, who gave me a whole new perspective of life, and allowed me to feel the unconditional love that cannot be described in words.

Nidal Zarifeh
Duisburg, Germany
Feb 2020

Abstract

The future generations of cellular systems promise the user a wide range of services and applications that require revolutionary enhancements in the network performance, in terms of throughput, capacity, latency, and reliability. Therefore, in order to fulfill the requirements, the current wireless systems need new technologies as revolutionary as the promised applications. Antenna arrays, especially massive Multi-Input Multi-Output (MIMO), Millimeter Waves (mmWaves), Nonorthogonal Multiple Access (NOMA), and In-Band Full-Duplex (IBFD) transmission, have been the most rising approaches for investigation. IBFD, or shortly known as Full-duplex (FD), is a promising technology that allows the device to simultaneously transmit and receive on the same frequency. Hence, the transceiver does not need any duplex scheme, neither in frequency nor in time domains, as it does in half-duplex (HD) transmission. Besides the potential to double the spectral efficiency, FD has many significant advantages. First, it can distinctly reduce the latency in wireless networks, which is a critical issue in 5G. Furthermore, it simplifies spectrum management and allows easier dynamic spectrum allocation, especially in cognitive radio (CR) systems. Also, it enables cellular systems to reuse frequency bands for radio access and backhauling. Moreover, FD is a potential solution for other wireless problems such as hidden terminals, congestion, and collision. However, the fact that the self-interference (SI) signal is usually $80 - 120$ dB stronger than the weak desired signal makes SI cancellation (SIC) the main challenge against the realization of FD. A hybrid SIC solution should be deployed, in propagation, analog, and digital domains, to accumulatively suppress the SI to the noise floor. Most of SIC methods are based on copying the transmitted signal, then subtracting it from the total received signal in order to eliminate SI. However, this methodology suffers from the sensitivity to the imperfections of analog components, i.e., the hardware impairments, which cause considerable changes to the copied signal; not to mention the effect of the SI channel.

In MIMO systems, the problem is even harder because of using multiple transceivers, where each one by its own has different imperfections (non-linearity, IQ imbalance, phase noise, etc.). The main motivation of this dissertation is to employ the multi-antenna feature in favor of SIC, instead of dealing with it as an additional problem to SIC.

Before addressing different multi-antenna technologies, IQ imbalance is investigated as one example of imperfections in FD transceiver, in order to demonstrate the complexity of hardware impairment calibration. An FD system is analyzed to show the considerable drop in SIC in the presence of IQ imbalance. Then, calibration methods are proposed. After that, the focus lies on three multi-antenna technologies, reflect-array (RA), co-located antenna selection (AS), and distributed antenna system (DAS). In general, during our work with these technologies, the following outlines are considered: The scenario assumes an FD base-station with HD users. Cross-polarization isolation is combined with isolation achieved by the tackled technologies. The system operates in wideband (5, 10, or 20 MHz), and with 5 GHz carrier frequency. Instead of using theoretical channel models, ray-tracing method is applied within realistic environments. The system is evaluated by bit error rate (BER), spectral efficiency, and FD over HD enhancement ratio FD/HD, which has a theoretical boundary value of 2.

The use of RA in FD mobile systems is proposed for the first time in literature. Using multi-feeder in dual-polarized RAs mitigates the leakage from the transmitter to the receiver, and the beam-forming allows further SI isolation. For FD AS investigation, three antenna selection criteria are proposed, 1) maximization of signal-to-noise ratio (SNR) without considering the SI channels, 2) maximization of signal to self-interference plus noise ratio (SSINR), where SI channels are estimated, and 3) maximization of channel gain ratio (CGR). FD AS is also investigated for distributed antenna systems. Then, experimental validation of the AS simulation is done with a real testbed in order to evaluate the FD system performance. Various setups are experimented in the testbed, such as changing the number of antennas, the type of isolation (vertical/horizontal), and the type of antennas (omnidirectional/directional). In fact, this testbed is considered one of few FD testbeds, and it is the first that enables AS in an FD base-station. In general, the achieved FD/HD enhancement ratio in simulations and experiments is in the range of $1.4 - 1.98$ for the different tackled technologies and different algorithms. However, in this work, the number of users is limited to maximum three users in each direction. Thus, more complex and dynamic scenarios are to be investigated. Nevertheless, the results show that the combination of FD transmission with low-complex multi-antenna techniques is feasible in technology, and promising in performance, validating its potential deployment in future wireless systems.

ZUSAMMENFASSUNG

„Full-Duplex“ (FD) ist eine vielversprechende Technologie, die es dem Gerät ermöglicht, auf der gleichen Frequenz zeitgleich Daten zu senden und zu empfangen. Im Gegensatz hierzu muss bei der üblicherweise verwendeten „Half-Duplex“ (HD)-Anwendung das Senden und Empfangen zeitlich getrennt werden. Neben der Möglichkeit der Verdopplung der spektralen Effizienz bringt FD weitere erhebliche Vorteile mit sich, wie beispielsweise deutlich geringere Latenzzeiten und ein vereinfachtes Spektrum-Management. Allerdings ist die Unterdrückung der „Selbstinterferenz“ (SI) eine wesentliche Herausforderung für die Realisierung von FD-Systemen. Zur SI-Unterdrückung („self-interference cancellation“, SIC) werden hybride Lösungen bevorzugt, die innerhalb der Übertragungskette sowohl in der analogen als auch der digitalen Verarbeitung ansetzen. Die meisten SIC-Methoden basieren auf der Nachbildung des übertragenen Signals und der anschließenden Subtraktion dieses Teilsignals vom empfangenen Signal. Diese Rückkopplungs-Methodik reagiert jedoch sehr empfindlich auf Nichtidealitäten der Hardware, die einen erheblichen Einfluss auf das nachgebildete Signal und den SI-Kanal haben. Diese Herausforderung ist in Mehrantennensystemen („multiple input - multiple output“, MIMO) aufgrund der Verwendung mehrerer Sender-Empfänger-Module, sogenannter Transceiver, noch stärker ausgeprägt, da in der Regel jeder dieser Transceiver abweichende Unzulänglichkeiten aufweist.

Das Hauptziel der vorliegenden Dissertation ist, die vorteilhafte Nutzung von Mehrfachantennen (MIMO) zur SI-Unterdrückung (SIC) aufzuzeigen, anstatt MIMO als eine zusätzliche Herausforderung für SIC aufzufassen. Vor der Betrachtung verschiedener Technologien für Mehrfachantennen-Systeme werden in dieser Arbeit zunächst IQ-Fehler (In-phase Quadrature-phase Imbalance) als ein Beispiel für Nichtidealitäten in einem FD-Transceiver untersucht. Hierbei wird die Komplexität der Kalibrierung zur Berücksichtigung von Hardware-

Unzulänglichkeiten aufgezeigt. Danach liegt der Fokus auf den drei Mehrfachantennen-Technologien, „Reflect-Array“ (RA), „Co-Located Antenna Selection“ (AS) und „Distributed Antenna System“ (DAS). Dem betrachteten Szenario liegt eine Breitband-FD-Basisstation mit HD-Nutzern zugrunde. Anstelle der Verwendung von theoretischen Kanal-Modellen wird die Methode der Strahlverfolgung („Ray-Tracing“) innerhalb realistischer Umgebungen angewandt. Die Bewertung des Systems erfolgt durch die Bitfehlerrate („Bit Error Rate“, BER), spektrale Effizienz und das Steigerungsverhältnis für den Datendurchsatz FD/HD, das einen theoretischen Grenzwert von 2 besitzt.

Die experimentelle Validierung der adressierten Mehrantennenschemata wird exemplarisch an FD AS durchgeführt. Hierzu wird im Testaufbau der Grad der erreichten SIC gemessen und damit die Leistung des FD-Systems bewertet. Untersucht werden verschiedene Anordnungen, wie beispielsweise die Variation der Anzahl der Antennen, des Antennentyps und der Isolation durch die Antennenpolarisationsrichtung. Der realisierte Testaufbau wird als das erste angesehen, der AS in einer FD-Basisstation implementiert. Im Allgemeinen liegt das in den Simulationen und Experimenten erzielte FD/HD-Steigerungsverhältnis für die untersuchten Technologien und die verschiedenen Algorithmen zwischen 1.4 und 1.98. In dieser Arbeit ist die Zahl der Nutzer auf maximal drei in jede Richtung begrenzt. Daher müssen für eine finale Beurteilung der Leistungsfähigkeit des Verfahrens noch weitere komplexere und dynamische Szenarien untersucht werden. Nichtsdestotrotz zeigen die Ergebnisse dieser Arbeit, dass FD-Transmission in Kombination mit gering-komplexer Mehrfachantennen-Technik praktisch anwendbar und in der Leistungsfähigkeit vielversprechend ist. Daher zeigt die in dieser Arbeit vorgeschlagene Methodik eine mögliche Verwendung von FD-Technologien in zukünftigen Mobilfunksystemen auf.

Contents

List of acronyms

3GPP	3rd Generation Partnership Project
5G	Fifth Generation of mobile network
ACK/NACK	Acknowledgement/Negative Acknowledgement
ADC	Analog to Digital Converter
ARQ	Automatic Repeat Query
AS	Antenna Selection
AWG	Arbitrary wave generator
AWGN	Additive White Gaussian Noise
Balun	Balanced-unbalanced
BER	Bit Error Rate
BS	Base-Station
CA	Conjugate Anti-symmetric
CAPEX	Capital expense
CGR	Channel Gain Ratio
COMP	Coordinated Multi-Point access
CP	Cyclic Prefix
CPE	Common Phase Error
CPRI	Common Public Radio Interface
CS	Conjugate Symmetric
CSI	Channel State Information
CST	Computer Simulation Technology
DAC	Digital to Analog Converter
DAS	Distributed Antenna System

DFT	Discrete Fourier Transform
DL	Downlink
DPD	Digital Pre-Distortion
DSA	Digital signal analyzer
eMBB	enhanced Mobile Broadband
FD	Full-Duplex
FDB	Full-Duplex Bidirectional
FDBS	Full-Duplex Base-Station
FDD	Frequency Division Duplex
FDMA	Frequency Division Multiple Access
FDR	Full-Duplex Relaying
FEC	Forward Error Correction
FFT	Fast Fourier Transform
FIIQ	Frequency-Independent IQ imbalance
FIR	Finite Impulse Response
FSIQ	Frequency-Selective IQ imbalance
GP	Guard Period
HD	Half-Duplex
HW	Hardware
IAB	Integrated Access and Backhaul
IBFD	In-Band Full-Duplex
ICI	Inter-Carrier Interference
IDFT	Inverse Discrete Fourier Transform
IEEE	Institute of Electrical and Electronics Engineers
IFFT	Inverse Fast Fourier Transform
IoT	Internet of Things
ISI	Inter-Symbol Interference
ITU	International Telecommunication Union
IUI	Inter-User Interference
LDPD	Linear Digital Pre-Distortion
LO	Local Oscillator
LS	Least Square
LTE	Long-Term-Evolution

MCGR	Maximization of Channel Gain Ratio
MIMO	Multi-Input Multi-output
ML	Maximum Likelihood
MMSE	Minimum Mean Square Error
mMTC	massive Machine Type Communications
mmWave	Millimeter Wave
MSNR	Maximization of Signal-to-Noise Ratio
MSSINR	Maximization of Signal-to-Self-Interference-plus-Noise Ratio
NLDPD	Non-Linear Digital Pre-Distortion
NR	New Radio
OFDM	Orthogonal Frequency Division Multiplexing
OPEX	Operational expense
PA	Power Amplifier
PAPR	Peak to Average Power Ratio
PC	Personal Computer
PEU	Pre-Equalization Unit
QAM	Quadrature Amplitude Modulation
RA	Reflect-Array
RAN	Radio Access Network
RAT	Radio Access Technology
RE	Resource Element
RF	Radio Frequency
RoF	Radio over Fiber
RRH	Remote Radio Head
RSI	Residual Self-Interference
Rx	Receiver chain
SC-FDMA	Single-Carrier FDMA
SF	Subframe
SI	Self-Interference
SIC	Self-Interference Cancellation
SISO	Single-Input Single-output
SLL	Side Lobe Level
SNR	Signal-to-Noise Ratio

SQNR	Signal-to-Quantization-Noise Ratio
SSINR	Signal-to-Self-Interference-plus-Noise Ratio
SSIR	Signal-to-Self-Interference Ratio
TDD	Time Division Duplex
TDMA	Time Division Multiple Access
Tx	Transmit chain
UE	User-Equipment
UHF	Ultra-High Frequency
UL	Uplink
URLLC	Ultra-Reliable Low-Latency Communications
USB	Universal Serial Bus
UWB	Ultra-Wideband
V2V	Vehicle to Vehicle
VR	Virtual Reality
WARP	Wireless open-Access Research Platform
WLAN	Wireless Local Area Network

Notation

x	Vector
$\mathbf{X}$	Matrix
$\mathbf{X}^{-1}$	Inverse of matrix $\mathbf{X}$
$\mathbf{X}^{*}$	Complex conjugate of $\mathbf{X}$
$\mathbf{X}^{T}$	Transpose matrix of $\mathbf{X}$
$\mathbf{X}^{H}$	Conjugate transpose (Hermitian) matrix of $\mathbf{X}$
$tr(\mathbf{X})$	Trace of matrix $\mathbf{X}$
$det(\mathbf{X})$	Determinant of matrix $\mathbf{X}$
$\|\mathbf{X}\|$	L-2 norm of matrix $\mathbf{X}$
$\|\mathbf{X}\|_F$	Frobenius norm of matrix $\mathbf{X}$
$\mathbb{E}(x)$	Mathematical expectation of random variable x
$\mathcal{R}e\{x\}$	The real part of complex variable or vector x
$\mathcal{I}m\{x\}$	The imaginary part of complex variable or vector x
$\mathcal{F}(x)$	Fourier transform of signal x
$\mathcal{F}^{-1}(X)$	Inverse Fourier transform of spectrum X
$*$	Convolution
$\odot$	Elementwise (Hadamard) product
$\mathbb{C}$	Complex field
$\mathbb{R}$	Real field
$\mathcal{P}$	A set
$[\mathbf{X}]_{\mathcal{P},\mathcal{Q}}$	A submatrix of matrix $\mathbf{X}$ indexed by the row indices in $\mathcal{P}$ and the column indices in $\mathcal{Q}$
$\mathcal{O}(.)$	The order of computation complexity
$\hat{x}$	Estimation of vector x

$\|x\|$	The magnitude of the complex number x
$\angle x$	The angle of the complex number x
$xmod2$	x modulo 2
$\mathbf{I}_N$	An $N \times N$ identity matrix

Chapter 1

Introduction

"It is generally not possible for radios to receive and transmit on the same frequency band because of the interference that results" [1]

- A. Goldsmith, 2005.

For now, let us forget about the quote above, and instead, let us talk about the current situation of mobile communication systems. In the last twelve years, two significant events stroke the world in the field of telecommunication. The earlier one was when the first revolutionary smartphone was produced, and the later was in 2010 when several Long-Term-Evolution (LTE) networks were launched commercially. Both of these waves created dramatic boosts in the traffic running through worldwide mobile networks. For example, the global mobile data traffic has increased from 0.4 exabytes (1 billion gigabytes) per month in 2011 to 12 exabytes per month at the end of 2017, then to 29 exabytes per month in 2019 [2]. It is clear that this is about a 73-fold within eight years. Along with the volume, there was a huge increase in terms of the number of connected devices which are more than 10.2 billion devices in 2019 compared to 2.2 billion in 2005 [2]. However, in the coming few years, the world will be hit by the tsunami of 5G, where revolutionary applications are planned to be provided, such as the Internet of Things (IoT), Vehicle to Vehicle (V2V) communication, and Virtual Reality (VR) applications. Besides, 5G promises the user to perform radical enhancements in the current service. These new and enhanced services do not only crave radical increases in data rates, but in addition, they generate a serious demand to increase the mobile system capacity in terms of the number of served devices. Estimations say that the traffic of mobile networks in 2025 will reach 1 zettabyte (1000 exabytes) which is about 35-fold of the current volume; meanwhile, there will be a dramatic boost in terms of the number of devices to reach more than 25 billion due to IoT [3, 4]. In order to provide

the promised wide range of applications and services, the standardization organizations, such as International Telecommunication Union (ITU) and the 3rd Generation Partnership Project (3GPP), have developed the vision of 5G into three main scenarios:

- **Scenario 1: eMBB** (enhanced Mobile Broadband) which focuses on providing high data rates.
- **Scenario 2: URLLC** (Ultra-Reliable Low-Latency Communications) which gives the priority to low-latency, strong security and ultra-reliability.
- **Scenario 3: mMTC** (massive Machine Type Communications) which is constrained to low power, low cost, and low complexity communications.

In current scientific researches, three main strategies are drawn to reach the mentioned scenarios, and especially for increasing the mobile system capacity:

- **Strategy I: New/under-utilized spectrum Exploitation**
  Along with spectrum aggregation, this is the first and most straightforward strategy. The bands around 5 GHz, and Millimeter Wave (mmWave) band, from 24-44 GHz, are strong candidates for the coming New Radio (NR) of the 5G mobile system and beyond [5, 6]. Besides the allocation of new spectrum, the under-utilized spectrum can be shared over different nodes within the same network, different RANs (Radio Access Network), and different RATs (Radio Access Technology). The later case can be performed when multi-RAT heterogeneous network is deployed in 5G with a centralized controller and coordinator [7]. Nevertheless, the three sharing cases can be deployed by the technology of Cognitive Radio (CR) [8, 9]. However, the complexity that is produced by CR algorithms is one of the disadvantages which have to be considered, especially in case of paired spectrum transmission, i.e., FDD (Frequency Division Duplex), where the spectrum management has to be done for uplink (UL) and downlink (DL) bands.
- **Strategy II: Reuse of resources**
  At present, the main way to achieve this target is by densifying the network. Spatial densification of cellular networks means that the coverage area is divided into smaller and smaller cells [10, 11]. This allows the system to reuse the frequency more, and hence increase the network capacity per area. Thus, micro-cells, small-cells, pico-cells, and femto-cells will be widely deployed in 5G rather than the macro-cells that are used as umbrellas to ensure

smooth coverage. However, network densification will trigger additional capital expense (CAPEX) and operational expense (OPEX) for the sites' installation, the backhauling, and the maintenance.

- **Strategy III: Improving spectral efficiency**
  This strategy has been, for decades, the favourite approach for both operators and researchers for reasons of affordability and reliability. Many methods have been investigated in this area, like advanced coding and modulation schemes [12–14], multi-cell interference management such as coordinated multi-point access (COMP) [15], smart antenna, and multi-antenna systems. However, in the last few years, it is known that these methods have almost reached their maximum limits, or they are too complicated with the current technologies.

Looking to the complexity/cost/limitation of these three strategies, one can ask the question: Is there a potential to refine these approaches and improve their outcomes. The answer lies in the words of the introductory quote.

1.1 Motivation and Scope

In-Band Full-Duplex (IBFD) transmission, or shortly known as Full-Duplex(FD), means that the transceiver is capable of transmitting and receiving on the same frequency at the same time. Until a decade ago, it was assumed that the wireless node cannot receive the desired signal from a remote node while it is simultaneously transmitting on the same frequency band. This assumption is due to the strong interference signal that is produced in the transmitter and reached the receiver circuits. This signal is referred to as self-interference (SI). However, the recent achievements in the semiconductor industry, Radio Frequency (RF) / antenna design, and digital technologies allow us to re-investigate this assumption aiming to achieve FD communication. Knowing that every communication device, from the previous century till the moment, is a half-duplex device, i.e., it is only capable of using half of the resources, urges the researches to explore the potentials of FD technology.

Intuitively, enabling wireless nodes with full-duplex operation offers the potential to double the spectral efficiency (bit/second/Hz) {scenario 1,2,3, strategy III}. However, FD technology carries also many other alluring benefits.

FD technology can reduce the latency by avoiding the waiting idle time in TDD (Time

Division Duplex) transmission, and also by simultaneously receiving feedback signals, i.e., channel state information (CSI), ARQ (Automatic Repeat Query), ACK/NACK (Acknowledgement/Negative Acknowledgement) control signaling, etc., from the receiver during transmission. This is very important in case of excessive latency for sensitive applications and multi-hop networks. Also, the additional capacity, provided by FD, can be used for a better Forward Error Correction coding (FEC) to decrease the packet loss rate, and subsequently to minimize the packet retransmissions which produce the major part of latency in RANs [16] {scenario 2,3, strategy III}.

Another assets of FD are the reliability and flexibility it provides for dynamic spectrum allocation, i.e., cognitive radio networks, either in case of in-band full-duplex or partially band-overlap FDD systems. This advantage grants less expensive unpaired spectrum, which is traditionally allocated for TDD operation, and also simplifies spectrum management {scenario 1,3, strategy I}.

Furthermore, FD technology will enable small cells in 5G and beyond to reuse the frequency resources for radio access and backhaul transmission. Self-backhauling, or Integrated Access and Backhaul (IAB), is proposed to enable easier deployment by reducing reliance on the availability of wired backhaul at each access node location [17, 18]. Together, FD and IAB would be very helpful, cost-wise and operation-wise, to go further in densifying the cellular network {scenario 1,3, strategy I, II}.

Moreover, full-duplex can be a potential solution for other wireless problems such as hidden terminals, congestion, collision, etc.

Based on the reasons mentioned above, full-duplex presents an interesting and promising topic of research for the next generations of mobile systems, including all the planned scenarios and strategies. Nevertheless, the deployment of FD technology can be summarized into four main applications:

- Full-Duplex Base-Station (FDBS), where UL and DL signals share the same band;
- Full-Duplex Bidirectional (FDB), in Machine-to-Machine (M2M) communication;
- Full-Duplex Relaying (FDR), especially in V2V communication;
- and backhauling.

In this thesis, the focus is on the first application. More details about the other FD applications and possibilities in 5G are found in [19–22]. It is worth mentioning that the benefits of FD

technology are valid for all other wireless systems, not only 5G. However, in this introduction, the focus was on 5G as it has, among the other wireless systems, the broadest range of applications, services, and scenarios. For a better understanding of the thesis motivation and scope, a brief understanding of SI cancellation (SIC) should be established, especially for multi-antenna systems.

Self-Interference Cancellation

As mentioned earlier, the main challenge of FD technology is the self-interference signal, i.e., the part of the transmitted signal that reaches into the receiver of the same node. SI signal is usually $80 - 120$ dB stronger than the weak desired signal that is coming from the remote node [23]. However, the trend of small cells in 5G provides an inherent capability to loosen this problem a little due to the lower cell edge path loss.

Contrary to how it seems, simply subtracting SI from the total received signal is not an adequate solution, because the assumption of knowing the transmitted signal by the receiver is inaccurate. Although the transmitted signal is fully known in its digital baseband form, it suffers later from unpredictable changes with all the imperfections of the analog elements, not to mention the SI channel between the transmit and receive antennas. Therefore, it is clear that more sophisticated solutions are required. In literature, it is well established that SIC has to be accumulatively achieved by a hybrid solution, i.e., a solution that is deployed in propagation, analog, and digital domains, to ensure that the residual SI (RSI) reaches the noise floor of the receiver. Each one of the three domains can cancel a few tens of dB's in order to cancel out the SI signal completely.

Another approach of SIC is to use an auxiliary transmitter chain to copy the signal in the digital domain and convert it to the analog domain, then subtract it from the total received signal. Note that before converting the signal to the analog domain, Digital Pre-Distortion (DPD) is applied to the copied samples to match the SI channel effect. However, this approach, as many SIC solutions that depend on subtracting the feedback signal, suffers from the effect of hardware (HW) impairments. These impairments lead to a considerable performance loss as it will be explained in the next chapters.

FD Multi-Antenna Systems

In Multiple-Input Multiple-Output (MIMO) systems, the challenge bar becomes even higher. Scalability is a serious issue in FD MIMO, as the number of analog elements, the number of transceivers, and the number of SI channels to be estimated, become much higher. This

complicates the task of SIC dramatically, especially in the presence of HW impairments.

Massive MIMO, as well, has been investigated in the presence of SI. However, scaling up MIMO means scaling up both the number of RF transceivers and antennas, which led to many other problems in SIC.

Although the cost of RF transceivers is becoming lower, thanks to the development of the semiconductor industry in the last decades, this cost is still significantly higher than the cost of antennas, not to mention the cost for bands above UHF (Ultra-High Frequency). In the near future, massive MIMO technology will still be confined to its cost, and therefore many recent works investigate low RF-complexity massive MIMO where many antennas, or known as a sub-array massive MIMO, where one transceiver and antenna/sub-array is selected [24].

Generally, besides scalability, all multi-antenna SIC techniques need further development and still face many challenges. First, the length of the pilot, which is used for SI channels estimation, is proportional to the number of antennas; hence, the accuracy of the channel estimation is limited by the coherence time and the noise correlation for long pilot sequences. Second, the effect of different types of hardware impairments on SIC performance becomes more pronounced and has to be analyzed and calibrated for the multi-antenna system with several transmitter and receiver chains. Finally and above all, the cost efficiency and the feasibility of FD realization for the aforementioned multi-antenna techniques are still a matter of question.

The motivation of this thesis is to investigate the potentials of FD technology with simple and cost-efficient multi-antenna techniques. The main idea is to avoid the traditional approach of SIC, i.e., copy/feedback/subtract, as explained earlier that this method is always susceptible to HW impairment of the analog components.

The methodology of the dissertation is the following: Instead of dealing with the multi-antenna feature as an additional problem to SIC, the aim is to employ this feature in favour of SIC.

The scope of this thesis is to investigate FD with three multi-antenna technologies:

1. FD in Reflect-Arrays (RA)
2. FD Antenna Selection (AS)
3. FD Distributed Antenna System (DAS)

In general, during our work with all these technologies, the following outlines are considered:

- The scenario is an FD base-station (BS) with half-duplex (HD) users.
- Cross-polarization isolation is combined with the isolation that achieved by the tackled technologies.
- The system operates in wideband (5, 10, or 20 MHz), and with a carrier frequency in the range of 5 GHz.
- Instead of using theoretical channel models, the ray-tracing method is applied within realistic environments.
- The wireless link properties are based on LTE interfaces and parameters (OFDM for DL, SC-FDMA for UL).
- The system is evaluated by bit error rate (BER), spectral efficiency, i.e., the bit-rate per Hz (bps/Hz), and the FD over HD enhancement ratio FD/HD, which has a theoretical boundary value of 2.

Besides the simulation and the analysis of the three technologies, a Full-Duplex BS with AS has been implemented as a testbed in our lab to measure the achieved SIC and to evaluate the FD system performance experimentally.

1.2 Dissertation Contributions and Organization

After the FD benefits to the preceding strategies are established, and the motivation of addressing the mentioned multi-antenna technologies is shown, the main contributions and chapters organization of this dissertation can be summarized as follows.

- **Chapter 2: Full-Duplex SISO system towards Multi-Antenna**
  This chapter presents the relevant literature review on the fundamentals of FD and SIC techniques. First, the benefits of FD technology in SISO (Single-Input Single-output) Systems are introduced, then the basic model of FD systems is presented, and the problem of SI is analyzed in detail. After that, SIC requirements in FD systems are determined. A brief look over the different techniques of SIC is done in order to classify them into four main categories: passive cancellation, analog active cancellation, digital active cancellation, and SIC with auxiliary chains. Hardware impairments are discussed, after that, to show the impact on SIC performance. Finally, a literature review of FD multi-antenna is presented.

  The content of this chapter is based on our book chapter:

- T. Kaiser and N. Zarifeh, "General principles and basic algorithms for full-duplex transmission," in Signal Processing for 5G: algorithms and implementations, F.-Long Luo and C. Zhang (eds.), Wiley, Chichester, 2016 (Chapter 16, pp.372-401).

- **Chapter 3: Hardware Impairment Complication: IQ Imbalance for Example**
  Before tackling the proposed multi-antenna techniques, the problem of IQ imbalance in the FD system is studied in this chapter. The chapter aims to show an example case of the HW impairment challenge, and the complexity of dealing with such problems. This chapter is based on cooperative work with Fraunhofer HHI institute, where IQ imbalance effect in the FD system is measured and calibrated. The chapter starts with a quick description of IQ imbalance problem, and the FD system is modelled in the presence of IQ imbalance. After that, methods of calibration using advanced pre-equalization units are proposed. Two methods of calibration are presented, firstly with a replicator unit, and secondly with distributed compensation units. Then, the results of the calibration are shown. Finally, a conclusion is drawn.

  As mentioned earlier, the content of this chapter is based on cooperative publication with Fraunhofer HHI institute:

  - R. Askar, N. Zarifeh, B. Schubert, W. Keusgen, and T. Kaiser, "I/Q Imbalance Calibration for Higher Self-Interference Cancellation Levels in Full-Duplex Wireless Transceivers," 1st Int. Conf. on 5G for Ubiquitous Connectivity, Levi, Finland, 26-27 Nov. 2014.

- **Chapter 4: Dual Polarized Reflect-Array in a Full-Duplex Base-Station**
  In this chapter, it is proposed, for the first time in literature, the use of reflect-array in FD mobile systems. Dual-polarized reflect-arrays are designed to be used in a full-duplex LTE BS with HD users. First, the main concepts in RA are introduced, and the advantages of using RA in FD systems are discussed. Then, the antenna design is described, and the system model is presented. After that, the system setup and the used ray-tracing tool are defined. Finally, the simulation results are shown and analyzed for different angular isolation values.

  The contributions of this chapter are published in the conference paper:

  - N. Zarifeh, M. Alissa, M. Khaliel and T. Kaiser, "Self-interference mitigation in full-duplex base-station using dual-polarized reflect-array," 2018 11th German Microwave Conference (GeMiC), Freiburg, 2018, pp. 180-183.

- **Chapter 5: Co-located and Distributed Antenna Selection in a Full-Duplex Base-Station**

  In this chapter, the use of antenna selection, in an FD indoor wideband femto-BS, is investigated in two cases, co-located, and distributed antennas. In the proposed scenario, UEs operate in HD TDD mode. At a certain time, part of them are acting as UL users, and the rest are receiving the DL signal. Meanwhile, the BS is working in FD mode, so it can simultaneously transmit its signal to the specific DL users and receive the signals from UL users. First, the motivation of using AS in FD BS is explained. Then, the system model is presented, and the channel model is described with the ray-tracing method. Next, the simulation setup is defined. The three antenna selection criteria are explained, 1) MSNR: maximization of SNR without considering the SI channels. 2) MSSINR: maximization of SSINR, where SI channels are estimated. 3) MCGR: maximization of channel gain ratio. Finally, the simulation results in both antenna setups are displayed and analyzed.

  The work in this chapter originated two conference papers:

  - N. Zarifeh, M. Alissa, T. Kreul and T. Kaiser, "Enabling full-duplex in a wideband indoor base-station using low-complex antenna selection," 2018 The Loughborough Antennas and Propagation Conference (LAPC), Loughborough, UK.

  - N. Zarifeh, M. Alissa, T. Kreul and T. Kaiser, "Antenna Selection Performance of Distributed Antenna Systems in Full-Duplex Indoor Base Station," 2019 12th German Microwave Conference (GeMiC), Stuttgart, 2019.

- **Chapter 6: Experimental Validation of Full-Duplex Base-Station with Antenna Selection**

  This chapter intends to experimentally validate the simulation of FD BS with AS which is presented in the previous chapter. Receive antenna selection is combined with cross-polarization and antennas conditional placement in order to achieve the required SIC. The testbed is explained in details, in terms of the setup, the signal processing, and the measurement environment. Next, the measurement results are shown considering different scenarios in the testbed, such as changing the number of antennas, the type of isolation (vertical/horizontal), and the type of antennas (Omnidirectional/directional).

  In fact, till the moment, there aren't many testbeds that could realize FD. Most of the previous hardware implementations focused on FDR. Recently, FD testbed has been realized with massive MIMO in [25]. Thus, this testbed is considered the first that

implements FD transmission in a BS with antenna selection.

The work in this chapter is published as a journal article:

- N. Zarifeh, Y. Zantah, Y. Gao and T. Kaiser, "Full-Duplex Femto Base-Station With Antenna Selection: Experimental Validation," in IEEE Access, vol. 7, pp. 108781-108794, 2019.

- **Chapter 7: Conclusions and Outlook**
  This chapter summarizes the main research challenges and highlights the achieved results. Furthermore, some constructive guidelines and recommendations are provided for future extension work.

To summarize, the structure and main contributions of this thesis with the relationship among the chapters are shown in Fig. 1.1.

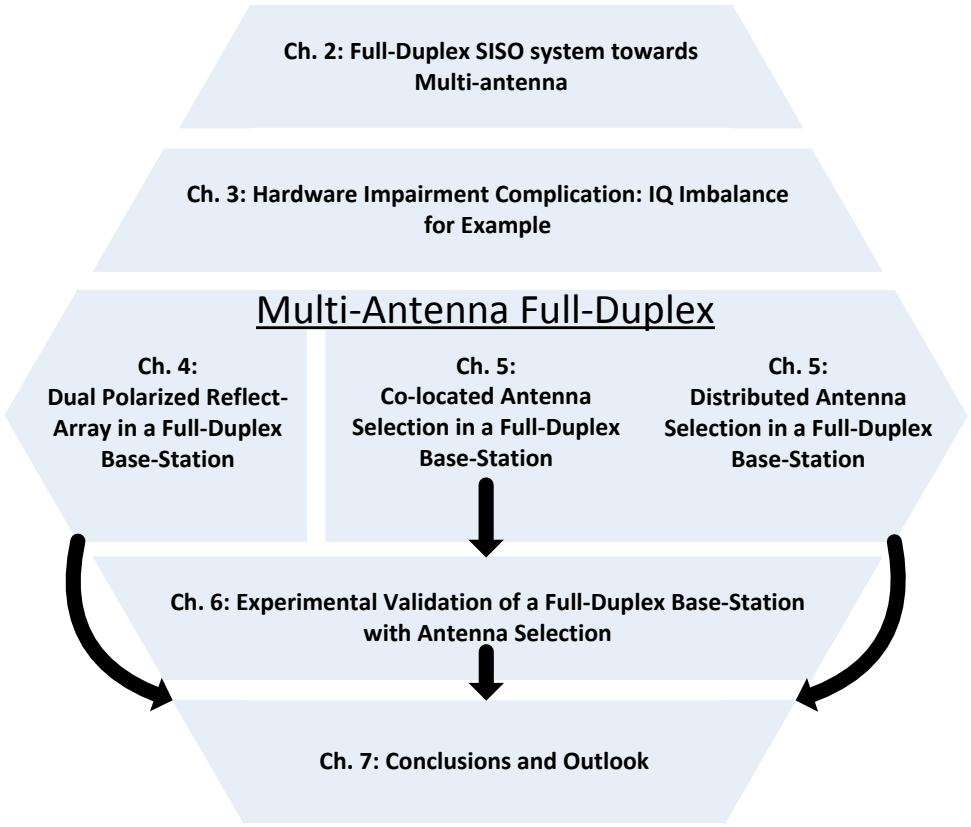

Figure 1.1: Schematic representation of the dissertation structure.

Chapter 2

Full-Duplex SISO system towards Multi-Antenna

The previous generations of mobile communication mainly depended on half-duplex transmission schemes, in which the transmitted and received signals are separated either

- in time domain, then Time Division Duplexing (TDD) is used as in Fig. 2.1(a)
- or in frequency domain, then Frequency Division Duplexing (FDD) is used as in Fig. 2.1(b)
- or in both, then it is Half-Duplex FDD as in Fig. 2.1(c).

Traditionally, the term ”Full-Duplex” (FD) was used in case the device has simultaneous bidirectional communication counter to ”Half-Duplex” (HD) which assumes time division duplex. Previously, ”full-duplex” mode assumed utilizing a pair of frequencies to transmit and receive simultaneously; however, the new employment of this term during recent years carries a new concept: the device can transmit and receive at the same time and over the same frequency as Fig. 2.1(d) depicts. Many papers use ”In-Band Full-Duplex” (IBFD) term to clarify this new concept as in [26, 27]; however, most of them refer to it by an abbreviated version: ”full-duplex”, which is adopted in this thesis as well.

As Fig. 2.1(d) depicts, the major challenge that is facing the implementation of full-duplex is the self-interference (SI) signal, i.e., the part of the transmitted signal that leaks into the receiver chain. Compared to the weak desired signal from the remote node, high power self-interference forms a significant issue to the receiver. Nevertheless, the trend of using short-range cells by new wireless networks provides an inherent capability to better manage the self-interference issue

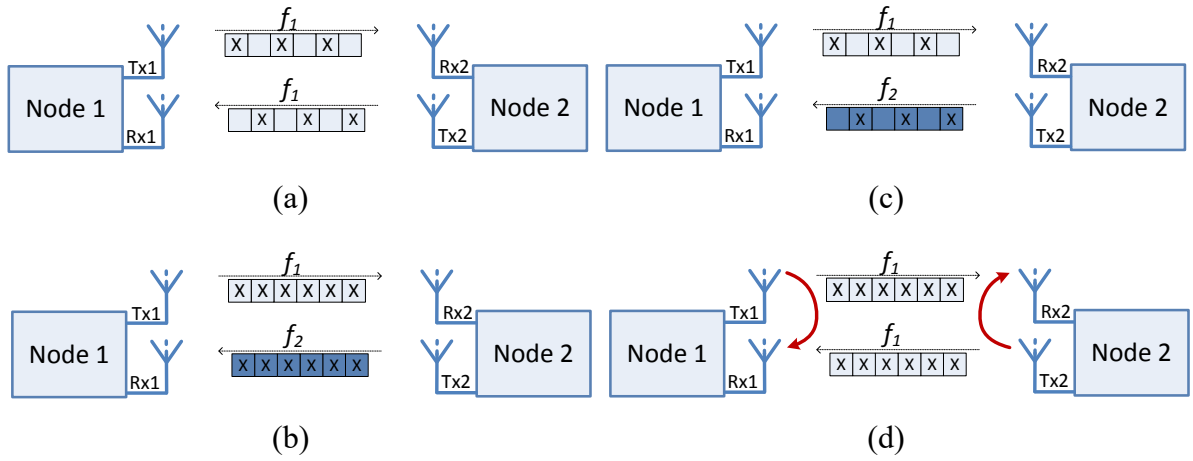

Figure 2.1: Duplex schemes (a) Time Division Duplex, (b) Frequency Division Duplex, (c) Half-Duplex FDD, (d) In-Band Full-Duplex with self-interference

due to the lower cell edge path loss, compared to the case in large cells [26].

A direct and straightforward question may be posed: in principle, the receiver knows the transmitted signal from its own transmitter which is causing self-interference, so would not it be easy to subtract the self-interference from the total received signal to cancel it out? The direct and straightforward answer to this question is: No; on the contrary, it is challenging, because the assumption of the receiver's knowledge of the transmitted signal is inaccurate. As a matter of fact, although the transmitted digital samples are fully known; the signal that reaches the end of the transmitter chain is quite different from its baseband original. This is due to the multistage process (digital to analog conversion, up-conversion, amplification, and all other imperfect analog components), not to mention the effect of SI channel between transmit (Tx) and receive (Rx) chains. The reasons above push researchers to explore further efficient and advanced techniques.

This chapter studies full-duplex technology from signal processing algorithm and implementation perspective. It explains full-duplex system requirements, self-interference, and Self-Interference Cancellation (SIC) techniques with related algorithms and implementation challenges. Also it shows the current achievements starting from SISO, in order to treat the problem from the basics, to MIMO case which still needs further development.

The rest of this chapter is organized as follows: In the next section, an analysis of the SI problem and a basic model of SI are shown. After that, the SIC requirements are presented, then the cancellation techniques in full-duplex SISO system are classified into four main categories:

- Passive SI suppression in propagation domain
- Active SIC in analog domain
- Active SIC in digital domain
- Auxiliary chain SIC

Afterward, hardware impairments and their impact on SIC are covered. Finally, the challenges of full-duplex multi-antenna system are discussed.

2.1 Self-Interference: Basic Analyses and Models

The main challenge toward full-duplex is self-interference, hence the big question is how to manage and suppress self-interference. SI was studied earlier in radar applications; the term "transmitter leakage" was used to describe the signal that leaks from the device transmitter to its own receiver. Generally, the transmitter signal is about 100 dB higher than the desired received signal. A considerable part of this transmitted signal leaks into the receiver chain, causing a severe issue in decoding the desired signal since it could be considered as a noisy signal that dramatically affects the Signal to Noise Ratio (SNR). In order to achieve the best performance of the full-duplex system, the SI signal has to be suppressed to reach the receiver's noise floor. For example, when the transmitted downlink power from an LTE cell is 20 dBm, and the noise floor of eNodeB's receiver is -104 dBm. This assumption means that 124 dB of cancellation has to be achieved in order to cancel out the SI signal entirely. This number is, of course, the worst-case. Generally, the difference between transmitted power and receiver noise floor is between 90 to 110 dB. It is essential to mention that these cancellation values cannot be achieved by one technique of cancellation; therefore, hybrid methods are proposed in order to meet the cancellation requirement.

Fig. 2.2 describes the two cases of antenna setup in wireless communication transceiver, the first uses two separated antenna, one for transmission and the other for reception, while the second uses one shared antenna for transmission and reception, and a circulator is employed to separate the signals. In both cases, the SI signal consists of two components; the first is caused by the direct path/circulator leakage (maybe adding here the mismatch between the transmission line impedance and the antenna's input impedance); while reflection paths cause the other component. The direct and reflected components of the SI channel are modelled as Rician and Rayleigh channels, respectively [28].

Another classification of self-interference is presented in [29], which shows the components

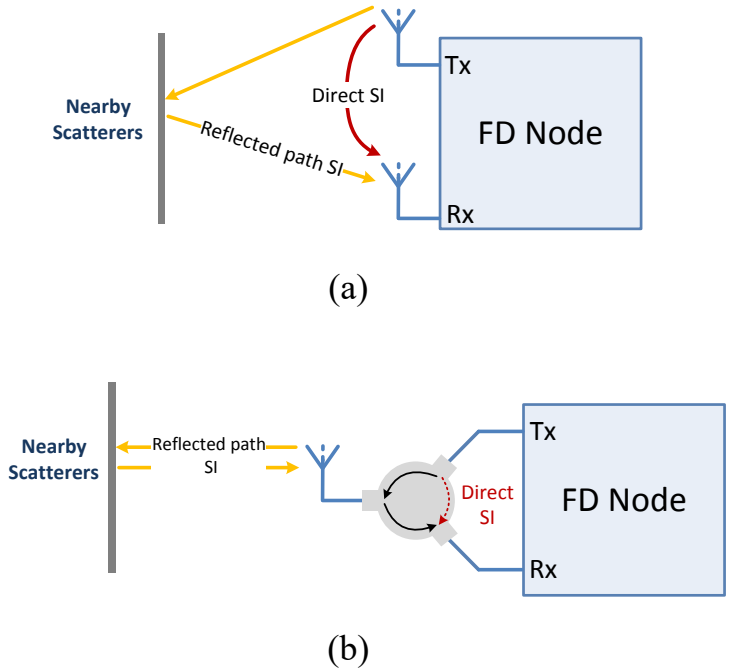

Figure 2.2: Two cases of antenna for Tx/Rx full-duplex node

as follows:

- Linear components

  This corresponds to the carrier itself, which is attenuated and reflected from the environment. The received distortion can be written as a linear combination of different delayed copies of the original carrier.

- Non-Linear components

  These components are created because the imperfect radio circuits take a signal x as an input and create outputs that contain non-linear cubic and higher-order terms such as x^3 and x^5. These higher-order signal terms have significant frequency content at frequencies close to the transmitted frequencies, which directly correspond to all the other harmonics [29].

- Transmitter noise

  It is also referred to as broadband noise [30]. It seems like an increase (about 50 dB above the receiver noise floor [29]) in the base signal level on the sides of the carrier at the receiver. It is by definition noise and is random; therefore, the only way to cancel transmitter noise is to get a copy of it where it is generated in the analog domain and cancel it there [29] as shown later.

For narrowband systems, the SI channel can be modeled as gain and delay functions; meanwhile, wideband systems require a more complicated model, because the reflected-path SI channel is often frequency-selective as a result of multipath propagation. In general, a basic equivalent baseband model in the digital domain is presented by

$$r(n) = r_d(n) + i(n) + w_r(n), \quad i(n) = r_{DSI}(n) + r_{SSI}(n) \tag{2.1}$$

where $r(n)$ is the total received complex baseband samples. $r_d(n)$ is the desired signal from the remote node. $r_{DSI}(n)$ is the complex samples caused by direct self-interference component signal between the Tx and Rx antennas in case of two antennas, or leaked signal in the circulator in case of one antenna. $r_{SSI}(n)$ is the complex samples caused by scattered self-interference components, and $w_r(n)$ is the additive white Gaussian noise (AWGN).

Both direct and scattered SI can be represented in detail as a combination of linear and nonlinear components. The suppression in the propagation domain can mitigate both linear and nonlinear SI at the same time, and with the same isolation value meanwhile, the techniques in the analog and digital domains have different cancellation performance for the two components.

2.2 SIC Requirements

The simple model above shows clearly that the FD system can reach maximum efficiency only when the SI signal $i(n)$ is suppressed to reach its own receiver's noise floor. The required cancellation has to meet specific requirements related to the system specifications such as the full scale of the analog-to-digital converter (ADC) and noise floor level. Generally, SIC is implemented in three domains: propagation, analog, and digital domains. Neither of these domains can meet the required cancellation value per se; therefore, hybrid solutions are proposed in the literature. This section explains the requirements of SIC and how to achieve them in the three domains.

The primary role of SIC in the propagation and analog domains is to avoid the saturation of the receiver due to the high power of the SI signal; this power exceeds the ADC dynamic range and limits its precision after the conversion as the desired signal is much weaker than SI. Thus the required cancellation before the low-noise-amplifier (LNA) has to be sufficient to prevent such effects. Detailed analysis and calculations of ADC and linearity challenges of the FD system are in [31]. To specify SIC requirements for an FD system mathematically, the

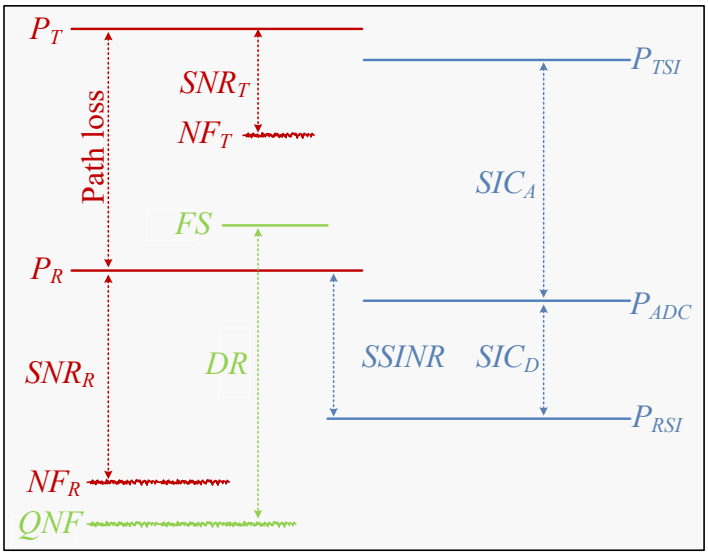

Figure 2.3: Dependencies of full-duplex system power levels

dependencies among FD transceiver specifications are illustrated in Fig. 2.3.

The specifications of the full-duplex system can be classified into three categories:

Main specifications

P_T Transmitter power level from the remote node

NF_T Transmitter noise floor

SNR_T Signal to noise ratio in the transmitter

P_R Power level of the desired received signal from the remote node

NF_R Receiver noise floor

SNR_R Signal to noise ratio in the receiver

ADC specifications

FS Full scale level of receiver ADC

QNF Quantization Noise Floor. It's practically 6 dB (1bit) below Receiver noise floor [26].

DR Dynamic Range of ADC

Self-interference Specifications

P_{TSI} Transmitted power from the own transmitter that causes SI

SIC_A Self-interference cancellation capability in propagation and analog domain

P_{ADC} Residual SI signal power after SIC before the ADC

SIC_D SIC achieved in digital domain

P_{RSI} Residual SI signal power after all cancellation operations

While the residual SI power P_{RSI} is higher than receiver noise floor level, the signal to self-interference plus noise ratio (SSINR) in full-duplex system is lower than the SNR of the half-duplex system receiver; this means that the maximum efficiency of full-duplex cannot be achieved. To clarify that, a numeric example is shown: $P_T = 0$dBm (as UE working in Femto BS) with working frequency: 2.6 GHz and line of sight (LoS) distance $= 50$ m, then the path loss is about 75 dB in free space calculations. $NF_R = -104$ dBm (with bandwidth 10MHz) then:

$$P_R = 0\text{dBm} - 75\text{dB} = -75\text{dBm}$$

$$\Rightarrow SNR_R = P_R - NF_R = -75 - (-104) = 29\text{dB}$$

Assuming: $P_{TSI} = 20$dBm (as Femto BS), $QNF = -110$dBm, $DR = 60$dB as a practical value for ADC based on the effective number of bits, then $FS = -110\text{dBm} + 60\text{dB} = -50\text{dBm}$

$$P_{ADC} = P_{TSI} - SIC_A = 20\text{dBm} - SIC_A < -50\text{dBm} \Rightarrow SIC_A > 70\text{dBm}$$

This means that, in this example, the sum of cancellation before ADC (i.e., propagation domain suppression and analog cancellation) has to be about 70 dB, or more, to avoid ADC saturation. For instance, in the work in [32] with certain conditions, an isolation of antenna in propagation domain achieves between 20 and 30 dB, and analog cancellation achieves between 20 and 45 dB.

Considering an example $SIC_D = 30$ dBm the residual SI power will be $P_{TSI} = P_{ADC} - SIC_D = -50 - 30 = -80$ dBm, so $SSINR = P_R - P_{RSI} = -75 - (-80) = 5$ dB instead of $SNR_R = 29$ dB in half-duplex system. The calculated minimum requirement $SIC_A = 70$ dBm means that the rest of cancellation has to be performed in the digital domain SIC_D to bring the residual SI signal below the noise floor. SIC_D has to exceed $-50 - (-104) = 54$ dB in order to reach the ultimate performance of the FD system; otherwise, a comparison in performance between full-duplex system and the half-duplex system should take place to evaluate the effectiveness of applying full-duplex. Similar calculations have been done in [29] for 802.11 WiFi system with more relaxed assumptions (Receiver noise floor $NF_R = -90$ dBm and higher full-scale level of receiver ADC $FS = -30$ dBm) and their solution met the SIC requirement for WiFi systems.

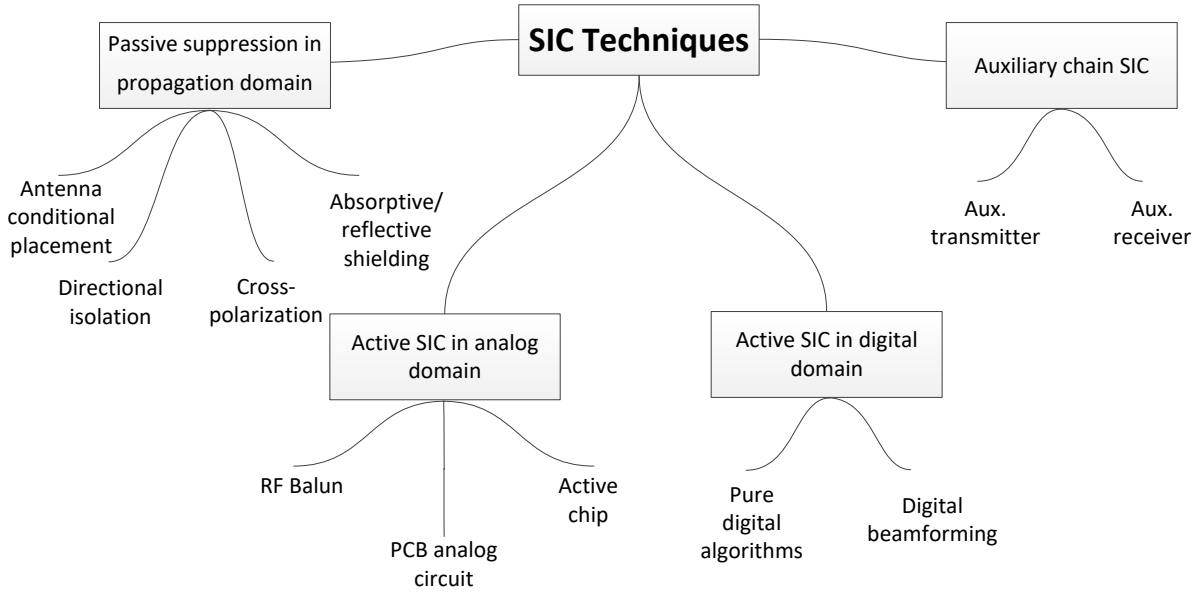

Figure 2.4: Categories of SIC techniques

2.3 SIC Techniques and Algorithms

Most SIC literature and results of full-duplex testbeds are for SISO systems; likewise, this chapter will mainly analyze SIC techniques and its properties in SISO case, then SIC techniques in MIMO are discussed. In general, SIC techniques can be classified into four main categories, as illustrated in Fig. 2.4:

- Passive SI suppression in propagation domain
  Conditional placement, directivity, polarization, and shielding;
- Active SIC in analog domain
  Tapping the transmitted analog signal and feeding it with a negative sign to the receiver;
- Active SIC in digital domain
  Replication of the transmission samples and feeding it with a negative sign to the receiver;
- Auxiliary Chain SIC
  Hybrid technique of the two previous methods, where replication and cancellation domains are different (i.e., one is analog and the other is digital) using additional ADC or DAC (digital-to-analog converter) as will be shown later.

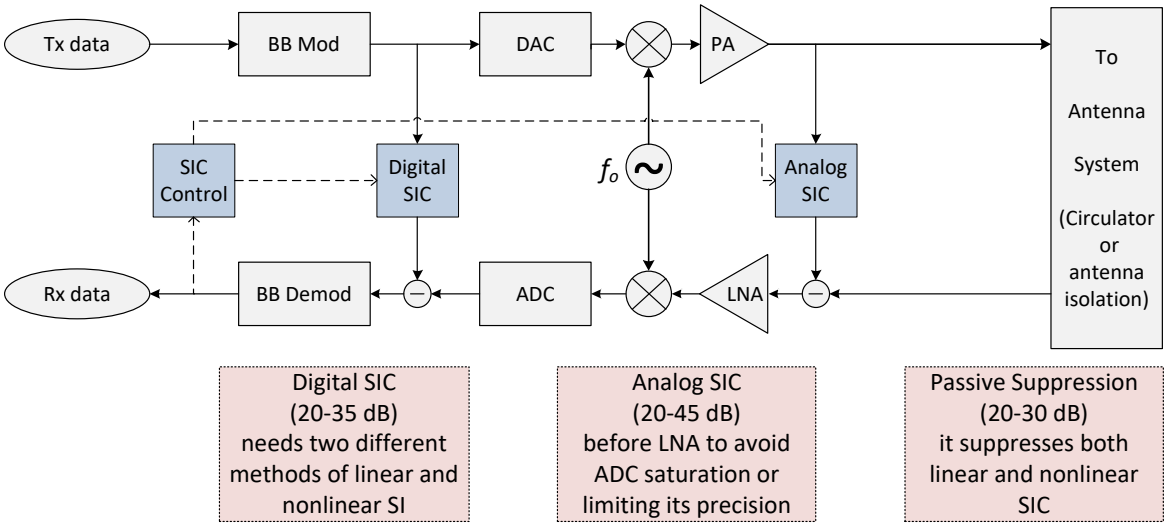

Figure 2.5: Example of hybrid SIC solution with performance average

Usually, any SIC solution is a combination of several techniques in order to meet the requirements. Fig. 2.5 illustrates an example with average performance value in each domain.

2.3.1 Passive Cancellation

Passive SI suppression is defined as the signal power attenuation imposed by the path loss due to the physical separation between transmitting and receiving antennas of the same device [20]. In case of shared antenna system, the suppression is done using a three-port RF circulator, as the ferrite within the device can be considered as a propagation domain [26]. Achievable isolation by circulator is from 15 up to 30 dB [19, 29, 33–35], and in case of wide band operation the maximum value would decrease [36–38]. In a separate antenna system, several SIC techniques can be used:

Antenna conditional placement [39–45] As shown in Fig. 2.6, the two transmit antennas are set at distances d and $d + \lambda/2$ away from the receive antenna. Offsetting the two transmitters by half a wavelength causes their signals to cancel one another [43]. For narrowband signals, this technique is proved experimentally to be sufficiently robust; however, the suppression performance dramatically falls in case of wideband signals.

Directional isolation [46, 47] Fig. 2.7(a) illustrates how directionality isolates the receiving antenna from the interfering signals of transmitting antenna. This technique could be useful for FD relaying scenario (FDR) as the receiving and transmitting directions are

generally separated from each other as in Fig. 2.7(b), therefore this approach would not work for point-to-point FD scenarios.

Absorptive/Reflective shielding [40, 42, 46] Electromagnetic shielding like copper or aluminum plates can enhance the isolation between antennas. However, one disadvantage that the shielding affects the far-field coverage patterns because it prevents the antenna from transmitting to/receiving from the shielding direction, hence it is relevant to be used in case of directional antennas as in Fig. 2.8. Absorptive shielding is preferred on the reflective shielding plates as the latter would couple with the transmit antenna and subsequently cause another component of self-interference. Experiments in [46], for instance, show that the absorption technique can achieve about 10 dB of isolation for 2.4 GHz, and intuitively this value depends on specifications of the absorption plate, signal frequency, and surrounding environment.

Cross-polarization [44, 46–48] Self-interference can be mitigated using orthogonal polarization as in Fig. 2.9. Achieving a low polarization match factor between the two antennas would increase the isolation from about 10 to 20 dB in an anechoic chamber and 6 to 9 dB in a reflective room as measured for 2.4GHz in [46].

Experiments in the propagation domain show, in optimal conditions, that up to 65 dB of SI can be suppressed with Omni-directional antennas [39,47], and up to 72 dB with directional antennas when implementing multi suppression techniques to achieve higher suppression performance [41,46]. This suppression applies to the entire signal, including linear and non-linear components as well as transmitter noise since it is pure RF signal attenuation [29]. Although passive SI suppression techniques are appealing for simplicity related reasons; however, they are highly sensitive to the wireless environment and its reflected paths which cannot be known during the design, not to mention that the device form-factor significantly limits their effectiveness: the smaller the device, the less room there is to implement such techniques [26].

2.3.2 Analog Active Cancellation

These techniques depend on the following methodology: a replica of the transmission signal to be generated and then adjusted to match the SI channel, making the replica similar to the SI signal as much as possible, in order to subtract it from the total received signal. This copy is created either in the analog domain, as in this subsection, or in the digital domain before the DAC. The SIC

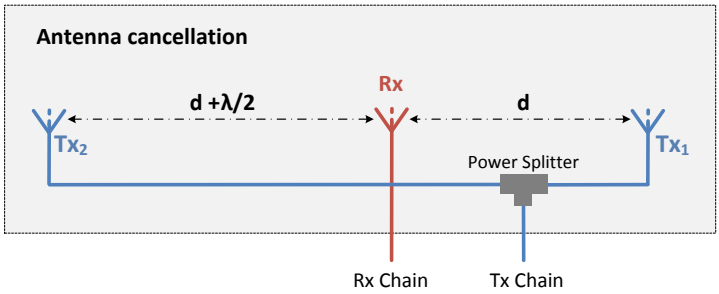

Figure 2.6: Example of antenna conditional placement

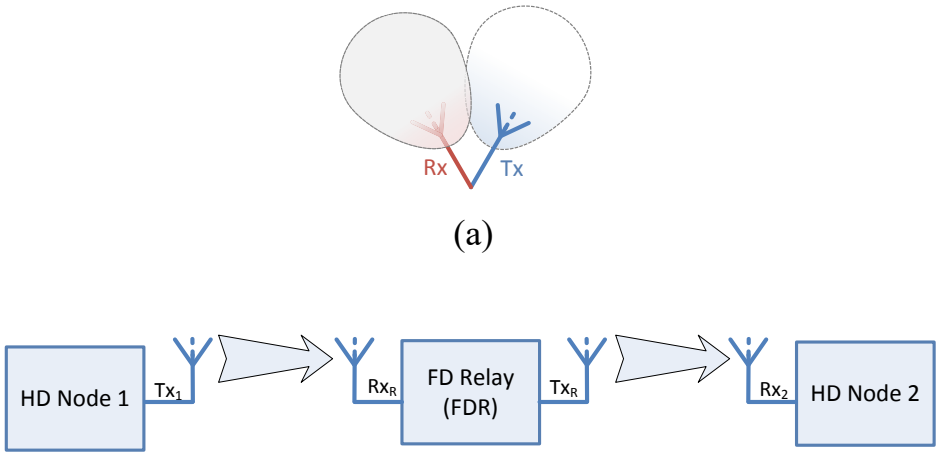

Figure 2.7: Directional Isolation

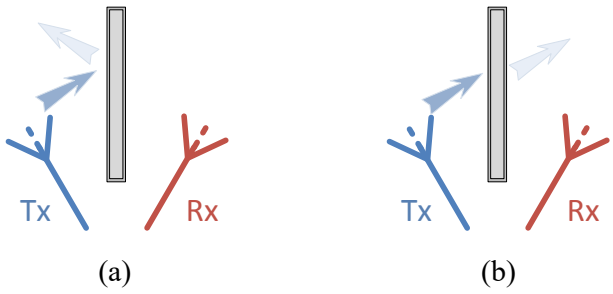

Figure 2.8: Antenna Shielding (a) Reflective (b) Absorptive

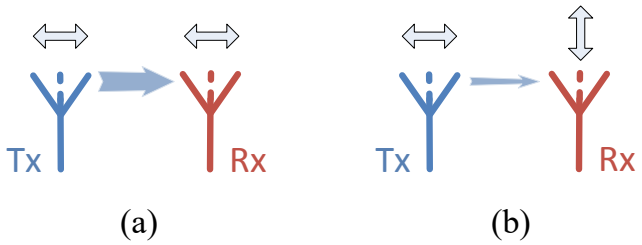

Figure 2.9: Cross-polarization isolation (a) Co-polarization (b) Cross-polarization

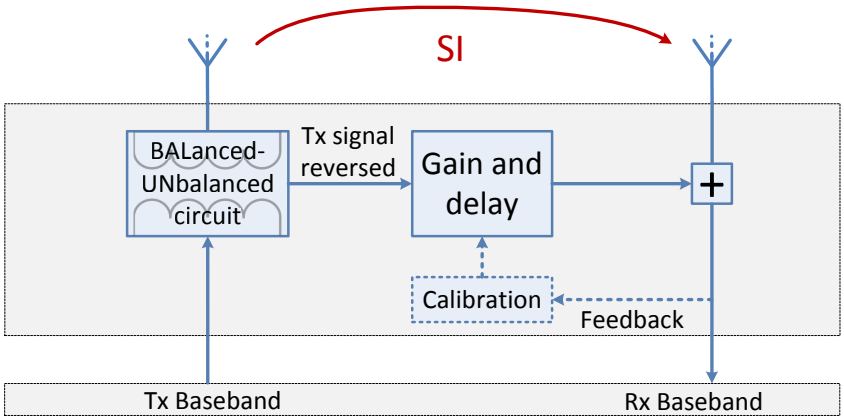

Figure 2.10: Balun Cancellation block diagram

signal stays in the same domain where it has been copied; therefore, no additional ADC/DAC is required. Replication of the transmission signal in the analog domain can be achieved by tapping the TX chain [29], using power splitter [28] or using Balun (balanced-unbalanced) circuit in case of two separate antennas [32]. Fig. 2.10 illustrates the Balun cancellation block diagram. Experiments in [32] show practically the benefits of the Balun in comparison with a phase shifter, mainly the flatter response within a wide frequency band.

After generating an exact negative replication of the signal (RF reference signal) from the invertor, the replica is adjusted by attenuation and delay elements to match the self-interference. In [32, 43, 49] adjusting the signal is achieved by a noise cancellation active chip Quellan QHx220 that is shown in Fig. 2.11. The chip takes the input signal from the Balun and separates it into an in-phase and quadrature components. A fixed delay is applied to the quadrature component; meanwhile, any variable delay can be achieved by controlling the gains of in-phase and quadrature components. Adding this adjusted reference signal to the total received signal from the Rx antenna will partially cancel out the SI signal. The cancellation which is achieved by

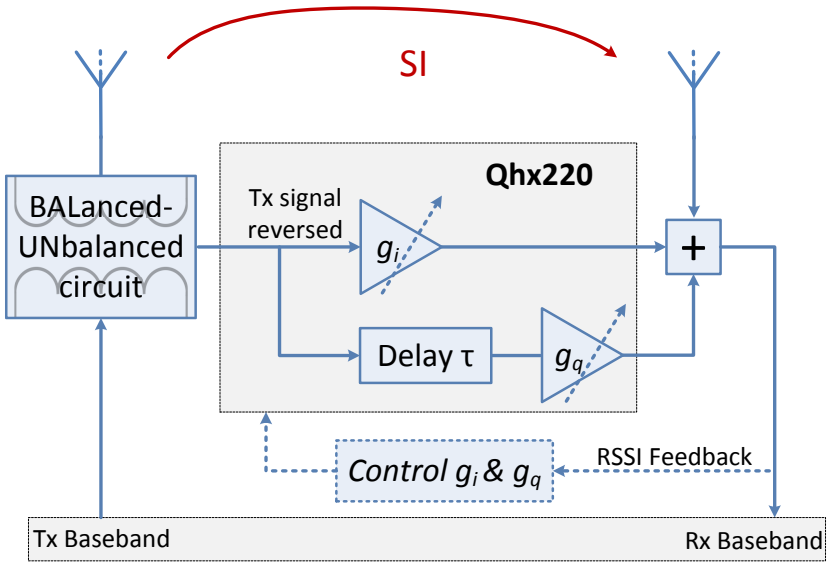

Figure 2.11: Block diagram of full-duplex system with Balun Active Cancellation. The RSSI values represent the energy remaining after cancellation

this method is limited to about 25 dB since it is susceptible, and it requires precise programmable delay with resolution as precise as 10 picoseconds, which is extremely challenging to build in practice [29]. One appealing aspect for this method, though, is the inexpensive cost of the QuellanQHx220 and similar chips; however, it cannot perform properly with wideband signals where the SI channel cannot be modeled as a complex gain and delay between the Tx and Rx chain. The fixed delay and controlling steps of the gains show limitations in the case of wideband operations. Moreover, Balun and QHx220 active chips produce nonlinear behavior that affects the performance of digital SIC which assumes the SI channel is a linear time-invariant (LTI) system [32].

Another method for adjusting the RF reference signal is proposed in [29]. While the previous adjusting method has limitations because of the fixed delay, a printed circuit board (PCB) can be designed with several delay micro-strip lines; each one has a different length and is connected to a tunable attenuator. The work in [29] shows that a linear combination of eight or sixteen adjusted replicas of the transmission signal can approximately build one SIC signal that can mitigate a considerable part of self-interference. The challenge here, in the ware-channel approach, is to reach an optimization algorithm for the variable attenuators like the algorithm in [29] which uses Nyquist theorem to deal with SIC as a sampling and interpolation problem. The achieved cancellation for WiFi wideband signal with eight and sixteen delay tabs was about 30 and 48 dB respectively without considering the circulator isolation.

Nevertheless, it is worth mentioning that for wideband signals, the *direct path SI* component can be mitigated using the same analog techniques described above. This is since the SIC direct path channel can be modeled as gain and delay functions with flat frequency behavior if that was considered during the antenna design. Meanwhile, the *scattered SI* components are frequency selective, and therefore they require an adaptive analog filter to cancel it out [26]. This point forms one motivation toward duplicating the transmission baseband signal to be cancelled in the digital domain with adaptive digital filter and further digital signal processing (DSP) algorithms which can mitigate both linear and non-linear self-interference as in [47, 50, 51].

2.3.3 Digital Active Cancellation

Assuming that SIC in propagation and analog domains ensures the minimum required cancellation that prevents ADC saturation, the digital cancellation aims to cancel the residual SI. This opens the door to apply advanced DSP algorithms to process the SI signal and cancel both linear and non-linear components. In this subsection linear SI cancellation is discussed, and later non-linear SI cancellation is studied when discussing hardware impairments and implementation challenges.

Earlier work of linear SIC in digital domain [43] proposes the same techniques that are used to digitally cancel the typical interference from any transmitter and solving the hidden node problem, when the desired packet is collided with another packet from the other transmitter [52–54]. Firstly, the receiver decodes the undesired packet, reconstructs it and then subtracts it from the originally received collided signal. For SI, a correlation operation is performed without the need for decoding because the undesired packet, which is its own transmitted samples, is already known by the receiver [43]. The correlation between the received signal and the clean transmitted signal is needed to detect the peaks which give the paths delay of the SI channel. Experimentally this method could not achieve more than 10 dB of cancellation, due to system non-linearity, jitter, and hardware limitations which are discussed later in this chapter. More advanced techniques are presented in [29, 32], for SI channel estimation and cancellation.

Baseband equivalent model

Full-duplex with linear SI may be modeled in digital baseband as follows [29]: At first the SI channel $h_s(n)$ is considered as a non-causal linear system which has the known preamble signal $x_{pr}(n)$. Any SI received sample $y(n)$ is modeled as a linear combination of transmitted samples

x_{pr} before and after the instant n. The non-causality assumption is possible as all IQ baseband samples x_{pr} are known.

$$y(n) = x_{pr}(n-k)h_s(k)+x_{pr}(n-k+1)h_s(k-1)+\ldots+x_{pr}(n+k-1)h_s(-k+1)+w_r(n) \quad (2.2)$$

where $w_r(n)$ is the receiver noise. To find $h_s(k)$, the above equation can be expressed as: $y = Ah_s + w_r$ where A is Toeplitz matrix of $x_{pr}(n)$:

$$A = \begin{bmatrix} x_{pr}(-k) & \cdots & x_{pr}(0) & \cdots & x_{pr}(k-1) \\ \vdots & & \vdots & & \vdots \\ x_{pr}(n-k) & \cdots & x_{pr}(n) & \cdots & x_{pr}(n+k-1) \end{bmatrix} \quad (2.3)$$

The problem is to find a maximum likelihood estimate of the vector h which means $minimize\|y - Ah_s\|^2$ as y and A are already known. Using convex optimization algorithm [55] computation of h_s coefficients is possible by multiplying each received samples of the preamble by the relevant column of the pseudo inverse of A matrix $a_i^\dagger$

$$\hat{h}_s = \sum (y_i.a_i^\dagger) \quad (2.4)$$

The residual signal after SI signal $\hat{i}(n)$ subtraction from total received signal $r(n)$:

$$r_{rs}(n) = r(n) - \hat{i}(n) = r_d(n) + \sum_{k=0}^{N-1} [h_s(k) - \hat{h}_s(k)]x(n-k) + z_r(n) \quad (2.5)$$

where $r_d(n)$ is the desired signal, and $z_r(n)$ is the noise after SIC.

This method is robust to noise as it includes the white noise in the channel estimation algorithm; however, an important challenge has to be taken into consideration about the coherence time of the SI channel. Many other SIC algorithms in the digital domain are proposed in the case of MIMO system, where this will be tackled later on in this chapter.

2.3.4 Auxiliary Chain Cancellation

This scheme [33, 39, 56] belongs to active SIC techniques, it copies the baseband IQ samples of the transmitted signal in digital domain, then it uses an additional transmitter chain (DAC, LPF, upconverter, PA, etc.) to generate the SIC signal and feed it back into the receiver in order to be subtracted from the total received signal. The SIC signal has to be adjusted (pre-distorted)

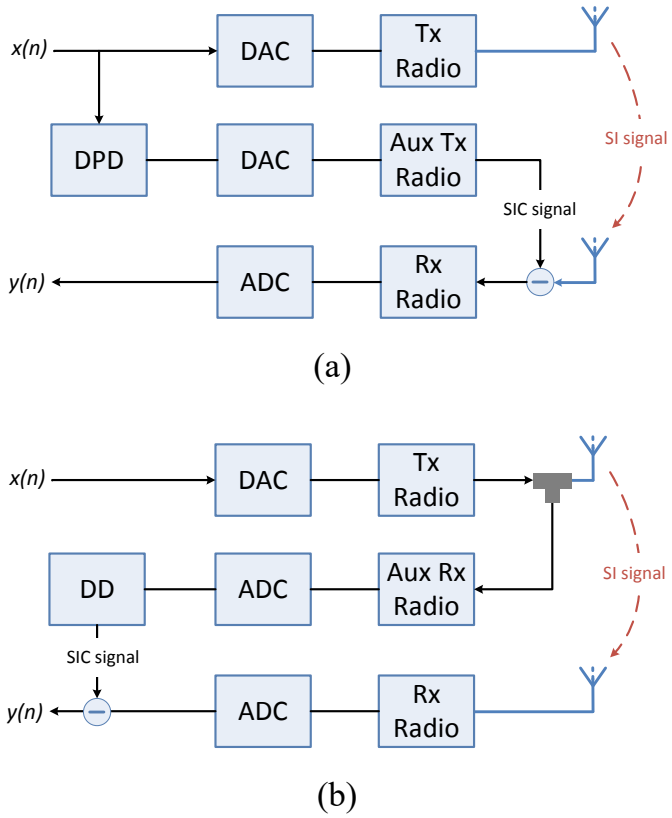

Figure 2.12: Auxiliary chain SIC (a) Auxiliary Tx (b) Auxiliary Rx

in the digital domain before the DAC to match the transmitted signal through the SI channel. Similar work is done in [28] proposing auxiliary receiver chain instead of auxiliary transmitter chain, this is the case when the transmitted signal is tapped in analog domain right before the antenna, and then fed back to the receiver's digital domain as in Fig. 2.12. However, like the auxiliary transmitter method, the SIC signal is also adjusted in the digital domain to employ digital signal processing algorithms. Auxiliary receiver chain method mitigates the effect of transmitter hardware impairments like phase noise and nonlinearities on SIC. Furthermore, a common oscillator for the chains -ordinary and auxiliary- is used to suppress the phase noise effect on the SIC signal.

Fig. 2.13 and Fig. 2.14 show the FD transceiver structure with auxiliary transmitter [33, 57], and its system model respectively.

$h_{ord}(n)$ The equivalent baseband channel between the generated waveform from DAC and the RF power amplifier (PA) output at the ordinary transmission chain

$h_{aux}(n)$ The equivalent baseband channel between the generated waveform from DAC and the PA output at the auxiliary transmission chain

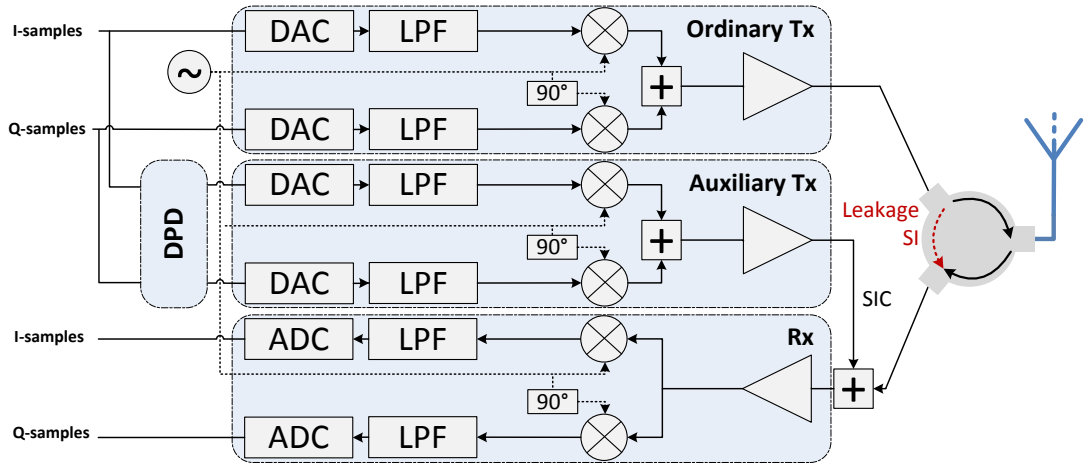

Figure 2.13: Structure of FD transceiver with auxiliary Tx SIC

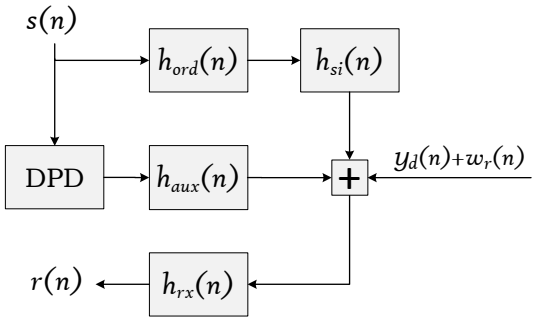

Figure 2.14: System model of FD transceiver with auxiliary Tx SIC

$h_{si}(n)$ The equivalent baseband channel of the SI radio channel

$h_{rx}(n)$ The equivalent baseband channel of the receiving chain

$s(n),\ r(n)$ The transmitted and the received complex baseband samples, respectively

The received baseband signal consists of the desired reception signal $y_d(n)$, the residual self-interference $i_{rsi}(n)$ and the noise $w_r(n)$.

Assuming that the two transmitter chains are identical, i.e., $h_{ord}(n) = h_{aux}(n)$, then Digital Pre-distortion function (DPD) has to emulate the estimated SI channel $\hat{h}_{si}(n)$. Then the residual SI in its baseband form is given as:

$$i_{rsi}(n) = [h_{si}(n) - \hat{h}_{si}(n)] * h_{rx}(n) * h_{ord}(n) * s(n) \tag{2.6}$$

The above equation illustrates clearly that the cancellation performance depends on mini-

mizing the error of SI channel estimation. Thus, a high cancellation value requires an accurate DPD model. The DPD model is calculated with preamble sequence, and it can be either linear (LDPD) as previously explained, or extended to non-linear (NLDPD) model in order to handle the nonlinearities of hardware components as it will be shown in the next section.

2.4 Hardware Impairment and Implementation Challenges

In principle, high power SI signal can be dramatically mitigated using a combination of the above SIC techniques in the propagation, analog, and digital domains. Experiments during the implementation of these techniques show that the performance is limited by hardware imperfections in the analog domain such as nonlinearities, phase noise, and IQ mismatch. These impairments have dissimilar effects of degradation on performance for different SIC techniques. One detailed example of IQ imbalance calibration in FD systems is addressed in the next chapter. Thus, another two main impairments are outlined here.

2.4.1 Non-linear SIC

Experiments in [29, 51] show that nonlinear components of SI can be 80 dB higher than the receiver noise floor. The major part of it may be eliminated along with the linear SI by SIC techniques in analog and propagation domains; however, the residual nonlinear SIC in the digital domain, which can be about 10 to 20 dB [29, 51], needs to be cancelled in the digital domain. Usually, the nonlinear SIC methods are added up to the linear methods to achieve optimal performance. The general model to approximate the nonlinear function uses Taylor series, so the output transmitted signal can be written as [29]:

$$y(n) = \sum_{m} a_m x_p^m(n) \tag{2.7}$$

where $x_p(n)$ is the ideal passband analog signal for the digital representation of $x(n)$. In [33] Volterra series is used in order to capture the memory effect. It can be shown that for practical wireless systems, only the odd orders of the polynomial contribute to the in-band distortion [58]. Furthermore, only a limited number of odd orders contribute to the distortion, and higher orders could be neglected [50]. In practical systems, the nonlinearity is typically characterized by the third-order intercept point (IP3), which is defined as the point at which the power of the third harmonic is equal to the power of the first harmonic [59]. Therefore, the above model can be

simplified to [50]:

$$y = x + \alpha_3 x^3 (assuming\ a\ unity\ linear\ gain\ \alpha_1 = 1) \tag{2.8}$$

The second term of the sum is presenting the nonlinear SI component which is transmitted, and it will cross the SI channel then suffer again from receiver nonlinearity; so the total nonlinear SI can be written as:

$$d = \underbrace{\alpha_3^t (x_{si})^3 * h_{si}}_{\text{Transmitter nonlinearity}} + \underbrace{\alpha_3^r (x_{si} * h_{si} + \alpha_3^t (x_{si})^3 * h_{si})^3}_{\text{Receiver nonlinearity}} \tag{2.9}$$

where α_3^t and α_3^r are the transmitter and receiver third-order nonlinearity coefficients. Expanding the above equation and neglecting the order higher than 3^{th} will give:

$$d = \alpha_3^t \underbrace{(x_{si})^3 * h_{si}}_{A} + \alpha_3^r \underbrace{(x_{si} * h_{si})^3}_{B} + 3\alpha_3^t \alpha_3^r \underbrace{(x_{si} * h_{si})^2 ((x_{si})^3 * h_{si})}_{C} \tag{2.10}$$

Accordingly, the main difference between the transmitter and receiver nonlinearity is that the former affects only the signal, while the latter affects both the signal and the wireless channel function [50]. In case of sending a preamble signal x_{pr}, the baseband representation of the received SI signal will be:

$$i = x_{pr} * h_{si} + d + z \tag{2.11}$$

where z is a random signal that sums up the white noise and the effects of all impairments -except nonlinearity- like phase noise and quantization error. As i, x_{pr}, h_{si} are known to the receiver, the equation can be:

$$i - x_{pr} * h_{si} = \hat{d} = d + z \tag{2.12}$$

and in matrix form:

$$\begin{bmatrix} \hat{d}_0 \\ \hat{d}_1 \\ \vdots \\ \hat{d}_N \end{bmatrix} = \underbrace{\begin{bmatrix} A_1 & B_1 & C_1 \\ A_2 & B_2 & C_2 \\ \vdots & \vdots & \vdots \\ A_N & B_N & C_N \end{bmatrix}}_{W} \begin{bmatrix} \alpha_3^t \\ \\ \alpha_3^r \\ \\ 3\alpha_3^t \alpha_3^r \end{bmatrix} + \begin{bmatrix} z_1 \\ z_2 \\ \vdots \\ z_N \end{bmatrix} \Rightarrow \hat{d} = W.\alpha + z \tag{2.13}$$

Using Least Squares estimator the matrix α, which represents the nonlinearity coefficients can

be found.

The simulation in [50] shows that this scheme, with the simplifications above, can achieve a performance which is less than 0.5 dB off the performance of a linear OFDM full-duplex system. However, this result is achieved by simulation, and therefore, it needs to be experimentally verified with an expectation of performance drop. Moreover, the complexity of the estimation algorithm has to be considered as a part of the SIC process, as it may limit its performance with a shorter coherence time of the self-interference channel. Many other simulations and experimentations have been conducted to study the nonlinearity in full-duplex system [27–29, 31, 33, 51, 60–62].

2.4.2 Phase Noise

The analyses and experiments in [63–66] show that the oscillator phase noise is one of the main SIC challenges which limit the performance of the FD system. Earlier literature assumes that when transmitter and receiver use a common local oscillator, the level of phase noise will remain on a tolerable level [67, 68], however, this consideration is not always valid especially in the case of orthogonal frequency division multiplexing (OFDM) systems. In [68] the WARP setup (wireless open-access research platform) shows that with a noise phase variance between 0.4° and 1.0°, the drop of SIC performance is about 20 to 25 dB for OFDM system as Fig. 2.15 shows. This can be justified as the phase noise causes two effects: Common Phase Error (CPE) and Inter-Carrier Interference (ICI) as shown in [69, 70]. The former may have acceptable levels as previously assumed, but the latter stimulates an enhancement on SIC performance, which is achieved by consecutively estimating and suppressing the ICI signal.

The conventional half-duplex techniques for ICI suppression in frequency domain [69–71] may be used in the FD system with two considerations in mind [63]: First, in FD systems, while suppressing the ICI associated with the self-interference signal, the signal of interest is considered as an unknown noise signal. Second, in full-duplex systems, the SI signal is known at the receiver side, thus eliminating the need to use decision feedback techniques to obtain the transmitted signal. Also, the work in [63] proposes that time-domain ICI estimation techniques introduced in [72, 73] could be modified and used in full-duplex systems. A low-complexity Least Square (LS) algorithm plus a filtering technique are used for ICI estimation in half-duplex systems. Despite its low complexity, using LS algorithm in full-duplex systems has to be carefully considered, mainly since the ICI has to be estimated in the presence of the signal-of-interest

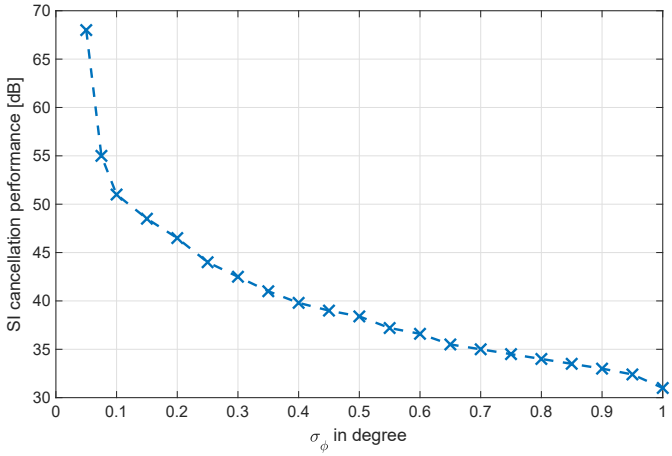

Figure 2.15: Amount of active analog cancellation in presence of phase noise with variance σ_ϕ

which is typically higher than the ICI power in typical operating scenarios. This high power will negatively impact the LS estimator quality [63].

Besides of LS estimator, other conventional estimation algorithms like minimum mean square error (MMSE) are used for phase noise suppression in full-duplex systems. Assuming that the reader is familiar with such algorithms, furthermore, a similar example of using them for IQ imbalance problem will be addressed, there is no need to demonstrate the employment of these algorithms further. The result of implementing these algorithms as in [63–66, 71] is achieving up to 10 dB of enhancement of the existing SIC schemes.

2.5 Full-Duplex for Multi-Antenna Systems

2.5.1 Problems and Techniques

In MIMO, one may set forth the following argument: The full-duplex can double the capacity, but also two or more antenna (half-duplex MIMO) can do the same without all these challenges of full-duplex. This would be true at first glance, and therefore, full-duplex MIMO may use one shared antenna for each Tx-Rx pair with a circulator, as shown in Fig. 2.16, in order to strengthen its viability. However, when multiple circulators are in place, a severe interference among the multiple shared antennas would occur, creating a bottleneck with respect to achieving full-duplex system feasibility [74]. Furthermore, multiple separate antennas have an advantage of exploiting the degree of freedom (DoF) in the spatial domain. As more powerful SIC schemes are required to make full-duplex MIMO systems feasible, the increased degree of freedom is

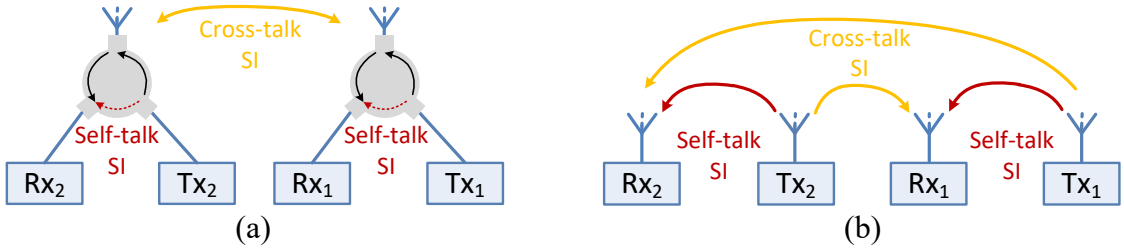

Figure 2.16: Self-interference in MIMO 2x2 (a) Shared antenna (b) Separate antenna

expected to provide an FD MIMO system with new solutions for SIC. However so far, convincing and practical designs of a full-duplex MIMO system, which can transmit and receive from all antennas simultaneously with sufficient SIC, are yet to be achieved. Hence, this section only addresses some of the proposed solutions.

Antenna techniques

Antenna conditional placement As shown before, this technique uses multi antennas to deconstruct the transmitted SI signal. The same technique can be extended to the MIMO case as in MIDU solution [41, 44]. MIDU performs a primary SIC in the propagation domain by employing antenna cancellation with symmetric placement of transmitting and receiving antennas as Fig. 2.17(a) depicts [44]. The achieved isolation is about 45 dB in open-space indoor; however, it has limited performance (only 15 dB) in indoor multipath environments since this solution can only mitigate the LoS SI component. The performance may be enhanced by using cross-polarization as in Fig. 2.17(b). In general, like in SISO, such techniques can be implemented only for narrowband systems, and they face major challenge regarding feasibility and scalability, not to mention the increasing cost of using $4N$ antenna to build N antennas MIMO system.

Directional isolation In the case of FD relaying, where the receiving and transmitting directions are generally separated from each other, it is possible to use MIMO to enhance the isolation.

Cancellation in analog domain

The same principle of analog SIC in SISO case is used in [61, 75] for MIMO case; tapping the SI signals from N_T transmitters with N_R copies from each one and then adjusting each SIC signal in order to match the SI channel between every Tx-Rx pair ($N_T \times N_R$ pair). The

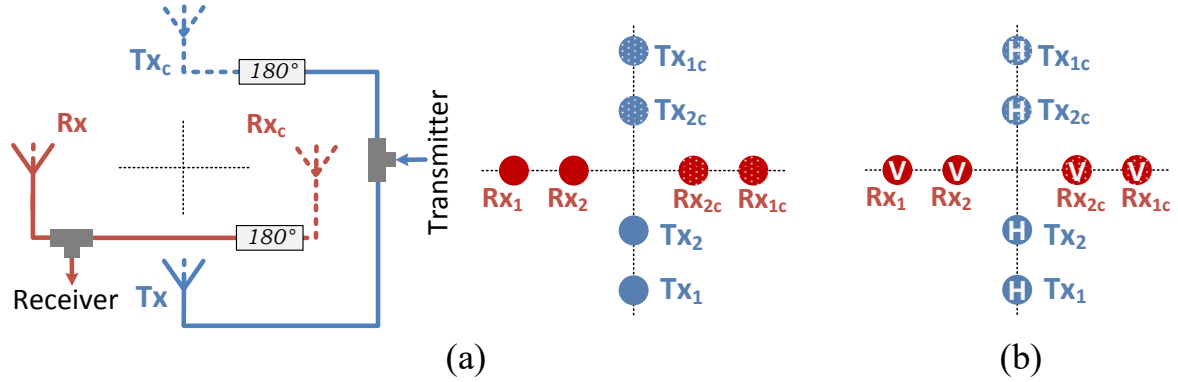

Figure 2.17: SIC in MIMO by antenna symmetric placemen (a) Multi cancellation level (b) Enhance with polarization

adjustment can be made by variable attenuators and phase shifters, or frequency-selective filters. In case 2×2 MIMO, the practical implementation may seem achievable with 4 SI channels; however, increasing the number of antennas will make this solution unpractical and expensive to implement.

Cancellation in digital domain

Earlier literature of digital SIC in MIMO focused on FD relaying applications as the case of relay has the advantage of antenna directional isolation that can be combined with digital beamforming. This combination can achieve considerable SIC value in case of decode-and-forward relays as in [76–81]. Later literature like [75, 82–84] analyzes bidirectional full-duplex system with digital schemes that depend on beamforming and phase rotation [85] to avoid SI, meanwhile [86] shows the first mature 3×3 MIMO full-duplex system that cancels the both components of SI signals (self-talk and cross-talk) almost to the noise floor. The proposed technique in [86] assumes that the co-located MIMO antennas share a similar environment since they share the same reflectors in this environment, and the distances to these reflectors are almost the same from the closely-spaced antennas. Thus, it can be assumed that for a specific transmit antenna, the cross-talk signals from other transmit antennas are similar to the self-talk signal with additional delays. Further, cross-talk across chains is naturally reduced compared to the chain's own self-talk because of physical antenna separation. Such simplifying assumption means that cross-talk and self-talk transfer functions can be expressed as a function of each other, with a modifying factor to account for the antenna separation. This allows modeling the system as a cascade of

transfer functions. Let $H_i(f)$ and $H_{ct}(f)$ be the transfer functions of the chain's own self-talk and cross-talk respectively. The overall relationship between these functions can be modeled as follows:

$$H_{ct}(f) = H_c(f)H_i(f) \tag{2.14}$$

where $H_c(f)$ is the cascade transfer function.

The critical observation is that $H_c(f)$ which cascaded with $H_i(f)$ results in the cross-talk transfer function, is a simple delay function. Further details about this work can be found in [86]. More analyses and experiments have to be conducted in order to verify the effect of such simplifying assumptions in different environments and systems.

Cancellation with auxiliary transmitter

Scaling this technique up toward MIMO implies that the number of auxiliary transmitter chains is equal to the number of receiving antennas N_R. In [47] a 2×1 MIMO OFDM system is modeled and analyzed as Fig. 2.18 shows. For each receiver chain, the previous SISO SIC technique is used, with SI channel estimation and pre-distortion the signal digitally. For the ordinary transmitter m, the pre-distortion factor $b_{i,m,n}$ is applied on the SI samples that leaks to the receiver antenna n based on the following equation [47]

$$b_{i,m,n}[k] = \frac{\hat{h}_{i,m,n}[k]}{\hat{h}^W_{i,n}[k]} \tag{2.15}$$

where i and k respectively are time and carrier indices of the time-frequency variable factor b. $h_{i,n}$ is the radio channel between the auxiliary transmitter n and receiver antenna n, meanwhile $h_{i,m,n}$ is the SI radio channel between the transmitter m and receiver antenna n.

Challenges and Limitations

Generally, in addition to scalability, all analog and digital SIC techniques still need further research and face many challenges in MIMO full-duplex systems:

- The length of the pilot, which is used for the estimation of SI channels, is proportional to the number of antennas. Thus, the estimation accuracy is limited by coherence time and correlation of the noise for long pilot sequences.
- The effects of hardware impairment, which were explained before in the SISO case, need

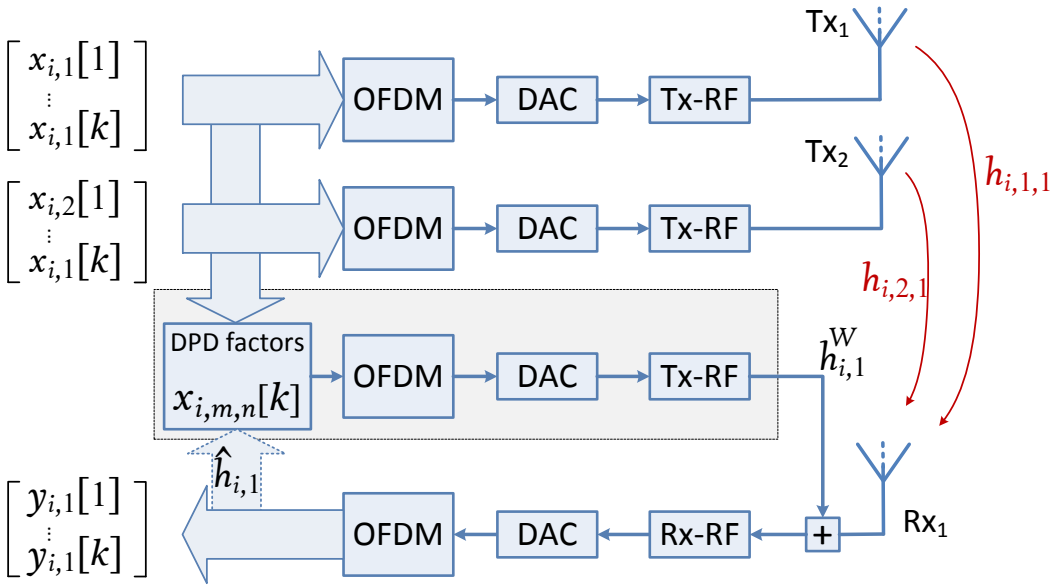

Figure 2.18: Block diagram of full-duplex MIMO 2x1 OFDM node using auxiliary Tx SIC

to be analyzed and calibrated for MIMO. Apart from simplified models like in [61], this is yet to be achieved. Nevertheless, anticipations regarding this issue indicate that the complexity of impairment calibration in the FD system may create a serious challenge as well.

- Cost efficiency and feasibility compared to half-duplex MIMO systems rates.

2.5.2 Conclusion

As shown earlier, in the case of multi-antenna systems, the main challenges are the scalability and the vulnerability of the SIC solution. Some works have been done with auxiliary chains as in [47, 87], or with complicated antennas conditional placement for narrowband systems [44], whereas the authors in [88, 89] are proposing a decoupling network as a SIC technique in the multi-antenna system. In all these works, the number of antennas is still limited to 2x2 due to the complexity of the proposed methods. Recently, beamforming with massive MIMO is considered in many papers like [25, 90, 91]. However, the massive MIMO will be confined to its cost, and therefore many recent works investigate low RF-complexity massive MIMO where many antennas, or known as a sub-array massive MIMO, where one transceiver and antenna/sub-array is selected.

As a conclusion, extending the traditional approaches of SIC for MIMO systems is not practical. Thus, different approaches for FD multi-antenna systems are proposed in this thesis. The proposed schemes avoid the high sensitivity to hardware impairment, as shown later. But before, let us present one detailed example case in which the impact of IQ imbalance impairment in an FD transceiver is minimized.

Chapter 3

Hardware Impairment Complication: IQ Imbalance for Example

In this chapter, the performance of a full-duplex transceiver is investigated in the presence of hardware impairment. The transceiver uses an additional transmit chain in order to create the self-interference cancellation signal. This approach is the traditional methodology for realizing FD. Both transmitters, and also the receiver, are impaired by frequency-dependent/independent IQ imbalance with different parameters. It is demonstrated that IQ imbalance deteriorates the achievable self-interference suppression level. After that, the calibration is performed with three different types of pre-equalization units to compensate for this deterioration. For simplicity in this work, the phase noise, generated in the local oscillator (LO), and other hardware imperfections are omitted to focus on the impact of IQ imbalance.

The chapter is organized as follows: The next section introduces the IQ imbalance problem and its impact on an FD transceiver. Then, the structure and the equivalent baseband model of an FD transceiver are shown with an active self-interference mechanism, which is impaired by IQ imbalance. After that, the advanced pre-equalization units, which can handle the IQ impairment, are proposed. Two approaches for IQ imbalance calibration are investigated, the replication and the compensation methods. Also, the pilot signal structure and the parameter estimation procedure are defined. Afterward, the simulation results and the conclusion are presented.

This chapter is based on our published book chapter [23] and the conference paper in cooperation with Fraunhofer HHI institute [57].

3.1 Introduction

The active cancellation mechanism requires an additional transmission chain, which is used to generate the SIC signal. Regardless of how accurately the transmission chains are manufactured, the original chain and the auxiliary one will not be identical. In fact, they are affected by the hardware impairments distinctly. One of these impairments is the IQ imbalance. IQ imbalance means asymmetric amplitude and phase between In-phase and Quadrature branch in the analog front-end. This is mainly due to the finite tolerances of electrical elements (resistors and capacitors) of the circuits. Two main effects of this problem are mirror-frequency interference and huge degradation of baseband pre-linearization of the power amplifier. The mismatch of the I and Q chains parameters causes imprecise SI signal generation, which leads to poor SIC performance.

Impairments Impact on Full-Duplex Transceiver

Essentially, the active cancellation mechanism relies on the precision of the SIC signal. Higher precision of the SIC signal can assure a significant improvement in SIC performance.

IQ imbalance is caused by the gain and phase mismatches between I- and Q-branches of the transmitter and receiver chains. This imbalance results in the complex conjugate of the ideal signal being added up on top of it with certain attenuation [27]. Thus, the output of an imperfect IQ mixer is a transformation of an input signal $x(t)$ where both direct and conjugated signals are filtered and then summed together [60]. This is typically called widely-linear transformation [92,93], and hence the IQ imbalance can be modeled as widely linear filters like in [60]. The output can be expressed as:

$$x_{IQ}(t) = g_1(t) * x(t) + g_2(t) * x^*(t) \tag{3.1}$$

where $g_1(t)$ and $g_2(t)$ are the responses for the direct and image components respectively [94].

The quality of the IQ mixer can be quantified with image rejection ratio (IRR), which can be defined as: $IRR(f) = 10\log_{10}(\frac{|G_1(f)|^2}{|G_2(f)|^2})$.

Taking LTE advanced system for example, 3GPP specifications limit the minimum attenuation for the in-band image component in the user equipment transmitters to 25 or 28 dB [95]. Such image attenuation is sufficient in the transmission path, but when considering the full-duplex device self-interference problem, the IQ image of the SI signal forms an additional interference

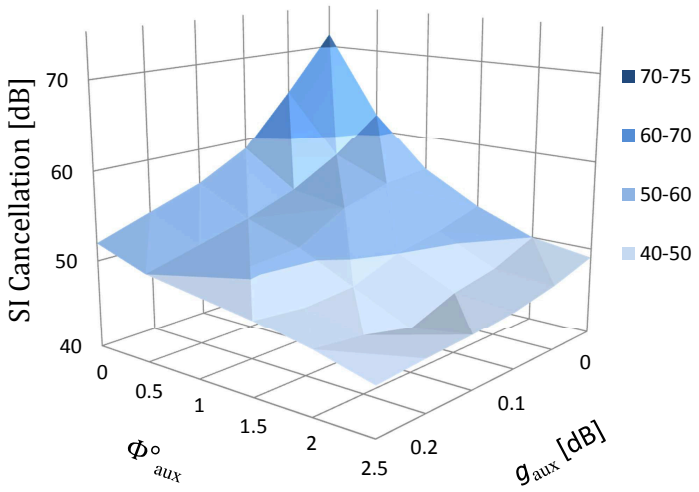

Figure 3.1: Self-interference suppression performance in the presence of IQ imbalance

that leaks into the receiver [60]. The performance of full-duplex transceivers in the presence of IQ imbalance is studied in detail in [57, 60, 82, 96]. They demonstrate that, with a practical IQ image rejection ratio for a full-duplex transceiver, it is necessary to mitigate the IQ image of the SI signal. Otherwise the loss of SSINR might be in the order of tens of decibel [27] which negates the benefit of using full-duplex. Fig. 3.1 shows the SIC performance in case of different gain and phase mismatch values in the auxiliary chain [57]. Taking, for example, practical values for gain mismatch $g < 0.05$ and phase error $\phi < 1^{\circ}$, the self-interference cancellation is 53 dB, and this means about 20 dB degradation of SIC performance from the best achieved cancellation. Therefore, the effect of IQ imbalance must be included in the design of baseband cancellation signal [57, 96].

3.2 Full-Duplex System Model with IQ Imbalance

The IQ imbalance can be calibrated by adjusting the cancellation signal in order to match the SI signal. This can be achieved by replicating the imbalance of the ordinary transmitter and correct the imbalance of the auxiliary transmitter. Considering the direct and quadrature signals are:

$$I(t) = \cos(wt), \qquad Q(t) = \sin(wt), \tag{3.2}$$

Table 3.1: The definitions of the FD IQ imbalance model

$h_{ord,I}(t)$, $h_{ord,Q}(t)$	The impulse response of the baseband filters in the ordinary transmitter at I- and Q- arm respectively
$h_{SI}(t)$	The equivalent baseband response of self-interference channel
$h_{aux,I}(t)$, $h_{aux,Q}(t)$	The impulse response of the baseband filters in the auxiliary transmitter at I- and Q- arm respectively
$h_{SIC}(t)$	The equivalent baseband channel between the up-converting quadrature frontend mixer at the auxiliary chain and the directional coupler at the receiver
$h_{rx,I}(t)$, $h_{rx,Q}(t)$	The impulse response of the LPF baseband filers at I- and Q- arm
g, ϕ	The gain and phase mismatch of the IQ imbalance for each chain (Ideally: $\phi_{ord} = \phi_{aux} = \phi_{rx} = 0$ and $g_{ord} = g_{aux} = g_{rx} = 1$)

and after IQ imbalance with gain g and phase error ϕ

$$\acute{I}(t) = \cos(wt), \qquad \acute{Q}(t) = g\sin(wt - \phi), \tag{3.3}$$

the above equations can be expressed in matrices:

$$\begin{bmatrix} \acute{I}(t) \\ \acute{Q}(t) \end{bmatrix} = \begin{bmatrix} 1 & 0 \\ -g\sin(\phi) & g\cos(\phi) \end{bmatrix} \begin{bmatrix} I(t) \\ Q(t) \end{bmatrix} \Rightarrow \begin{bmatrix} \acute{I}(t) \\ \acute{Q}(t) \end{bmatrix} = \begin{bmatrix} 1 & 0 \\ r_\beta & r_\alpha \end{bmatrix} \begin{bmatrix} I(t) \\ Q(t) \end{bmatrix}, \tag{3.4}$$

where r_α and r_β are the replication parameters. These parameters can be used to replicate the IQ imbalance of the ordinary transmitter in the SIC signal. The correction parameters c_α and c_β can be extracted by inversion:

$$\begin{bmatrix} I_c(t) \\ Q_c(t) \end{bmatrix} = \begin{bmatrix} 1 & 0 \\ \tan(\phi) & (g\cos(\phi))^{-1} \end{bmatrix} \begin{bmatrix} \acute{I}(t) \\ \acute{Q}(t) \end{bmatrix} \Rightarrow \begin{bmatrix} I_c(t) \\ Q_c(t) \end{bmatrix} = \begin{bmatrix} 1 & 0 \\ c_\beta & c_\alpha \end{bmatrix} \begin{bmatrix} \acute{I}(t) \\ \acute{Q}(t) \end{bmatrix}. \tag{3.5}$$

The parameters c_α and c_β can be used to correct the IQ imbalance of the auxiliary transmitter in the SIC signal.

Before explaining further the proposed calibration algorithms, let us check in Fig. 3.2 and Fig. 3.3 the structure and the equivalent baseband model of the FD transceiver in the presence of IQ imbalance in the three chains [57] (ignoring, for now, the calibration units, PEU and PAU, in both figures). The direct down converter structure of the quadrature modulator is modelled as in [97].

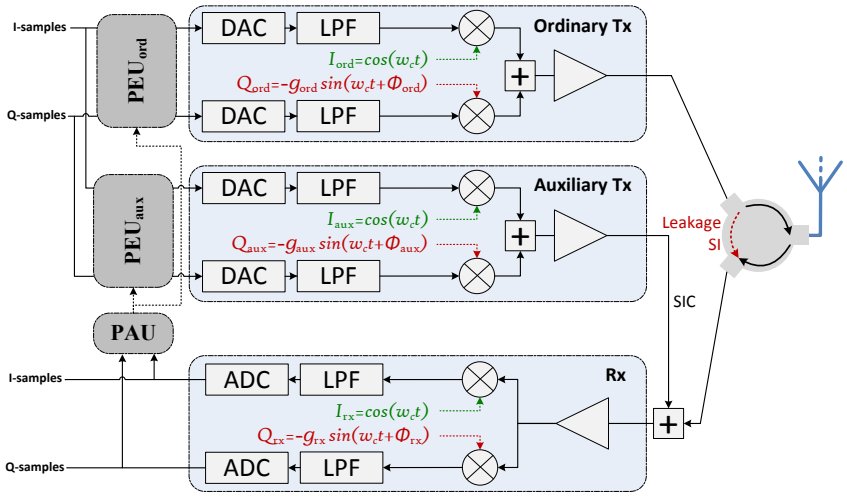

Figure 3.2: Structure of an FD transceiver with IQ imbalance

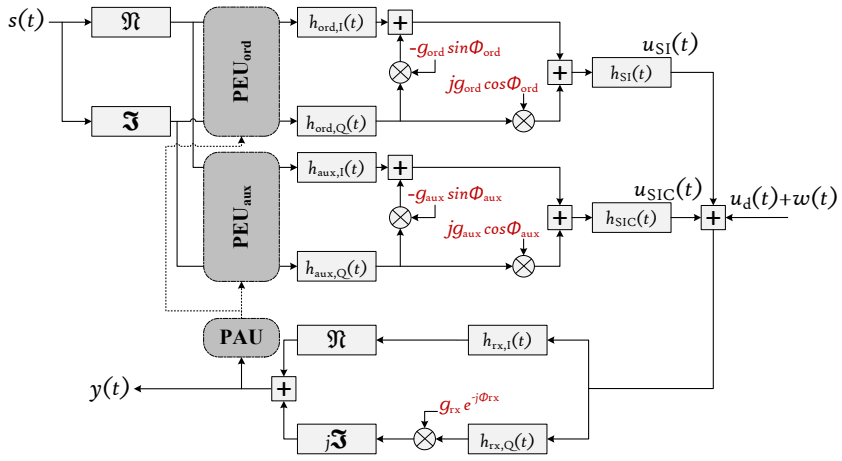

Figure 3.3: The equivalent baseband model of an FD transceiver with IQ imbalance. The model incorporates IQ imbalances in their equivalent baseband models

The equivalent baseband model of the RF self-interference signal is

$$u_{SI}(t) = \mathcal{R}e\{s(t)\} * h_{ord,I}(t) * h_{SI}(t) + g_{ord}(\jmath \cos\phi_{ord} - \sin\phi_{ord})\mathcal{I}m\{s(t)\} * h_{ord,Q}(t) * h_{SI}(t). \quad (3.6)$$

Similarly, the equivalent baseband model of the RF SIC signal is

$$u_{SIC}(t) = \mathcal{R}e\{s(t)\} * h_{aux,I}(t) * h_{SIC}(t) + g_{aux}(\jmath \cos\phi_{aux} - \sin\phi_{aux})\mathcal{I}m\{s(t)\} * h_{aux,Q}(t) * h_{SIC}(t). \quad (3.7)$$

3.3 Advanced Pre-Equalization Units

Ideally, the self-interference signal $u_{SI}(t)$ and the self-interference cancellation signal $u_{SIC}(t)$ have to be exactly identical in order to achieve perfect cancellation. However, in practice, the basic model of linear pre-equalization for SIC with an auxiliary transmitter $G_{\mathrm{L}}(f) = \frac{H_{\mathrm{ord,I}}(f)H_{\mathrm{SI}}(f)}{H_{\mathrm{aux,I}}(f)H_{\mathrm{SIC}}(f)}$ [33] is not considering the IQ imbalance in the full-duplex transceiver. This model assumes a perfect match between the I- and Q-arm in all transceiver chains, i.e., $h_{\mathrm{ord,I}}(t) = h_{\mathrm{ord,Q}}(t)$, $h_{\mathrm{aux,I}}(t) = h_{\mathrm{aux,Q}}(t)$ and $h_{\mathrm{rx,I}}(t) = h_{\mathrm{rx,Q}}(t)$. Moreover, this model expects that the LO signals are perfectly rotated by $90°$ and have the same amplitude, so $\phi_{\mathrm{ord}} = \phi_{\mathrm{aux}} = \phi_{\mathrm{rx}} = 0$ and $g_{\mathrm{ord}} = g_{\mathrm{aux}} = g_{\mathrm{rx}} = 1$. However, with practical transceivers where the IQ imbalance is unavoidable, the linear model has a poor performance. The channel estimations are corrupted by the IQ mismatch, ergo, the estimated pre-equalization function $\tilde{G}_{\mathrm{L}}(f) = \frac{\tilde{H}_{\mathrm{ord,I}}(f)\tilde{H}_{\mathrm{SI}}(f)}{\tilde{H}_{\mathrm{aux,I}}(f)\tilde{H}_{\mathrm{SIC}}(f)} + \epsilon$ is deviated from its ideal value.

Adding the following units aims to estimate then calibrate IQ imbalance of SIC signal to match the SI signal:

- $[PAU]$ Parameter Acquisition Unit
- $[PEU_{ord}]$ Ordinary Pre-Equalization Unit
- $[PEU_{aux}]$ Auxiliary Pre-Equalization Unit

Two algorithms for calibration are proposed: Replicator unit method, and distributed compensation units method.

3.3.1 Replicator unit method

In this case, the PEU_{ord} will not be used; meanwhile, the PEU_{aux} will perform the two required functions on SIC signal; the first is to replicate the IQ imbalance of the ordinary transmitter, and the second is to correct the IQ imbalance of the auxiliary transmitter. This can be done by sending a pilot signal in order to estimate the parameters g_{ord}, ϕ_{ord}, g_{aux} and ϕ_{aux} by the PAU in the receiver, and then feed it back to the PEU_{aux}. Knowing these four parameters enables the PEU_{aux} to calculate the replication values $r_{ord,\alpha}$, $r_{ord,\beta}$ and the correction parameters $c_{aux,\alpha}$, and $c_{aux,\beta}$ as explained previously.

Frequency-independent IQ imbalance replicator

Fig. 3.4 (a) shows the structure of frequency-independent IQ imbalance (FIIQ) replicator which is loaded into the pre-equalization unit $\mathrm{PEU_{aux}}$. The FIIQ replicator is an advanced linear model able to cope with the IQ imbalance in its frequency-independent model at both transmission chains. It is clear that the FIIQ replicator structure contains three main parts to match the three required tasks. The first part is used to replicate the IQ mismatch of the ordinary transmitter using the multipliers $r_{\mathrm{ord},\alpha}$ and $r_{\mathrm{ord},\beta}$. The middle part $g(t)$ contains the SI and the SIC channels, i.e., it is the basic linear model. The last part is to compensate the auxiliary chain frequency-independent IQ imbalance using the multipliers $c_{\mathrm{aux},\alpha}$ and $c_{\mathrm{aux},\beta}$.

The frequency domain representation of the FIIQ replicator parameters are given by

$$G(f) = -\frac{H_{\mathrm{ord,I}}(f)H_{\mathrm{SI}}(f)}{H_{\mathrm{aux,I}}(f)H_{\mathrm{SIC}}(f)}, \tag{3.8a}$$

$$r_{\mathrm{ord},\alpha} = \jmath g_{\mathrm{ord}} \cos\phi_{\mathrm{ord}}, \tag{3.8b}$$

$$c_{\mathrm{aux},\alpha} = \frac{1}{g_{\mathrm{aux}} \cos\phi_{\mathrm{aux}}}, \tag{3.8c}$$

$$r_{\mathrm{ord},\beta} = -g_{\mathrm{ord}} \sin\phi_{\mathrm{ord}}, \tag{3.8d}$$

$$c_{\mathrm{aux},\beta} = \tan\phi_{\mathrm{aux}}. \tag{3.8e}$$

Note that $g(t) = \mathcal{F}^{-1}\{G(f)\}$ is a Finite Impulse Response (FIR) filter with time domain complex coefficients and the rest of the FIIQ parameters are scalar multipliers.

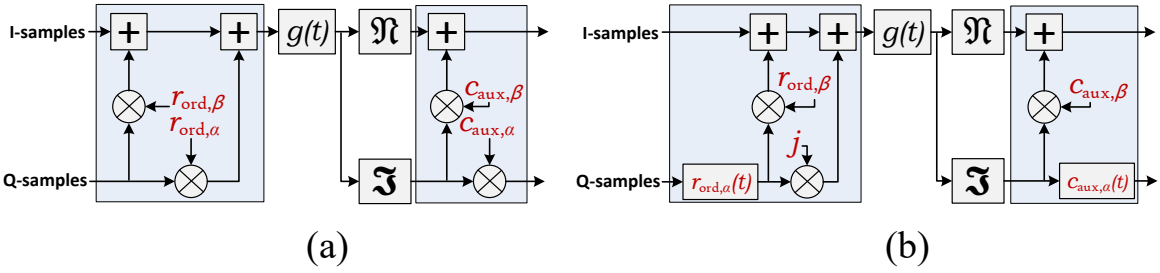

Figure 3.4: Structure of IQ imbalance replicator (a) Frequency independent (b) Frequency Selective

Frequency-selective IQ imbalance replicator

Fig. 3.4 (b) shows the structure of the frequency-selective IQ imbalance (FSIQ) replicator. Taking into account the frequency-selective behavior of the IQ imbalance allows a better estimation of the self-interference and self-interference cancellation radio channels by mitigating the influence of IQ mismatch on the estimation procedure. In fact, the IQ imbalance parameters are also estimated and integrated into the FSIQ replicator structure. The FSIQ replicator is designed to compensate for the IQ imbalance, which occurs at the auxiliary chain, and to replicate the IQ imbalance of the ordinary chain. By that, the FSIQ replicator prepares an RF self-interference cancellation signal that matches the RF self-interference signal, for which the multipath self-interference radio channel and the IQ imbalance in the both models, the frequency-independent and frequency-selective one, are considered. Similar to the FIIQ case, the FSIQ replicator occupies the $\mathrm{PEU}_{\mathrm{aux}}$, whereas the $\mathrm{PEU}_{\mathrm{ord}}$ is kept empty unoccupied for different purposes.

The FSIQ replicator parameters, in their frequency domain representation, can be expressed as

$$G(f) = -\frac{H_{\mathrm{ord,I}}(f)H_{\mathrm{SI}}(f)}{H_{\mathrm{aux,I}}(f)H_{\mathrm{SIC}}(f)}, \tag{3.9a}$$

$$R_{\mathrm{ord},\alpha}(f) = \frac{H_{\mathrm{ord,Q}}(f)}{H_{\mathrm{ord,I}}(f)} g_{\mathrm{ord}} \cos\phi_{\mathrm{ord}}, \tag{3.9b}$$

$$C_{\mathrm{aux},\alpha}(f) = \frac{H_{\mathrm{aux,I}}(f)}{H_{\mathrm{aux,Q}}(f) g_{\mathrm{aux}} \cos\phi_{\mathrm{aux}}}, \tag{3.9c}$$

$$\hat{r}_{\mathrm{ord},\beta} = -\tan\phi_{\mathrm{ord}}, \tag{3.9d}$$

$$c_{\mathrm{aux},\beta} = \tan\phi_{\mathrm{aux}}. \tag{3.9e}$$

where:

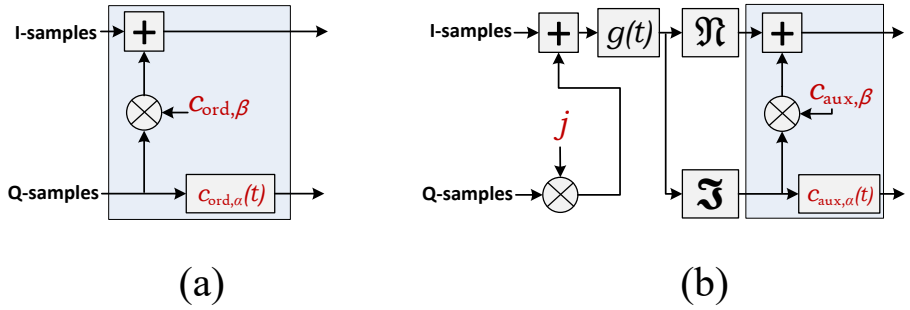

(a) (b)

Figure 3.5: IQ imbalance compensation units (a) in the ordinary Tx (b) in the auxiliary Tx

- $g(t) = \mathcal{F}^{-1}\{G(f)\}$ is a FIR filter with time domain complex coefficients,
- $r_{\mathrm{ord},\alpha}(t) = \mathcal{F}^{-1}\{R_{\mathrm{ord},\alpha}(f)\}$ and $c_{\mathrm{aux},\alpha}(t) = \mathcal{F}^{-1}\{C_{\mathrm{aux},\alpha}(f)\}$ are FIR filters with time domain real coefficients,
- The rest of the FSIQ parameters $\hat{r}_{\mathrm{ord},\beta}$ and $c_{\mathrm{aux},\beta}$ are scaler multipliers.

3.3.2 Distributed compensation units method

In distributed compensation, each PEU corrects the IQ imbalance of its own branch as Fig. 3.5 shows. As long as the IQ imbalance at the ordinary chain is completely compensated, there is no need to replicate its behavior at the auxiliary chain anymore. Regardless of full-duplex application, the main advantage of the distributed model is the fact that IQ imbalance of the ordinary transmission signal is digitally corrected, which is desirable for the remote reception node.

The same parameters which are used in the FSIQ replicator, set of parameters (3.9), are used for the distributed model except of (3.9d) and (3.9b); these parameters are replaced by $c_{\mathrm{ord},\beta} = \tan\phi_{\mathrm{ord}}$ and $C_{\mathrm{ord},\alpha}(f) = \frac{H_{\mathrm{ord,I}}(f)}{H_{\mathrm{ord,Q}}(f) g_{\mathrm{ord}} \cos\phi_{\mathrm{ord}}}$, respectively.

The distributive property of this model might be considered as disadvantage in some practical implementations where the access to the digital domain of the ordinary chain is not recommended or probably not possible [57].

3.3.3 Self-Interference Channel and IQ imbalance parameter estimation

Pilot signal structure and parameters

An OFDM signal is used as a pilot to estimate the parameters. Both DC and edge subcarriers are null [98]; meanwhile, the pilot subcarriers consist of a modified Frank-Zadoff-Chu sequence [99]. In the time domain, the pilot consists of two segments, as shown in Fig. 3.6d, with the following configuration. As in Fig. 3.6d, the first segment has a conjugate symmetric (CS) property in the frequency domain , i.e., $S_{\mathrm{p,cs}}(f) = S^{*}_{\mathrm{p,cs}}(-f)$ [100]. The inverse Fourier transform of this CS spectrum is a pure real signal in the time domain. The second segment has a conjugate anti-symmetric (CA) property in its frequency representation, i.e., $S_{\mathrm{p,ca}}(f) = -S^{*}_{\mathrm{p,ca}}(-f)$ [100], see Fig. 3.6c. The time domain signal of the second segment is a pure imaginary signal.

Then, the continuous frequency domain mathematical representation of the pilot signal segments is

$$S_{\mathrm{p,cs}}(f) = \mathcal{R}e\left\{S_{\mathrm{p}}(f)\right\} - \jmath\ \mathrm{sgn}(f)\mathcal{I}m\left\{S_{\mathrm{p}}(f)\right\}, \tag{3.10a}$$

$$S_{\mathrm{p,ca}}(f) = \jmath S_{\mathrm{p,cs}}(f), \tag{3.10b}$$

where $S_{\mathrm{p}}(f)$ is the spectrum of the FZC sequence, as in Fig. 3.6a.

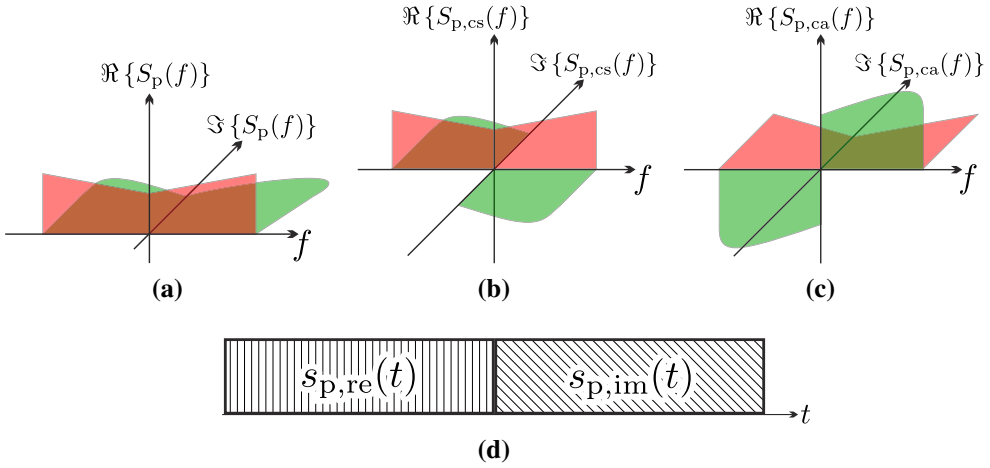

Figure 3.6: Pilot signal structure; (a) Unmodified FZC sequence (b) Pilot signal first segment spectrum, (c) Pilot signal second segment spectrum, (d) Time domain representation of the pilot signal.

The proposed structure for the pilot aims to improve the channel estimation by mitigating the influence of the IQ mismatches. It further allows estimating the IQ imbalance out of the two

segments of the pilot signal. The parameters of the pilot signal are summarized in Table 3.2.

Table 3.2: The OFDM pilot signal parameters

Parameter	Value and Unit
Number of subcarriers	512
Number of null subcarriers	96
Number of active subcarriers	416
Number of repetitions	10 times
Cyclic prefix (CP) length	16 samples

Estimation procedure

The pilot signal is sent consecutively through the ordinary and auxiliary chains to the own receiver. The parameter acquisition unit (PAU) estimates the required parameters based on the implemented model of pre-equalization. Within the estimation phase, perfect synchronization is assumed. It is a rational assumption due to the proximity between Tx and Rx, which is resulting in high SNR of the received pilot signal. The perfect timing property allows us to split the estimated pilot into two consecutive segments precisely. The estimated frequency responses of the ordinary chain are given by:

$$Y_{\mathrm{ord},\alpha}(f) = S_{\mathrm{p,cs}}(f) H_{\mathrm{ord,I}}(f) H_{\mathrm{SI}}(f) H_{\mathrm{rx,I}}(f), \tag{3.11a}$$

$$Y_{\mathrm{ord},\beta}(f) = g_{\mathrm{ord}} \left(\jmath \cos\phi_{\mathrm{ord}} - \sin\phi_{\mathrm{ord}}\right) S_{\mathrm{p,ca}}(f) H_{\mathrm{ord,Q}}(f) H_{\mathrm{SI}}(f) H_{\mathrm{rx,I}}(f). \tag{3.11b}$$

The estimated frequency responses of the auxiliary chain are given by:

$$Y_{\mathrm{aux},\alpha}(f) = S_{\mathrm{p,cs}}(f) H_{\mathrm{aux,I}}(f) H_{\mathrm{SIC}}(f) H_{\mathrm{rx,I}}(f), \tag{3.12a}$$

$$Y_{\mathrm{aux},\beta}(f) = g_{\mathrm{aux}} \left(\jmath \cos\phi_{\mathrm{aux}} - \sin\phi_{\mathrm{aux}}\right) S_{\mathrm{p,ca}}(f) H_{\mathrm{aux,Q}}(f) H_{\mathrm{SIC}}(f) H_{\mathrm{rx,I}}(f). \tag{3.12b}$$

The receiver chain is assumed to be ideal and does not suffer from any IQ mismatch, i.e., $h_{\mathrm{rx,I}}(t) = h_{\mathrm{rx,Q}}(t)$, $g_{\mathrm{rx}} = 1$ and $\phi_{\mathrm{rx}} = 0$. Such assumption is practically applicable by means of digital-down-converter [101] with higher sampling rate of the receiver's ADC.

Using 3.11 and 3.12 with the perfect knowledge of the pilot baseband 3.10, four estimated

frequency responses can be found to be given by:

$$H_{\mathrm{ord},\alpha}(f) = \frac{Y_{\mathrm{ord},\alpha}(f)}{S_{\mathrm{p,cs}}(f)}, \quad H_{\mathrm{ord},\beta}(f) = \frac{Y_{\mathrm{ord},\beta}(f)}{S_{\mathrm{p,ca}}(f)},$$
$$H_{\mathrm{aux},\alpha}(f) = \frac{Y_{\mathrm{aux},\alpha}(f)}{S_{\mathrm{p,cs}}(f)}, \quad H_{\mathrm{aux},\beta}(f) = \frac{Y_{\mathrm{aux},\beta}(f)}{S_{\mathrm{p,ca}}(f)}.$$

These estimated responses are employed to calculate the PEU parameters. The first parameter, which is broadly used in each PEU, can be computed as follows

$$G(f) = -\frac{H_{\mathrm{ord},\alpha}(f)}{H_{\mathrm{ord},\beta}(f)}. \tag{3.13}$$

The CS frequency responses are similarly computed from the estimated responses to be given by

$$C_{\mathrm{ord},\alpha}(f) = \frac{1}{R_{\mathrm{ord},\alpha}(f)} = \frac{H_{\mathrm{ord},\beta}(f)}{H_{\mathrm{ord},\alpha}(f)} + \frac{H^*_{\mathrm{ord},\beta}(-f)}{H^*_{\mathrm{ord},\alpha}(-f)}, \tag{3.14}$$

$$C_{\mathrm{aux},\alpha}(f) = \frac{H_{\mathrm{aux},\beta}(f)}{H_{\mathrm{aux},\alpha}(f)} + \frac{H^*_{\mathrm{aux},\beta}(-f)}{H^*_{\mathrm{aux},\alpha}(-f)}. \tag{3.15}$$

The phase mismatchs of the ordinary and auxiliary chain are calculated by averaging over the frequency to be given by

$$\phi_{\mathrm{ord}} = \arctan\left(-\frac{\jmath}{B}\int_{-B/2}^{+B/2} \frac{\frac{H_{\mathrm{ord},\beta}(f)}{H_{\mathrm{ord},\alpha}(f)} - \frac{H^*_{\mathrm{ord},\beta}(-f)}{H^*_{\mathrm{ord},\alpha}(-f)}}{\frac{H_{\mathrm{ord},\beta}(f)}{H_{\mathrm{ord},\alpha}(f)} + \frac{H^*_{\mathrm{ord},\beta}(-f)}{H^*_{\mathrm{ord},\alpha}(-f)}} \mathrm{d}f\right) \tag{3.16}$$

$$\phi_{\mathrm{aux}} = \arctan\left(-\frac{\jmath}{B}\int_{-B/2}^{+B/2} \frac{\frac{H_{\mathrm{aux},\beta}(f)}{H_{\mathrm{aux},\alpha}(f)} - \frac{H^*_{\mathrm{aux},\beta}(-f)}{H^*_{\mathrm{aux},\alpha}(-f)}}{\frac{H_{\mathrm{aux},\beta}(f)}{H_{\mathrm{aux},\alpha}(f)} + \frac{H^*_{\mathrm{aux},\beta}(-f)}{H^*_{\mathrm{aux},\alpha}(-f)}} \mathrm{d}f\right) \tag{3.17}$$

where B is the bandwidth of the pilot signal.

In implementation, the coefficients of the FIR filter are calculated by taking the DFT of the pilot signal subcarriers with maximum length equal to the pilot signal CP.

3.4 Results

The behavior of the full-duplex transceiver has been simulated, and the PEU models have been tested under realistic system behavior. The LO parameters concerning the frequency-independent

IQ imbalance are included in Table 3.3. The frequency-selective IQ mismatches are simulated as 9-order FIR filters.

Table 3.3: FIIQ imbalance simulation parameters

	Ordinary	**Auxiliary**	**Receiving**
Gain mismatch g	0.7485 /dB	0.5877 /dB	0.2996 /dB
Phase mismatch ϕ	5.5°	2.7°	2°

Fig. 3.1 shows the gain and phase mismatches versus the achieved amount of self-interference suppression. The ordinary chain is kept ideally operating without any IQ imbalance, whereas the IQ imbalance in the auxiliary chain is gradually increased in order to report the results of the linear PEU under such conditions. The linear PEU is compared to the FIIQ replicator under IQ mismatch transceiver behavior in its frequency-independent model. The used parameters of IQ imbalance are listed in Table 3.3. The simulation includes two configurations, and their results are shown in Table 3.4. In the first configuration, an ideal receiving chain is assumed, while in the second configuration a receiving chain corrupted with IQ imbalance is simulated. The results show that the FIIQ replicator outperforms the linear PEU under frequency-independent IQ imbalance transceiver behavior. The receiver IQ imbalance disturbs the estimation phase and consequently decreases the accuracy of the estimated parameters. Hence, the FIIQ replicator has a better performance when the Rx IQ is disabled.

Table 3.4: The achieved self-interference suppression under FIIQ imbalance behavior

	Rx-IQ disabled	**Rx-IQ enabled**
Linear	47.2 dB	47.1dB
FIIQ replicator	71.8 dB	61.6 dB

Lastly, the proposed PEUs models are simulated under FSIQ imbalance behavior. Two configurations are considered: with and without receiver IQ imbalance. The simulation results are shown in Table 3.5.

The results in the table show the significant deterioration in the FIIQ replicator performance when a frequency-selective model of IQ imbalance are used. The FIIQ replicator presents a relatively poor performance even with an ideal implementation of the receiving chain. The FSIQ replicator has approximately similar results to the distributed PAU. Both of the FSIQ replicator and the distributed PAU demonstrate the best performance in suppressing the self-interference even with a highly realistic model of the IQ imbalance, i.e., frequency-independent

Table 3.5: The achieved self-interference suppression under FSIQ imbalance behavior

	Rx-IQ disabled	**Rx-IQ enabled**
Linear	46.2 dB	45.7 dB
FIIQ replicator	51.3 dB	51.1 dB
FSIQ replicator	71 dB	56.6 dB
Distributed PEU	70.5 dB	57.3 dB

and frequency-selective. The IQ imbalance of the receiving chain has a considerable negative impact on these PAUs.

3.5 Conclusion

Different advanced pre-equalization schemes have been proposed in this work to calibrate the impact of IQ imbalance in FD transceivers. The proposed schemes show a better performance, i.e., a higher level of SIC, in comparison with the basic linear model. The FSIQ replicator and the distributed PEU show the best performance compared to the simpler FIIQ replicator. The FSIQ replicator and the distributed PEU are pretty similar with respect to their complexity and performance, but they are different in structure. For implementation purposes, the FSIQ replicator might be a good option without any additional modification in the ordinary chain.

This work focuses on the impact of IQ imbalance for full-duplex systems, while the impact of nonlinear distortions, as they are mainly stemming from the power amplifier, has been neglected. The importance of considering the nonlinearity in full-duplex systems has been investigated in [31], and first nonlinear digital self-interference cancellation techniques have been reported in [29, 33, 50, 51]. Nevertheless, this work shows the challenge of dealing with one hardware impairment in an FD transceiver. It is clear that including further imperfections to be calibrated will increase the complexity dramatically, not to mention the complication that results in the case of multi-antenna. Thus, the traditional approach of SIC, which depends on SI subtraction, has to be avoided for multi-antenna systems. In the next chapters, new approaches are presented for realizing the FD transmission in multi-antenna systems.

Chapter 4

Dual Polarized Reflect-Array in a Full-Duplex Base-Station

After showing, in the previous chapter, that the traditional approach of SIC, i.e., feedback with auxiliary chain, produces much complexity to soften its sensitivity to different hardware impairment; other approaches are proposed to employ multi-antenna techniques in favour of SIC. The first multi-antenna technique included in this thesis is reflect-arrays (RA). This chapter proposes the exploitation of reflect-arrays for spatial self-interference isolation, aiming to enable a base-station to operate in FD mode. An ultra-wideband (UWB) RA is designed to enable full-duplex transmission in an indoor/outdoor LTE base-station with HD users. Two cross-polarized beams are generated using two separate feeders to meet the SIC requirements of achieving high isolation between the downlink and the uplink signals. The self-interference components are analyzed to evaluates the direct and back-scattered SI paths in the designed RAs, and to estimate the amount of SI isolation that can be achieved in the wideband system. Instead of using theoretical channel models, the ray-tracing method is applied within realistic environments.

One may argue that the isolation can be done using two horn antennas instead of reflect-arrays; however, the later allow to do the beam-forming electronically, and this cannot be performed by horn antennas without an impractical mechanical system. Moreover, the reflect-arrays avoid any Tx-RX leakage on the electronic board of the base-station. On the contrary to array antennas, massive MIMO is not the potential candidate for 5G systems due to its design complexity and less adaptability with shorter wavelengths [102].

The work of this chapter was partially published in [103], which is the first work that proposed the use of RA in full-duplex mobile communication. Both reflect-array and full-duplex

technologies are strong candidates to be used in 5G [102].

4.1 Introduction

4.1.1 Reflect-Array Basics

"Reflect-array antenna" is a type of radiating structures that are consist of an array of radiating elements. These elements can reradiate the energy that is transmitted to them through free space from one or more feeders. Thus, reflect-array can be seen as a hybrid antenna system that has the desirable capabilities of the phased array antennas and the parabolic reflector antenna [104, 105]. These combined features are:

- wide beam scanning and forming abilities,
- multi-beam capability,
- spatial feeding,
- easy integration with RF circuitry,
- lightweight,
- and finally, low cost.

Fig. 4.1 depicts one reflect-array. RA consists of a free space located feeder that spatially illuminates a reflecting surface of radiating elements. Each element is called a cell. In principle, the adjustment of the geometrical properties of the array cells is performed to realize the desired aperture field distribution [106, 107]. In contrast to conventional phased arrays with, that use microstrips transmission lines and thus suffer from excessive loss at higher frequencies [108], reflect-arrays utilize the free space as a medium for the transmission of the electrical signal from the feeder to the cells, and subsequently, avoid any degradation in the gain performance as a result of loss in the feeding system [109].

The RA antenna beam may be steered either mechanically or electronically. The mechanical steering approaches suffer from low scan rate, high scan volume, low scan resolution, and high-cost [110]. Meanwhile, the electronic steering methods use variable lumped elements that are embedded in the array cells and controlled via analog biasing lines. Thus, electronically steering the beam is more efficient, faster without any need for moving parts, more robust, and more reliable. Most designs so far use lumped elements such as P-I-N and varactor diodes. Thus, the objective is to steer the beam utilizing the electronically controlled tuning devices. These

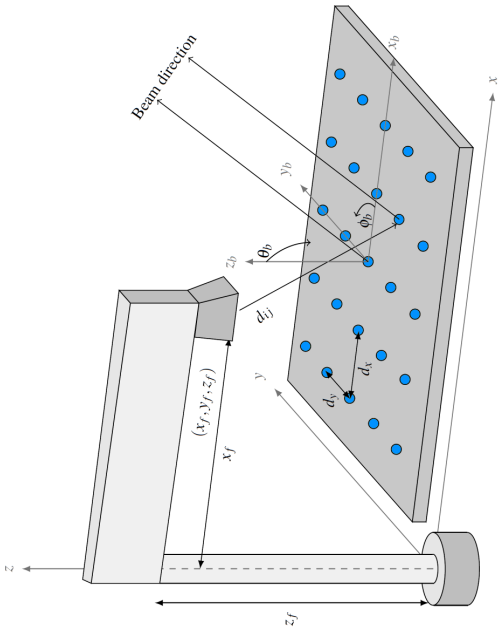

Figure 4.1: RA structure: The elements array and the feeder.

elements can be aperture coupled or directly connected to the RA cell. Although the aperture coupling configuration provides wide bandwidth because of the independent optimization to the tuning device, it suffers from design complexity [111]. The received wave by each cell is reradiated after being modulated by a certain reflection phase. Hence, the RA antenna is a phase-only synthesis problem, where the reradiation pattern is controlled by tuning the distribution of the reflection phase over the array surface. Thus, the reflecting surface can be designed and controlled to reradiate the electromagnetic wave in a single beam or multi-beams with the desired pattern and direction. Previously, RA was considered a narrow bandwidth antenna, and this well-known limitation was due to the narrowband nature of the microstrip patches and different spatial phase delays between the feed and each element of the reflect-array [112]. Recently, many works have been done to have better performance of RA in wide/UWB such as [106, 113–115]. The high gain performance can be obtained by increasing the size of the RA which can produce sharp beams; however, this would also increase the different spatial phase delays between the feed and each element of the reflect-array [116].

4.1.2 Reflect-Arrays for FD Transmission

As shown in Chapter 2, several SIC techniques have been presented in propagation domain to mitigate SI, for example: Antenna conditional placement [39, 45], Directional isolation

[46, 47], Absorptive/Reflective Shielding [40, 46], and Cross-polarization [46, 48]. In average, the mentioned techniques achieve only about 15 dB of isolation practically. In optima conditions, like a narrow band system in an anechoic chamber, the isolation may reach 70 dB.

Massive MIMO has been proposed for 5G system because of the compatibility with small cells [25, 90, 91]. However, Massive MIMO is complicated and less adaptable with shorter wavelengths [102]. On the other hand, RA is getting the attention again, because it is much simpler, more flexible, and considerably cheaper compared to Massive MIMO. This makes RA a strong candidate technology in some 5G scenarios [102].

The novelty of this work is that it proposes, for the first time in literature, the use of RA to perform SIC in the propagation domain for mobile communication. The UWB RA, which is designed in [113], is considered to enable FD in an indoor/outdoor base-station. The design is customized to meet the FD requirements, where two cross-polarized RAs with two feeders are used to generate the DL and UL beams, from and to HD users. This chapter also analyzes the components of SI in the direct and back-scattered paths and the amount of isolation which is achieved using reflect-arrays in a wideband system.

The rest of the chapter is organized as follows: In the next section, the RA antenna design is described, then the system model is presented. After that, the simulation setup is explained. Then, the results of the simulation are shown, and the advantages and disadvantages of the approach are discussed. Finally, the conclusion is presented at the end of the chapter.

4.2 Antenna Design

The low cross-polarization level between the two arrays is essential to isolate the UL and DL beams. Accordingly, an UWB orthogonal beams RA antenna is developed. One possible way is to use the double-ring structure a cell by making gaps across the rings in the cross-polarized direction; hence, the cross-polarization patterns are cancelled. However, a polarization selective dipole is preferred in order to increase the isolation between the co-polarized and cross-polarized reradiated fields.

Fig. 4.2(a) depicts the primary cell of the designed RA, where the 360° phase response is achieved using two closed resonant dipoles. Arranging an array of the same dipoles cells horizontally or vertically produces the co-polarized and cross-polarized beams. For this reason, at first, the calculations are done to find the best cell dimensions and substrate parameters for one polarization, and they are optimized for bandwidth enlargement. After that, these lengths

are calculated to produce the cross-polarized beams at two different directions to minimize the cross-polarization levels.

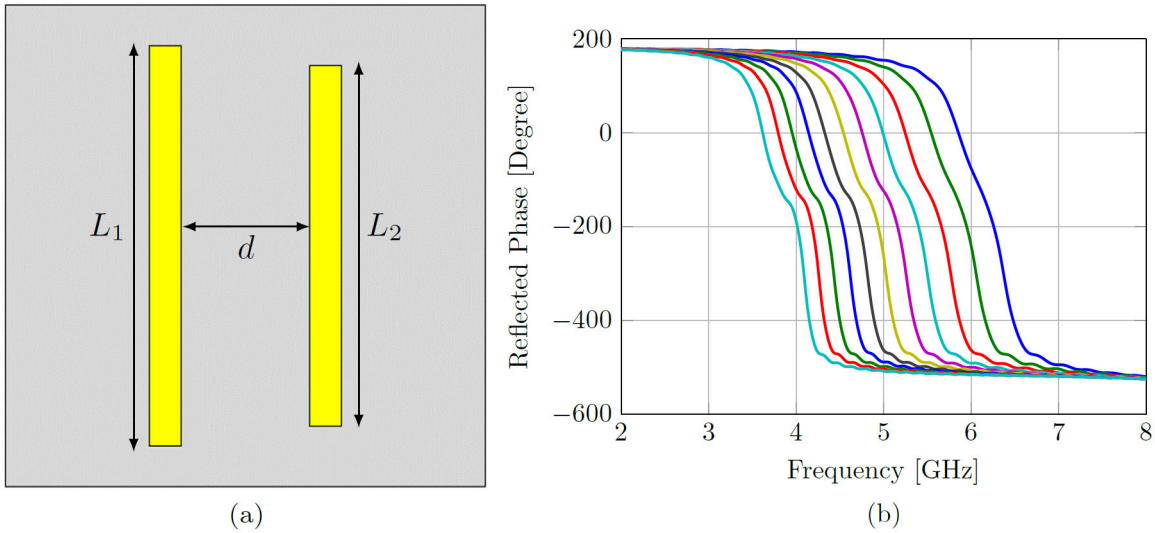

Figure 4.2: UWB RA cross-polarized cell: (a) Cell shape consists of two coupled dipoles with relative lengths $L_2 = 0.9L_1$. (b) Reflected phase with the frequency at different lengths of the first dipole.

The cross-polarized RA configuration is shown in Fig. 4.3. Two spatially separated orthogonal feeders are utilized to illuminate the RA cells, and subsequently different beam pattern in each polarization is produced.

The relative dipole lengths are calculated to produce a central offset beam directed at, for example, ($\theta = 30°$, $\phi = 0°$) for the vertical polarization and the other horizontally polarized beam is directed at ($\theta = -30°$, $\phi = 0°$), where θ and ϕ are the azimuth and the elevation angles respectively. In order to steer the beams around the center direction electrically, there are several approaches. The first one is using an electrically tunable impedance surface of a metal-dielectric composite texture. An applied bias voltage in the surface can control the resonance frequency, and the reflection phase distribution over the array cells [117]. Similar method can be done using a liquid crystal substrate [118], or using a set of varactor diodes [119].

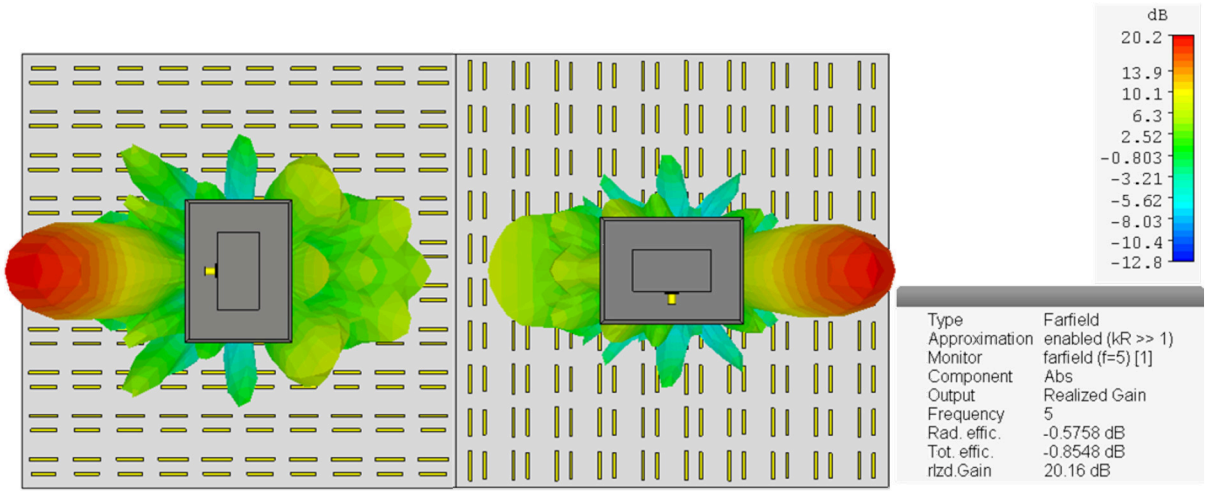

Figure 4.3: The radiation patterns of the cross-polarized reflect-arrays.

4.3 System Model

The received signal at the base-station can be modelled as:

$$y_{UL} = \sum_{i=1}^{U} h_{u,i} x_{u,i} + h_{SI,d} x_{DL} + \sum_{j=1}^{D} h_{SI,s} x_{d,j} + w_r, \tag{4.1}$$

where $x_{u,i}$ is the desired signal from the user i and $h_{u,i}$ is the related UL channel. $x_{d,j}$ is the DL signal to the user j, meanwhile x_{DL} is the sum of all DL signals. $h_{SI,d}$ is the direct SI channel, and $h_{SI,s}$ is the back-scattered SI channel. U and D are the numbers of uplink and downlink users respectively. w_r is the white Gaussian noise. For the user-pairing case, one user for each direction is considered. The scenario of multi-users is realized when dividing the users based on their locations into two groups, one for UL and the other of DL. For each group a main beam is formed to transmit and receive the signals. For each pair, the received signal from the UL user (TxUE1) at the base-station is:

$$y_{UL} = h_{u,1} x_{u,1} + (h_{SI,d} + h_{SI,s}) x_{d,2} + w_r, \tag{4.2}$$

Meanwhile, the received signal at the DL user (RxUE2) is:

$$y_{d,2} = h_{d,2} x_{d,2} + h_{IUI} x_{u,1} + w, \tag{4.3}$$

where h_{IUI} is the channel from UL user (TxUE1) to the DL user (RxUE2) that carries the interference.

4.4 Simulation Setup

Computer Simulation Technology (CST) microwave studio is used to design the UWB RA and generate the radiation patterns. The considered base-station scenarios are carried out using Wireless Insite at 5 GHz for applying the ray-tracing method to get the impulse responses of the channels in the scenario. This method is preferred, instead of using theoretical channel models, to get more realistic outcomes. Next, the DL, UL, and SI channels' coefficients are exported to MATLAB for the baseband processing. Fig. 4.4 shows the simulated environments in (a) indoor as a multi-room office and in (b) outdoor as an urban area. This simulation is confined to one user in each direction with different distances of the two users and omni-directional antennas.

The baseband system is an LTE link which is based on 4-QAM (Quadrature amplitude modulation) OFDM with 5/10/20 MHz bandwidth and sampled by 30.72 MHz. The transmitted power from each transmitter is 0 dBm.

4.5 Results

The simulation results of the RA design are presented in Fig. 4.5, where Ludwig's third definition [120] is used to define the cross-polarized patterns. In the case of $\theta = \pm 30^{\circ}$, the RA antenna gain is about 20 dB, and this is 4 times higher than the gain of the horn antenna feeder. The results show also that the cross-polarization level is about -35 dB. The Side Lobe Level (SLL) is below 10 dB. The operation bandwidth is about 1 GHz for both polarizations. Please note that the asymmetry of the vertical and horizontal polarization patterns is due to the feeder and cells asymmetry.

Tables 4.1, 4.2, and 4.3 show the average received power of the four signals in line-of-sight propagation and the components of SI, for the angles $\pm 20^{\circ}, \pm 30^{\circ}, \pm 40^{\circ}$ respectively. To fairly compare the different angles, the first column shows equal values of the DL received power at the DL user (RxUE2), and the UL received power from the UL user (TxUE1). The next four columns show the SI total power, the signal to self-interference ratio (SSIR), the SI direct path power, and the SI strongest scattered path, respectively. In the last column, the Inter-User-Interference (IUI) from UL users to DL users is shown.

(a)

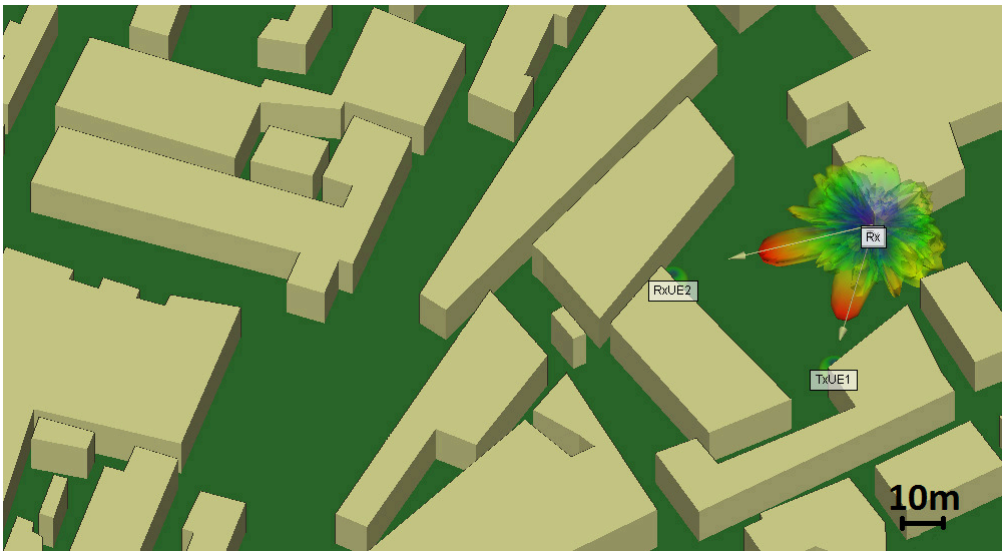

(b)

Figure 4.4: The environment of simulation: (a) Indoor (b) Outdoor.

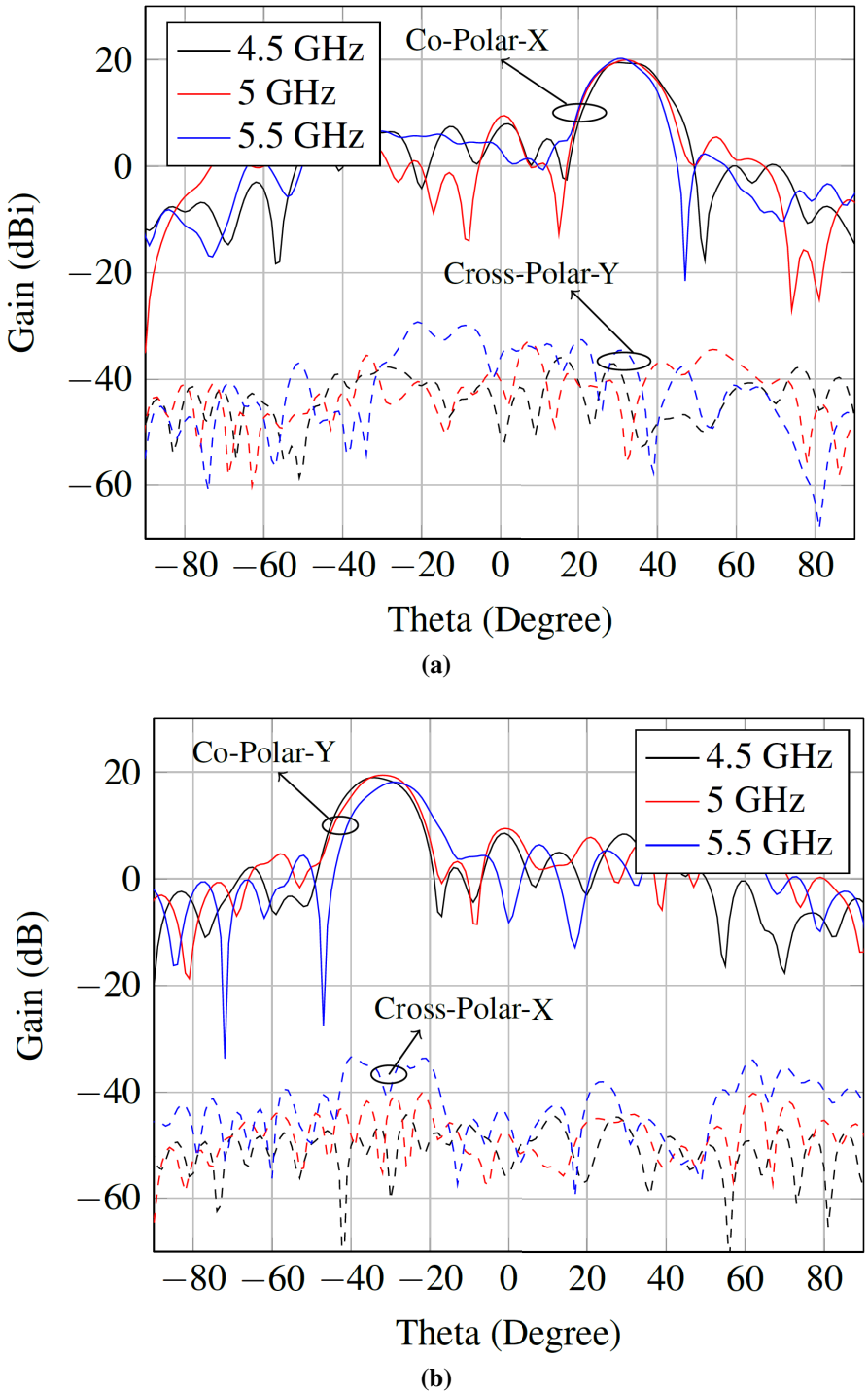

Figure 4.5: The radiation patterns of the dual-polarized RA antenna illustrating in UWB operation: (a) horizontal (b) vertical

Table 4.1: The average power of the four received signals and the signal to self-interference ratio $\pm 20^{\circ}$

$\theta = \pm 20^{\circ}$ $P_T = 0$ dBm LoS	**UL & DL (dBm)**	**Total SI (dBm)**	**SSIR (dB)**	**SI direct (dBm)**	**SI 1st scatter (dBm)**	**IUI (dBm)**
	Indoor					
Co-polar	-41	-36	-5	-41	-70	-55
X-polar		-79	38	-95	-80	-98
	Outdoor					
Co-polar	-63	-39	-24	-41	-88	-72
X-polar		-96	33	-95	-101	-105

Table 4.2: The average power of the four received signals and the signal to self-interference ratio $\pm 30^{\circ}$

$\theta = \pm 30^{\circ}$ $P_T = 0$ dBm LoS	**UL & DL (dBm)**	**Total SI (dBm)**	**SSIR (dB)**	**SI direct (dBm)**	**SI 1st scatter (dBm)**	**IUI (dBm)**
	Indoor					
Co-polar	-41	-45	4	-50	-72	-62
X-polar		-94	53	-103	-89	-101
	Outdoor					
Co-polar	-63	-49	-14	-50	-86	-78
X-polar		-101	38	-103	-110	-112

From the tables, it can be noticed that:

- The downlink and uplink received signals have less power in the outdoor because of the longer paths. The path loss is about 20 dB more in outdoor. This is because the average distance in outdoor is 30m, meanwhile, in indoor it is about 3m.

- The direct SI power, which is produced by the side lobes, has the same power in both environments, but it decreases with larger angle separation. The cross-polarization provides 103 dB mitigation of the direct SI; meanwhile it is only 50 dB with co-polarized arrays for $\pm 30^{\circ}$. The average enhancement in the direct SI isolation using cross-polarization is about 50 dB for the three angles.

- The rich scattering environment in the indoor makes the cross-polarization isolation less

Table 4.3: The average power of the four received signals and the signal to self-interference ratio $\pm 40^\circ$

$\theta = \pm 40^\circ$ $P_T = 0$ dBm LoS	**UL & DL (dBm)**	**Total SI (dBm)**	**SSIR (dB)**	**SI direct (dBm)**	**SI 1st scatter (dBm)**	**IUI (dBm)**
	Indoor					
Co-polar	-41	-55	14	-59	-78	-66
X-polar		-91	50	-104	-92	-107
	Outdoor					
Co-polar	-63	-58	-5	-59	-85	-80
X-polar		-102	39	-104	-110	-116

effective, moreover, it causes higher scattered SI compared to the outdoor.

- Also, the use of cross-polarization provides higher mitigation of IUI (from TxUE1 to RxUE2). For example with $\pm 30^\circ$, the mitigation enhancement by cross-polarization compared to co-polarization is $-62 - (-101) = 39$ dB in the indoor and 34 dB in the outdoor.

- The FD system cannot perform without the use of cross-polarized arrays as the SSIR would be very low in the case of co-polarization.

The total SSIR value reflects the average isolation ratio of the SI, which is achieved by cross-polarization and angle separation. The average value for the three angles is 47 dB in indoor, and 37 dB in outdoor. Such values could be achieved with two horn antennas instead of reflect-arrays. However, the later allows us to do the beam-forming electronically, and horn antennas can not perform this without an impractical mechanical system. Moreover, the reflect-arrays avoid any Tx-RX leakage on the electronic board of the base station.

Finally, to evaluate the use of the proposed setup with an LTE base-station, a system simulation is done, and the performance is evaluated by the bit error rate and the achieved sum rate. Fig. 4.6 shows that the BERs of the FD and HD systems are almost the same. However, there is a slight performance loss at high SNR values where the self-interference becomes the dominant limiting factor instead of the white noise.

Fig. 4.7 shows the sum rate of the base-station. For separation angle values bigger than 60°, the rate is almost the same. The FD/HD enhancement of the system is a little less than double because of the residual SI. This RSI may be cancelled by digital SIC techniques.

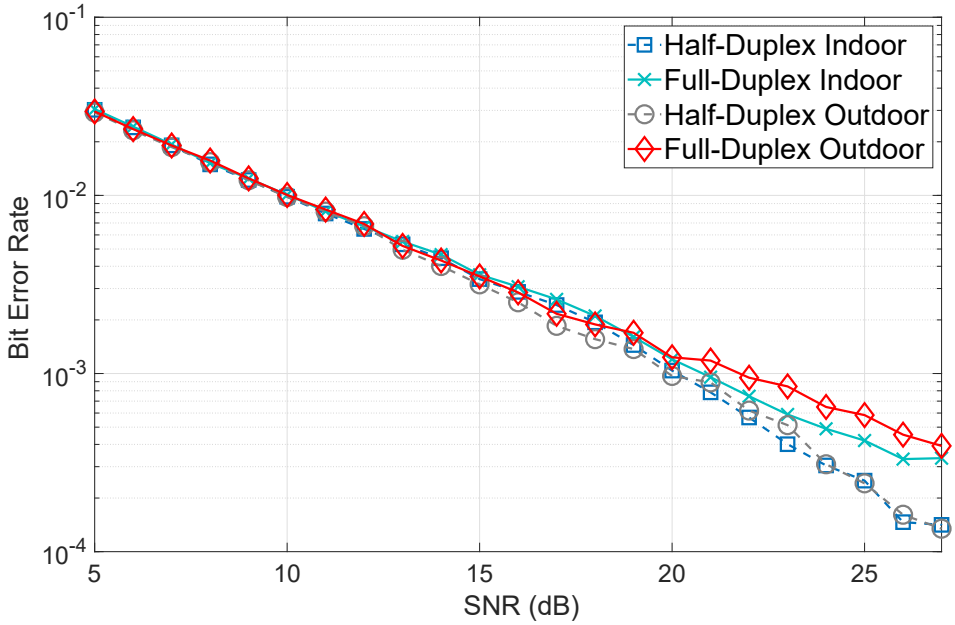

Figure 4.6: Bit error rate of FD and HD systems using cross-polarized RA

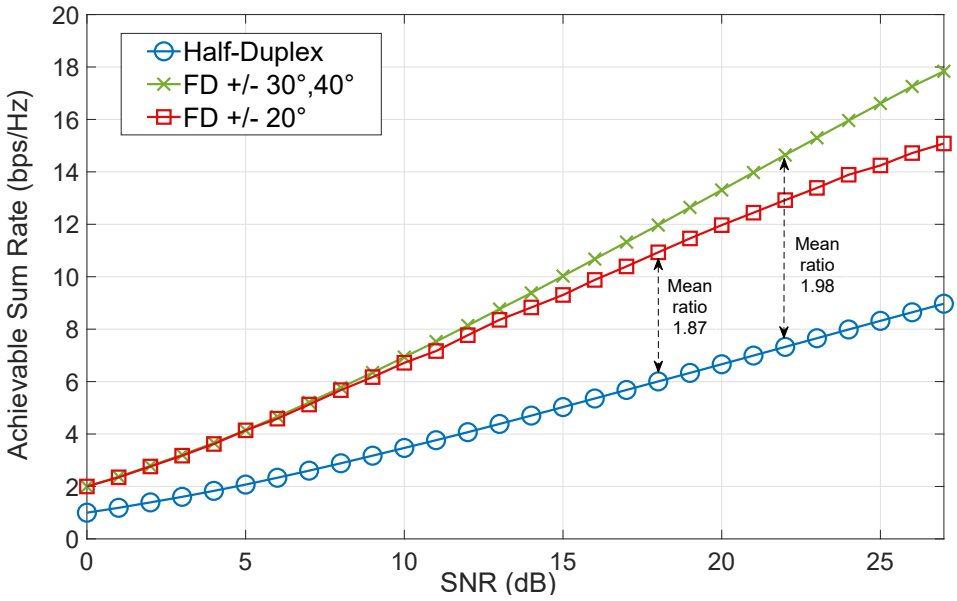

Figure 4.7: Achievable sum rate of FD and HD OFDM systems using cross-polarized RA

4.6 Conclusion

In this chapter, the use of reflect-array in FD mobile systems is proposed for the first time in literature. Dual-polarized reflect-arrays are designed to be used in a full-duplex LTE base-station. The different self-interference components are analyzed in indoor and outdoor environments.

Evaluation of the system performance is done considering the BER and the sum rate of the base-station in a simple case of two HD users, and three values of angular separation. The results show that the enhancement FD/HD ratio would reach almost the theoretical boundary of two in this case. As the work was confined to a simple scenario, further work can be done, like increasing the number of users and doing the beam-forming to different users' positions. The system performance can be enhanced in this complicated scenario by applying digital cancellation schemes to remove the residual self-interference. Also, the studied scenario can be useful for UL/DL users pairing.

In the next chapter, another multi-antenna technology (antenna selection) is presented to analyze its benefits for SIC in an FD base-station in both cases, co-located and distributed antennas.

Chapter 5

Co-located and Distributed Antenna Selection in a Full-Duplex Base-Station

Antenna Selection (AS) cancellation is a simple cost-efficient technique for multi-antenna FD systems. Rather than RF elements, antennas are inexpensive. In many application scenarios, the additional hardware and the high complexity can be avoided with AS where only some RF switches are needed instead of multi-transceiver chains. This forms a motivation to use AS as an alternative SIC multi-antenna technique to reduce hardware costs and complexity dramatically. The use of narrowband AS in FD was adopted in [121–123]. The works in [124, 125] analyze the performance of AS theoretically and with a simple simulation of a bidirectional FD multi-antenna system. In [126], a theoretical analysis is done to use FD AS for backhauling of multiple small cell network. In wideband systems, Our work [127] proposed a practical method of wideband AS to enable full-duplex in an indoor LTE femto base-station (femto-BS). We also presented a similar work in [128] with a distributed antenna system (DAS) in order to enhance the channel diversity. These two simulation works are the basis of this chapter. Meanwhile, the experimental validation of AS in an FD BS is presented in the next chapter.

5.1 Introduction

Receive antenna selection is combined with cross-polarization and antennas conditional placement in order to perform the required SIC. HD uplink user-equipments (UE) are used to estimate the effect of downlink (DL) SI on the uplink (UL) reception at the FD BS. In the proposed scenario, UEs operate in HD TDD mode. At a certain time, part of them are acting as UL users,

and the rest are receiving the DL signal. Meanwhile, the BS is working in FD mode, so it can simultaneously transmit its signal to the specific DL users and receive the signals from UL users. Another deployment scenario is IAB with the same setup. For example, at a certain moment all the users are transmitting UL signals, and the FD BS receives them and simultaneously transmits the backhaul signal to the core network in the same frequency band.

Three AS criteria are used, 1) MSNR: maximization of SNR without considering the SI channels. 2) MSSINR: maximization of SSINR, where SI channels are considered. 3) MCGR: maximization of channel gain ratio, as will be explained later. The performance of the system is evaluated by bit-error-rate (BER), sum-rate per Hz, residual SI (RSI), and FD/HD sum-rate enhancement ratio.

Along with the performance improvement MIMO technology offers, comes a considerable limiting factor represented by the resulting complexity due to using a dedicated RF chain for each employed antenna in conventional MIMO systems. Consequently, this would highly increase the implementation costs which escalate along with the number of employed antennas [129].

AS technique provides the possibility to reduce the accompanying costs while maintaining many of the advantages that MIMO systems offer, by using a limited number of RF chains and selecting a subset of antennas from the total available antennas. This way, the number of RF chains will be reduced to the number of the selected antennas, and the implementation costs of the MIMO system will be reduced. The best set of antennas to be selected is determined by deploying a specific antenna selection criterion. AS can be deployed at the receiver side and/or at the transmitter side as well, with the condition that the Channel State Information (CSI) for all MIMO channels, must be known at the receiver and/or at the transmitter side respectively [130]. This condition can be met by training the MIMO channels through using pilot signals, in order to be able to estimate the channel at the receiver side, and to feedback the estimated CSI to the transmitter in case of AS implementation at the transmitter side. Nevertheless, in this simulation work, perfect knowledge of the channels is assumed; meanwhile, in the experimentation work, all the channels will be estimated as shown in the next chapter.

5.2 System Model

Since the essential objective of this work is the evaluation of the AS performance in mitigating the SI in an FD BS, for simplicity, a maximum of three UL single-antenna users are considered in different locations $N_U = \{1, 2, 3\}$. Further work can be done to evaluate the DL reception at

different DL users, and to analyze the inter-user interference from UL users to DL users. The FD system model is denoted in Fig. 5.1. A femto-BS is considered with N_R receive antennas, and a single transmit antenna that transmits the DL signal ($N_T = 1$). In the HD system, and for each user the UL signal is given by the following linear model

$$y = \sqrt{E_x}\, H\, x + w_r, \tag{5.1}$$

where x is the transmitted symbol from the UL user, H is the $N_R \times 1$ channel vector. E_x is the transmission power and w_r is AWGN following the complex Gaussian distribution with zero mean and $\sigma^2 I_{N_R}$ covariance matrix. σ^2 is the noise covariance and I_{N_R} is the $N_R \times N_R$ identity matrix. Then, the SNR is given by $\rho = E_x/\sigma^2$. When AS is implemented at the receiver side in the BS, with the assumption of complete knowledge of the CSI at the receiver, one antenna is selected out of the N_R receive antennas of the BS. The signal model of the received signal using the selected receive antenna is

$$y_s = \sqrt{E_x}\, h_s\, x_s + w_s, \tag{5.2}$$

where h_s is the channel response of the selected antenna, and w_s is the AWGN.

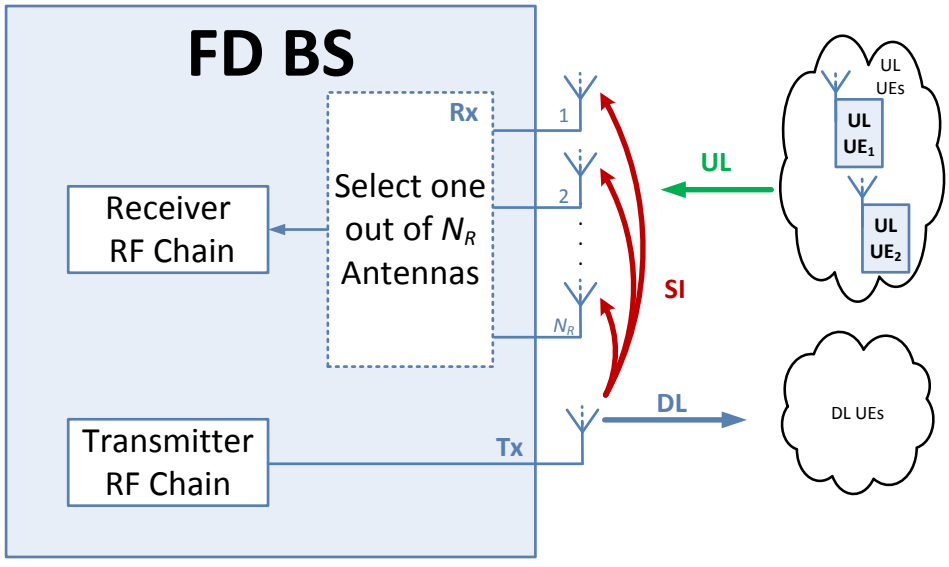

Figure 5.1: FD AS system model

The FD system is assumed to be applied in an indoor environment; consequently, the UL signal and the SI signal experience multipath propagations. The impulse response of the channel

between the UE's transmit antenna, and one of the N_R receive antennas is given by the following model

$$CIR(t,\tau) = \sum_{p=1}^{P(t)} \alpha_p(t)\, e^{-j\varphi_p(t)} \delta(\tau - \tau_p(t)), \tag{5.3}$$

where τ_p, α_p and φ_p are the delay, the attenuation, and the phase shift of the pth path. The frequency domain response is obtained by applying Fourier transform to the impulse response as

$$H(f) = \int_{-\infty}^{+\infty} CIR(\tau)\, \mathrm{e}^{-2\pi f \tau}\, d\tau. \tag{5.4}$$

OFDM waveform is used to overcome the Inter-Symbol Interference (ISI), which is a result of the multi-path propagations. The transmit symbol vector in the frequency domain is of size $N_{used} \times 1$, where N_{used} is the number of used subcarriers in the OFDM symbol. After receiving the transmitted signal using all the N_R receive antennas, and estimating propagation channels, the received symbol vector in frequency domain at the receiver baseband is given for $N_R \cdot N_{used} \times N_{used}$ by the frequency domain channel matrix

$$H = \begin{bmatrix} H(0) & \cdots & 0 \\ \vdots & \ddots & \vdots \\ 0 & \cdots & H(N_{used}-1) \end{bmatrix}, \tag{5.5}$$

where each diagonal element $H(k)$ represents the $1 \times N_R$ channel vector for the k_{th} subcarrier

$$H(k) = \sum_{l=1}^{L-1} G(l)\, e^{-i\frac{2\pi kl}{N_{used}}}, \tag{5.6}$$

where $G(l)$ is the $N_R \times 1$ vector for the l_{th} delay of the channel impulse response.

After AS implementation, the received signal from the UL user u at the BS using the selected antenna is given by

$$y_u(k) = h_{ul}(k)x_{ul}(k) + \underbrace{\alpha\,\beta\,h_{si}(k)x_{dl}(k)}_{\text{self-interference}} + \underbrace{\sum_{q=1,q\neq u}^{N_U} H_q(k)x_q(k)}_{\text{inter-user-interference}} + w(k), \tag{5.7}$$

where $x_{ul}(k)$ is the uplink transmitted signal from the specific UL user u, and $h_{ul}(k)$ is the forward uplink channel response. $h_{si}(k)$ is the SI channel response between the BS's downlink transmit antenna and the selected receive antenna. $x_{dl}(k)$ denotes the transmitted downlink signal. β is the SI digital attenuation factor, where the maximum value of β is one when no digital SIC is implemented, and α denotes the SI suppression factor in the analog and propagation domains, so it sums the impacts of AS, cross-polarization, and the SI channel path loss. The summation in (5.7) denotes the unwanted signals from other UL users. This term may be neglected if single-carrier frequency division multiple access (SC-FDMA) is used. In LTE, SC-FDMA guarantees the orthogonality of the uplink multiplexing. $w(k)$ is the AWGN in the receiver of the BS. Meanwhile the DL received signal at the $d^{\text{th}} \in \{1, .., N_D\}$ user $y_d(k)$ can be written as

$$y_d(k) = h_{dl}(k)x_{dl}(k) + \underbrace{\sum_{m=1,m\neq d}^{N_D} h_m(k)x_m(k)}_{\text{interference from DL users}} + \underbrace{\sum_{u=1}^{N_U} h_{ud}(k)x_u(k)}_{\text{interference from UL users}} + w_d(k), \tag{5.8}$$

where $h_{dl}(k)$ is the DL channel of all sub-carriers for the user d while w_d represents the AWGN at the d^{th} DL user.

5.3 Selection Criteria

In general, the optimal AS is realized by selecting the antenna, or a subset of antennas, that achieves the maximum capacity with full rank channel matrix. In real implementation, with practical approximation, the optimal AS criterion is to maximize the SNR in an HD system, or the SSINR in an FD system. In this experiment, three AS criteria are deployed.

5.3.1 Maximization of Signal-to-Noise Ratio (MSNR)

In this criterion, the BS selects the antenna a_j that maximizes the received SNR as

$$Select \quad a_j = \arg\max\{\rho\}. \tag{5.9}$$

ρ is the mean SNR, and it is the given by

$$\rho = \frac{S}{N}, \tag{5.10}$$

where S is the uplink received signal power, and N is noise power. ρ can be calculated from (5.7) and with neglecting the SI part.

5.3.2 Maximization of Signal-to-Self-Interference-plus-Noise Ratio (MSSINR)

In [127], optimal receive AS criterion is proposed and investigated for the purpose of SI mitigation in the BS of a wideband FD system. In this criterion, the BS selects the antenna a_j with the maximum achieved SSINR

$$Select \quad a_j = \arg\max\{\Gamma\}. \tag{5.11}$$

Γ is the mean SSINR, and it is given by

$$\Gamma = \frac{S}{N + SI}, \tag{5.12}$$

where S is the desired forward received signal power, N is the noise power, and SI is the power of the undesired self-interference signal. Γ can be calculated from (5.7).

5.3.3 Maximization of Channel Gain Ratio (MCGR)

With this criterion, the selected receive antenna is the one that achieves the maximum ratio Π between the forward channel gain and SI channel gain according to

$$Select \quad a_j = \arg\max\{\Pi\}. \tag{5.13}$$

Π is the CGR, and it is given by:

$$\Pi = \frac{\|h_{ul}\|}{\|h_{si}\|}, \tag{5.14}$$

where the channels responses are estimated during the channel training phase as will be explained later.

For multi-user in the UL, the three criteria are extended to maximize the sum value of all UL users. Then the MSNR criterion complexity is given by $\mathcal{O}(N_{used} \times N_U \times {N_R}^2)$, meanwhile it is $\mathcal{O}(N_{used} \times N_U \times {N_R}^2 \times N_T)$ for MSSINR, and $\mathcal{O}(N_{used} \times N_U \times N_R \times N_T)$ for MCGR criterion.

5.4 Simulation Setup

The FD femto BS scenario is simulated using Wireless Insite and MATLAB. The ray-tracing method is employed to capture a precise site-planning assessment and to get the impulse responses of the multipath channels. Rather than theoretical models, the ray-tracing method allows precise specification of the environment, and it provides detailed channel characterizations for a practical scenario. Built-in omnidirectional antennas are used in the ray-tracing tool with linear horizontal or vertical polarization for each direction. The DL, UL, and SI channels coefficients are exported to MATLAB for the baseband processing as a wideband OFDM system. Fig. 5.2 shows the simulated environments in an indoor femto-BS as a multi-room office where BS antennas are mounted on the 3m height ceiling, and the users are 1m high. A summary of the simulation parameters in this setup is presented in Table 5.1.

The performance is evaluated by bit error rate (BER), and sum rate per user in average, i.e., the sum of uplink and downlink rates in BS for an average user while changing the SNR. The results are averaged over three values for number of users $N_U = \{1, 2, 3\}$ in each direction, and in random positions.

5.5 Results

Employing the combined solution yields a good SI mitigation in the analog domain, even before applying the digital SIC. In simulation, the applied techniques in the propagation domain provide about $\alpha = -75$ dB of mitigation in average, meanwhile further enhancement is achieved when digital SIC is applied with $\beta = -20$ dB. The SI channel path loss provide about 35 dB of cancellation, meanwhile the AS and cross-polarization provide about 40 dB together. In general,

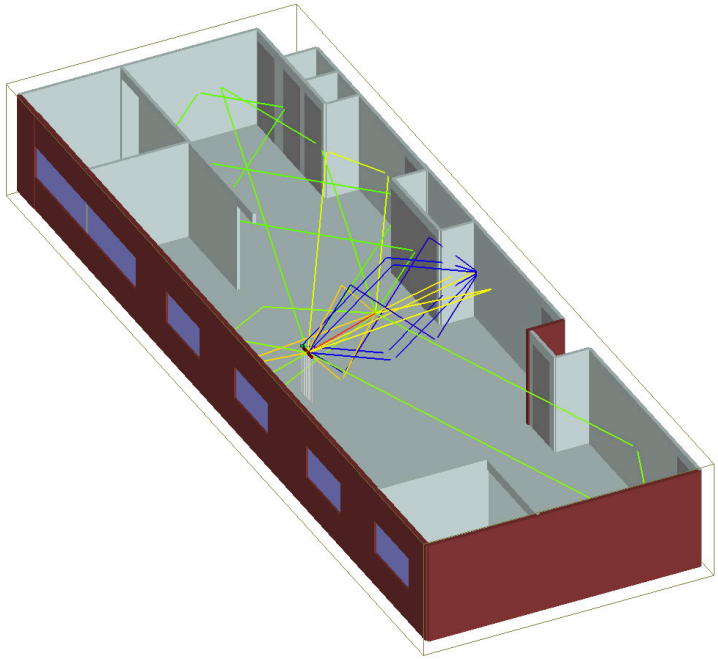

Figure 5.2: The indoor environment of simulation

Table 5.1: Summary of simulation parameters

Parameter	Value	Description
F_c	5 [GHz]	Carrier frequency
F_s	30.72 [MSa/s]	Sampling rate in baseband
N_{fft}	2048	FFT size of OFDM
N_{used}	300	The number of active subcarriers
Δ_F	15 [KHz]	Subcarrier spacing
B	4.5 [MHz]	Bandwidth
N_{cp}	256	The number of samples in CP
τ_{sym}	75 [μs]	Time duration of one OFDM symbol
τ_{cp}	8.33 [μs]	Time duration of one CP
N_R	$4, 8, 16$	The number of receive antennas
N_U	$1, 2, 3$	The number of users
$\mathcal{A}$	4	Alphabet size of constellation mapping, 4-QAM

a small decrease in the performance of UL/DL is expected for moving/handheld devices, as the cross-polarization may not be perfect in this case. However, the mitigation of SI in BS achieved by cross-polarization remains almost the same. Fig. 5.3 shows the performance comparison of the two algorithms with and without cross-polarization in the case of 8 BS receive antennas. Since no channel coding is implemented in the simulation, the calculated error rate here is uncoded BER. The channel capacity of the system when no antenna selection is implemented is given by

$$C_{NoAs} = \log_2(1 + \rho_a), \tag{5.15}$$

where ρ_a is the average estimated SNR per receive antenna before AS. When the HD AS criterion is employed, the channel capacity is calculated by

$$C_{HD_{sel}} = \log_2(1 + \rho_{sel}), \tag{5.16}$$

where ρ_{sel} is the estimated SNR at the selected antenna, and is calculated as in (5.10). Meanwhile, the rate can be calculated as in the HD system, except using SSINR instead of SNR.

$$C_{FD_{sel}} = \log_2(1 + \Gamma_{sel}), \tag{5.17}$$

where Γ_{sel} can be calculated as in (5.12).

Similarly, Fig. 5.4 shows the effect of changing the number of receive antennas using the practical AS algorithm. From Fig. 5.4(a) it is clear that the degree of freedom provided by 16 antennas in the case of FD can ensure a comparable performance (BER) with an HD system of 4 or 8 antennas. The gain, in this case, is doubling the capacity as in Fig. 5.4(b).

Finally, Fig. 5.5 shows the enhancement ratio of FD capacity over HD capacity for both algorithms. The ratio in the practical algorithm is about 1.85 compared to nearly 2 in the case of the optimal selection, with comparable BERs.

5.6 Distributed Antenna System

After showing the results of the proposed AS FD system, the focus now is to evaluate the effect of using distributed antennas instead of co-located antennas. The earliest literature about DAS is [131], where it was presented as a solution to cover the dead spots and reduce the large-scale

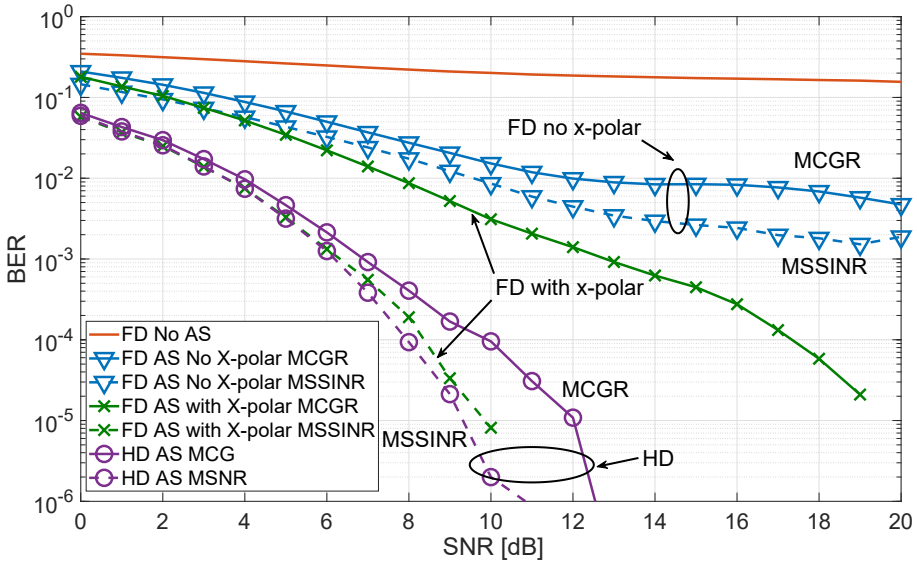

(a)

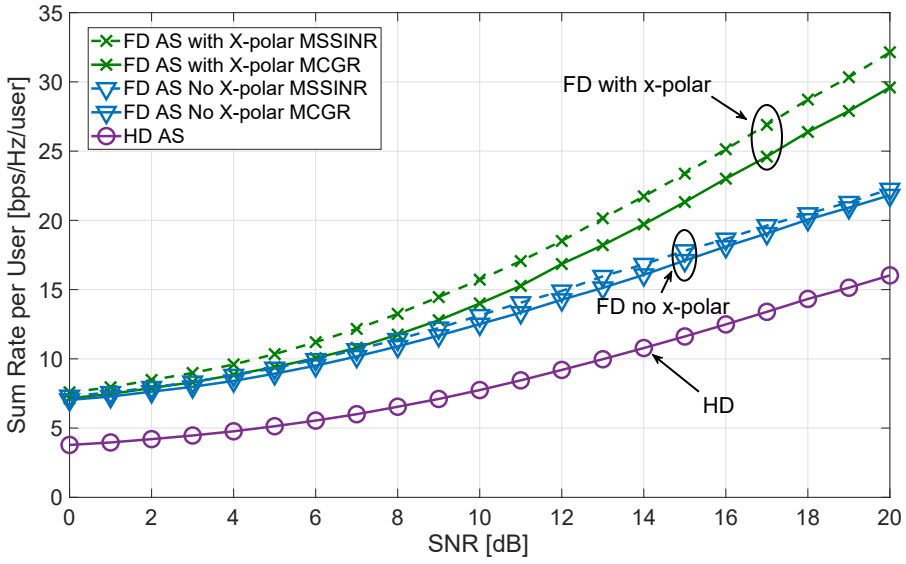

(b)

Figure 5.3: Performance comparison of the two algorithms in case of 8 receive antennas (a) BER (b) Sum rate per UE

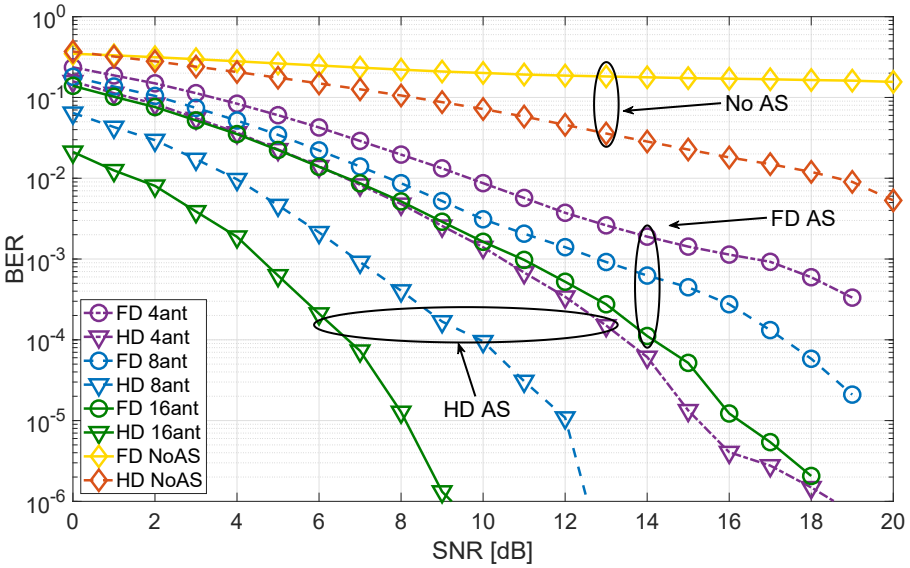

(a)

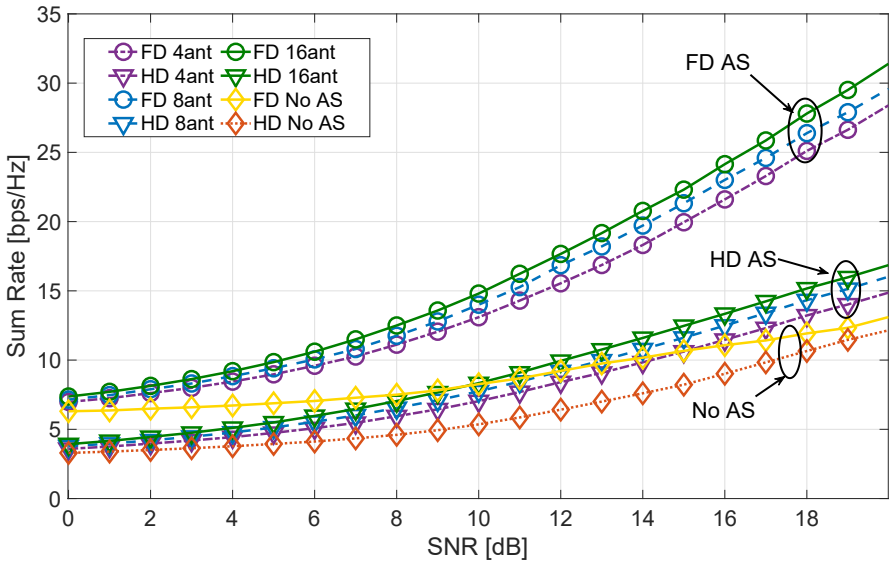

(b)

Figure 5.4: Performance comparison for different numbers of receive antennas (a) BER (b) Sum rate per UE

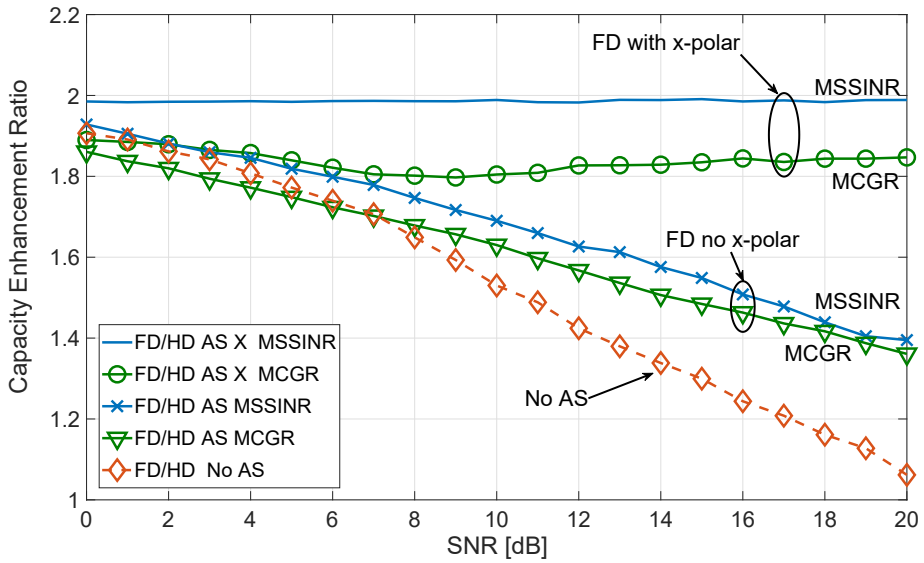

Figure 5.5: FD/HD capacity enhancement for the optimal and the practical algorithms

fading impact in indoor wireless communications, then many literature analyzed the benefits of DAS like coverage extension, link reliability enhancement, and power saving in cellular systems [132–141]. Thus, DAS has acquired great attention in 3GPP standardizations [142]. Moreover, it is one of the promising antenna techniques to be used in 5G, especially to form user-centric manner virtual cells [143]. In DAS, many remote antennas and remote radio heads (RRHs) are distributed over a certain area and connected to the central base station by coaxial cables, or by optical fibers using Common Public Radio Interface (CPRI) or a similar flexible interface. The latter setup is known as Radio over Fiber (RoF).

The attractive advantages of DAS over co-located antennas, such as higher diversity gain and power efficiency, urge to investigate more about the exploitation of DAS in FD systems. Distributing BS antennas may make SIC easier as it allows SI to be mitigated in the propagation domain. DAS provides a more degree of freedom in selecting the weakest SI channels between the transmitter and the receiver.

Many works have been done to analyze FD DAS theoretically. The earliest literature focused on Full-Duplex Relaying (FDR) as in [144, 145], meanwhile the work in [146, 147] analyzed the resource allocation and the energy efficiency in FD BS with distributed antenna, and the hybrid duplex was proposed in [148]. To the best of our knowledge, all of the prior works studied antenna selection and DAS in FD cell theoretically, proposing resource allocation algorithms without any focus on the SIC that can be achieved by DAS. The aim here is to investigate AS in a

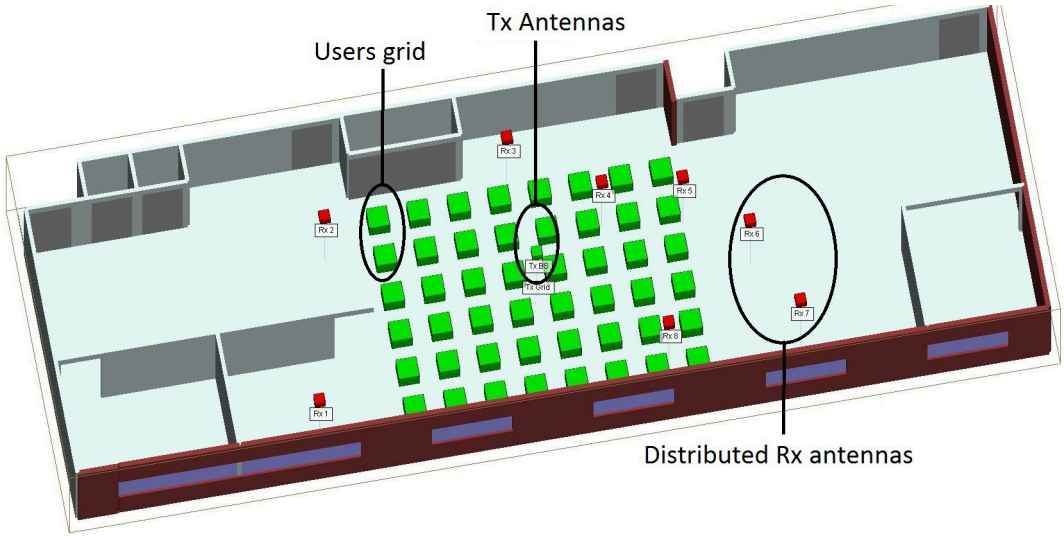

Figure 5.6: The indoor environment of simulation

practical scenario of femto BS with distributed antennas in comparison with co-located antennas. Fig. 5.6 shows the simulated environment of an indoor femto-BS as a multi-room office, where BS co-located/distributed antennas are mounted on the 3m high ceiling, and the users grid is 1m high.

Fig. 5.7 shows the BER performance for different operating modes with 8 receive antennas. The BER of FD modes is almost similar in both distributed antenna and co-located scenarios, and very close to the HD case with antenna selection. It is clear that applying FD does not cause considerable degradation of the performance compared to the no antenna selection case.

In terms of capacity, Fig. 5.8 presents the sum-rate performance of the simulated channels using antenna selection with 4 and 8 antennas for both distributed and co-located antennas systems. The FD capacity enhancement is clear when comparing to HD mode. The performance of co-located and distributed antenna systems in HD transmission is almost the same; however, in FD mode, the distributed antenna provides slightly better performance. The performance difference between FD distributed and co-located antennas in the case of co-polarization is greater compared to the cross-polarization case; this is because distributing the receive antennas away from the transmit antennas makes the SI polarization isolation much less effective. From this figure, it may be seen that there is limited enhancement by distributing the antennas in the cross-polarization case; however, the enhancement can be observed clearer as a ratio as in Fig. 5.9.

The capacity enhancement ratio FD/HD in distributed antenna mode is better than the co-located antenna selection case. The enhancement ratio deviation is found to be more pronounced

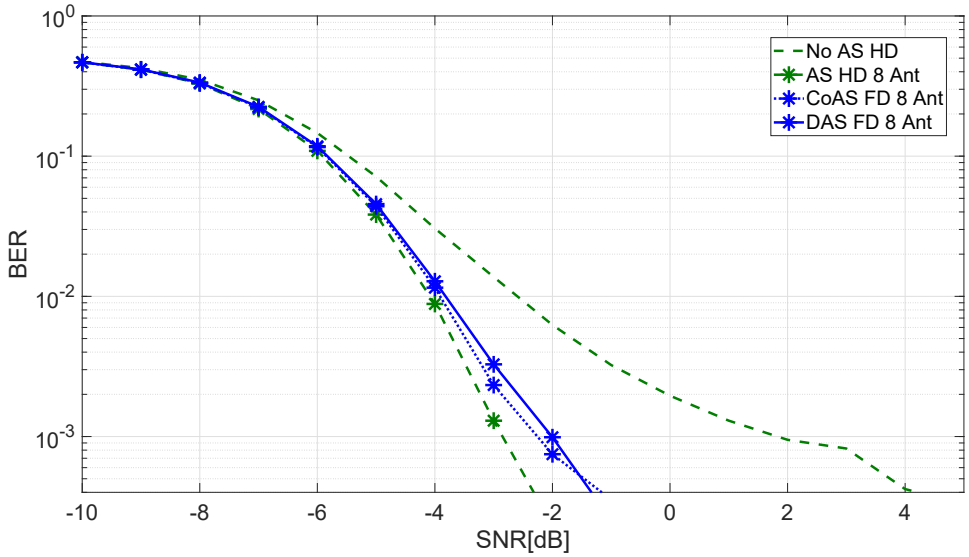

Figure 5.7: BER performance comparison of co-located and distributed antenna selection in case of 8 receive antennas

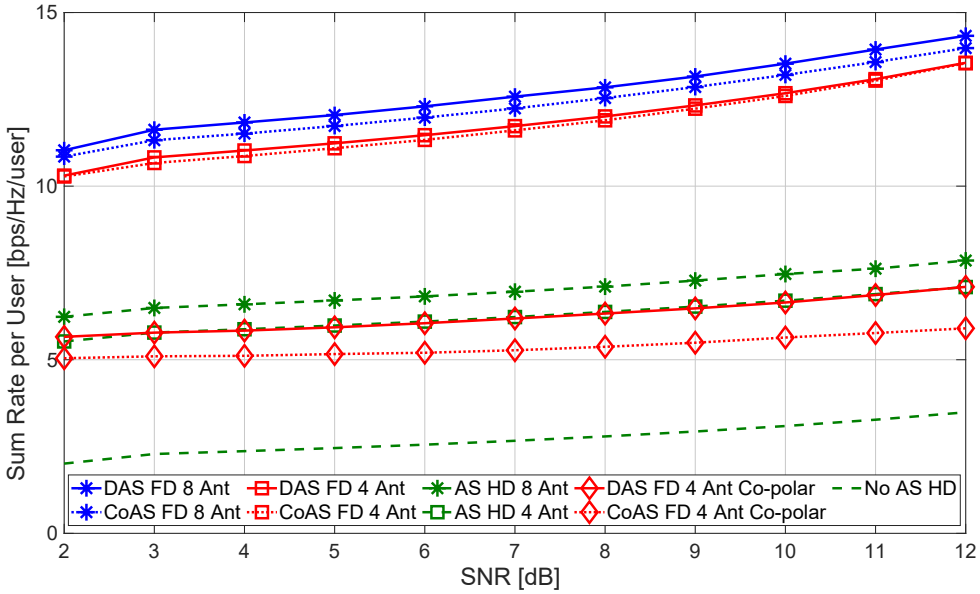

Figure 5.8: Sum rate comparison of co-located and distributed antenna selection

in case of 8 antennas compared with 4 antennas.

Finally, Fig. 5.9 shows that, in both distributed and co-located cases, the 4-antenna scenario achieves a higher enhancement ratio compared to the 8-antenna scenario. This indicates that increasing the number of antennas will not lead to a scalar increase in performance.

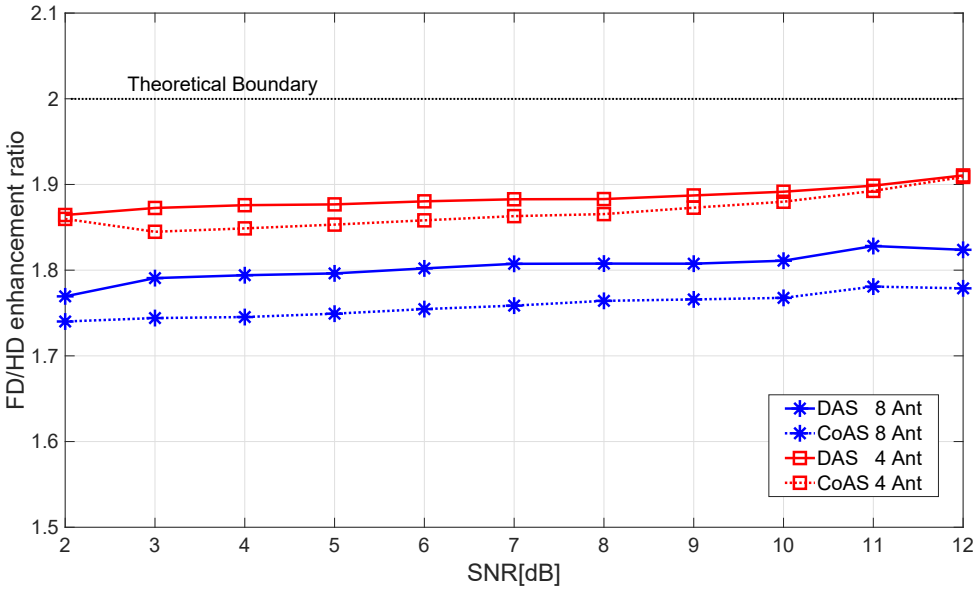

Figure 5.9: FD/HD enhancement ratio of co-located and distributed antenna selection

To conclude, the impact of distributing the receive antennas on SIC can be outlined as follow

- The path loss between the transmit and the receive antennas causes higher SI isolation.
- Distributing the receive antennas provides better diversity to select the antenna that guarantees minimum SI in the base station.
- The SI isolation, which is attained by the cross-polarization, is almost ineffective in case distributed antennas. This is due to the rich scattering SI channel in the indoor environment.

5.7 Conclusion

In this chapter, receive antenna selection is employed to enable FD transmission in a femto base-station. The proposed scheme combines wideband antenna selection and cross-polarization. A ray-tracing tool is used to precisely characterize the indoor multi-path channel environment instead of using theoretical channel models. A baseband analysis is conducted to evaluate the performance of the full-duplex system. Different AS criteria are simulated and compared in terms of performance and complexity. Both co-located and distributed antenna systems show

similar performance. The simulations show promising results for both. However, the simulation can be extended to more complex antenna selection scenarios. The work was confined to a small number of users; therefore, further investigation is required with a larger number of users. Nevertheless, the presented simulation is the basis for implementing an FD base-station with antenna selection in a real testbed, as shown in the next chapter.

Chapter 6

Experimental Validation of a Full-Duplex Base-Station with Antenna Selection

6.1 Introduction

The work in this chapter presents the hardware validation of the simulation work in the previous chapter. This work aims to experimentally enable the FD transmission in an indoor wideband femto-BS with antenna selection.

Various scenarios are experimented in the testbed, such as changing the number of antennas, the type of isolation (vertical/horizontal), and the type of antennas (Omnidirectional/directional). Three AS criteria are used, 1) MSNR: maximization of SNR without considering the SI channels. 2) MSSINR: maximization of SSINR, where SI channels are estimated. 3) MCGR: maximization of channel gain ratio, as will be explained later. The performance of the system is evaluated by the bit-error-rate (BER), the sum-rate, the residual SI (RSI), and FD/HD sum-rate enhancement ratio.

In this chapter, the details of the built-up testbed of the FD BS are described. First, the full structure of the testbed is presented, including hardware structure, signal structure, and transmission/reception workflow. Next, the signal processing chain and several key signal processing modules, e.g., synchronization, channel estimation, are described. Afterward, the testbed integration and the measurement environment are explained. Then, the measurement results are presented with various cases regarding the used criteria, the number and the type of antennas, and the antenna separation structure. Finally, the conclusions are drawn at the end of the chapter. The work presented in this chapter is published in [149].

6.2 Testbed Setup

The FD system model is denoted in Fig. 5.1. The system is assumed to be applied in an indoor environment; consequently, the UL signal and the SI signal experience multipath propagations.

6.2.1 Hardware Structure

Fig. 6.1 demonstrates the block diagram of the testbed setup. The setup consists of the following equipment:

1. **Controlling PC** where the following tasks are done:
    - Generation of the transmit data in MATLAB
    - Digital signal processing of the transmit and receive data
    - Applying the proposed antenna selection criteria according to the adopted scenario
    - Sending control commands to the employed equipment
2. **Arbitrary wave generator (AWG)** where the digital transmit data are converted to an analog wideband RF signal and prepared to be sent over the air via the transmit antennas.
3. **Digital signal analyzer (DSA)** where the analog received RF signals are down-converted, digitized, and transferred to the PC for further processing in MATLAB.
4. **Arduino platform** which is responsible for controlling the RF switch for selecting the receive antenna. The Arduino platform receives its control commands from MATLAB via Universal Serial Bus (USB) interface.
5. **RF switch** the RF switch has three control pins connected to Arduino platform, which correspond to eight switch ports, each port is connected to a single receive antenna.

6.2.2 Signal Structure

The main aim of this experiment is to investigate the performance of the FD system with practical implementation errors, realistic channels, and wideband signals. Thus, the signal structure adopted in the testbed should be thoughtfully designed, including the frame structure, the resource grid structure of the channel training pilots and user payload data, which will be explained in this section.

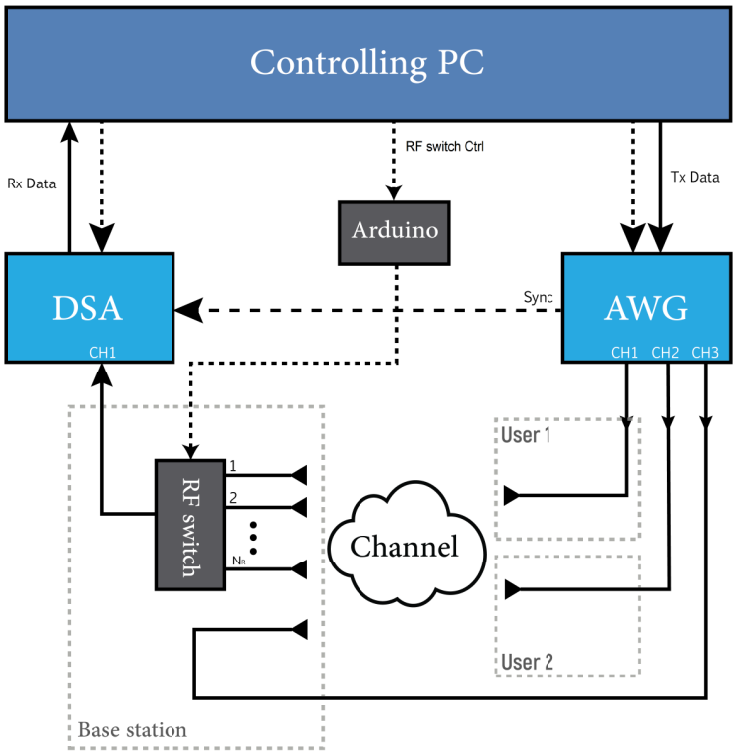

Figure 6.1: Block diagram of the FD antenna selection testbed

Frame design

In order to decide which is the best receive antenna by deploying the antenna selection criterion, channel training must be initially arranged. This order is manifested in the frame design in the testbed for the HD and the FD scenarios. In the HD scenario presented in [24], each frame is comprised of two subframes, subframe 0 ($SF0$) and subframe 1 ($SF1$). $SF0$ is dedicated essentially for forward channels training, that is why it is composed of N_R identical slots, where N_R is the number of the BS's receive antennas. Each slot contains:

- One pilot OFDM symbol: to train one of the N_R receive antennas.
- Payload data OFDM symbols: which are used to calculate the BER of the corresponding channel after demodulation.
- Guard period (GP): the RF switching between the antennas is done in this period.

$SF1$ is essentially dedicated for transmitting the actual payload data. After the AS criterion is deployed, and the best antenna is determined, $SF1$ is transmitted and then received using the selected antenna. $SF1$ consists of payload data OFDM symbols and only one pilot OFDM symbol. Although both subframe $SF0$ and $SF1$ consist of pilot-payload-blocks, their functions

are different: $SF0$ is mainly used for channel training and short payload data transmission; while $SF1$ is mainly used for long payload data transmission/reception, as it uses the high reliable selected antenna. Besides, since no antenna selection is made in $SF0$, the payload data transmission in this subframe can emulate the system without specific selection functionality, which serves as a benchmark for the antenna selection algorithms.

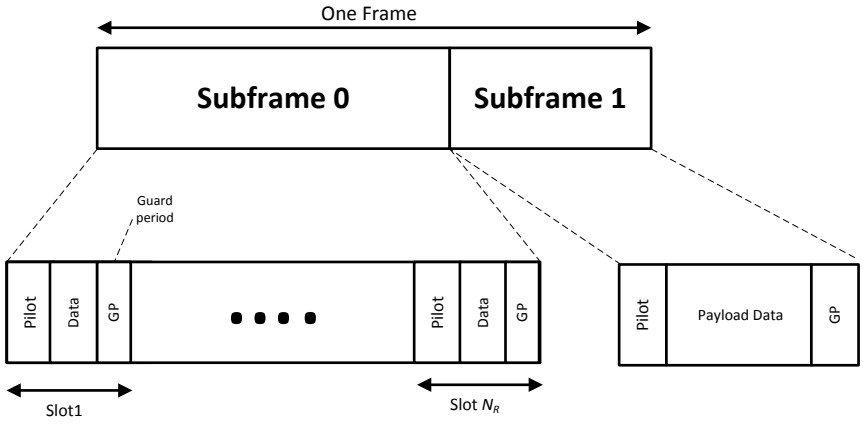

Figure 6.2: HD Frame structure

Fig. 6.2 shows the frame structure, as in [24], for the HD system, where there is no downlink transmission.

In the FD scenario, the channel training stage must be considered for the uplink forward channels, as well as for the SI channels, and there will be simultaneous uplink and downlink transmissions after selecting the antenna. Therefore the frame structure must be modified for the FD scenario. Fig. 6.3 shows the extended frame structure for the FD scenario. The uplink subframe 0 ($SF0_{UL}$) is dedicated to forward channels training; meanwhile, the SI calibration subframe 0 ($SF0_{Cal}$) is dedicated to SI channels training. $SF1_{UL}$ and $SF1_{DL}$ in the FD scenario are the uplink subframe 1 and the downlink subframe 1 respectively, which are dedicated for the actual uplink payload data transmission and the actual downlink transmission respectively. $SF1_{UL}$ and $SF1_{DL}$ have the same structure as $SF1$ in the HD scenario.

It is important to notify here, that the SI channel calibration must be used when the experiment runs for the first time, yet it does not necessarily have to be executed for each frame. This is because the SI channels have fewer variations than the UL forward channels, and the SI channels are more affected by the form factor of the BS, unlike the forward channels which are more subject to the surrounding environment and UEs locations. Consequently, when no SI channels calibration is required, $SF0_{Cal}$ can be omitted from the FD frame structure.

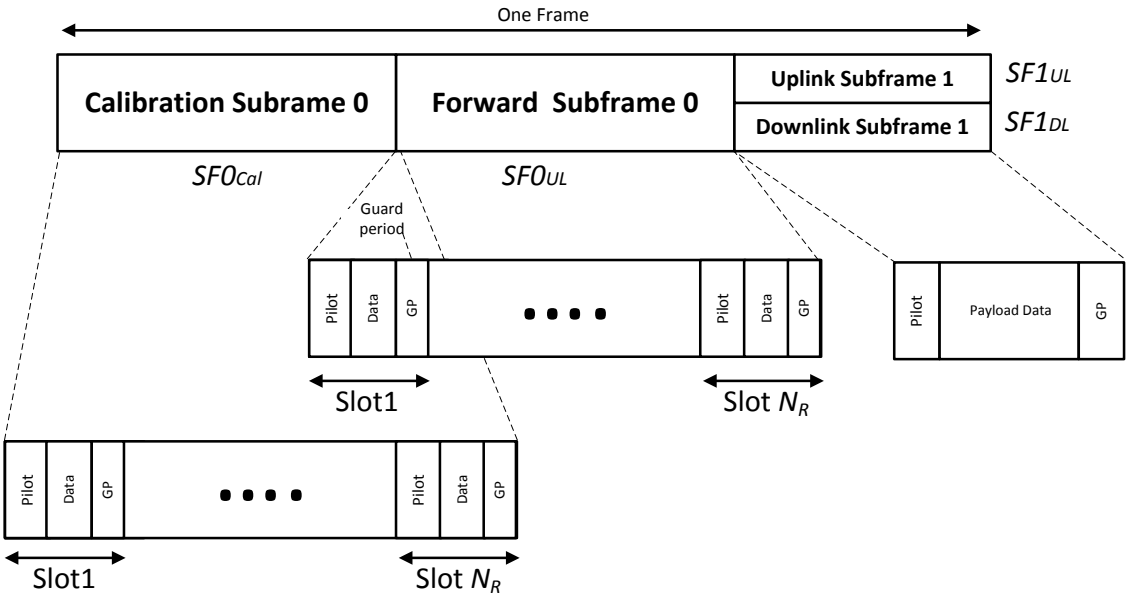

Figure 6.3: FD Frame structure, with SI channels calibration

OFDM Waveform Configuration

The wideband OFDM waveform is used as it is described in many practical communication standards, such as LTE, and 802.11 Wireless Local Area Network (WLAN). The number of subcarriers is $N_{fft} = 2048$, which is the size of the Fast Fourier transform (FFT) in OFDM modulation. Only the central $N_{used} = 300$ subcarriers around the DC subcarrier are active, and the high-frequency subcarriers are inactive with zero values. The DC subcarrier has a zero value to omit the DC offset that affects the dynamic range of the AWG DACs and DSA ADCs. The subcarrier spacing is $\Delta_F = 15$ kHz as in the LTE standard. Hence, the bandwidth of the waveform can be calculated as $B = N_{used}\Delta_F = 4.5$ MHz. The waveform in the baseband has a sampling rate of $F_s = 30.72$ MHz, so the sampling period $T_s \approx 32.55$ ns. The number of samples for CP is $N_{cp} = 256$, which has the time duration of $\tau_{cp} = N_{cp}T_s = 8.33\ \mu s$. Therefore, one OFDM symbol, including CP, occupies the time duration $\tau_{sym} = 1/\Delta_F + \tau_{cp} = 75\ \mu s$.

Pilot-payload-block Structure

Fig. 6.4 depicts the structure of one pilot-payload-block in the time-frequency domain. Each OFDM subcarrier is denoted as a square box. Each column of N_{fft} subcarriers denotes one OFDM symbol in the frequency domain. As mentioned earlier, in an OFDM symbol, only the

central N_{used} subcarriers are active to carry pilots or payload data, while the other subcarriers are inactive. The active subcarriers are called Resource Elements(RE). In the first OFDM symbol, the REs carry only pilots, while the REs in the rest OFDM symbols carry payload data. The pilots in the first OFDM symbol are arranged in interleaved configuration with the separation of P_{plt}, and the pilots of different users are allocated with different REs to keep orthogonality among them as shown in the figure. There are totally $N_D^{(0)}$ and $N_D^{(1)}$ OFDM symbols for the payload data in $SF0$ and $SF1$, respectively.

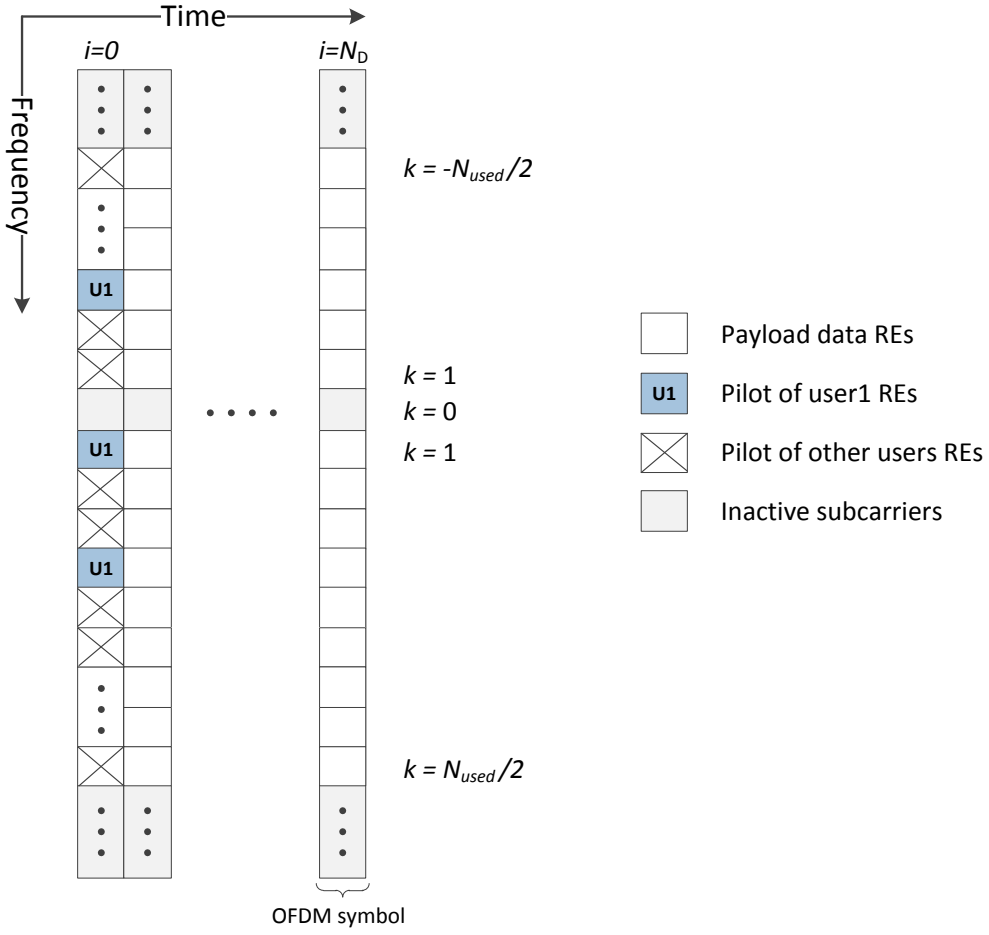

Figure 6.4: Pilot-payload-block structure and the REs allocation for user-1 pilots

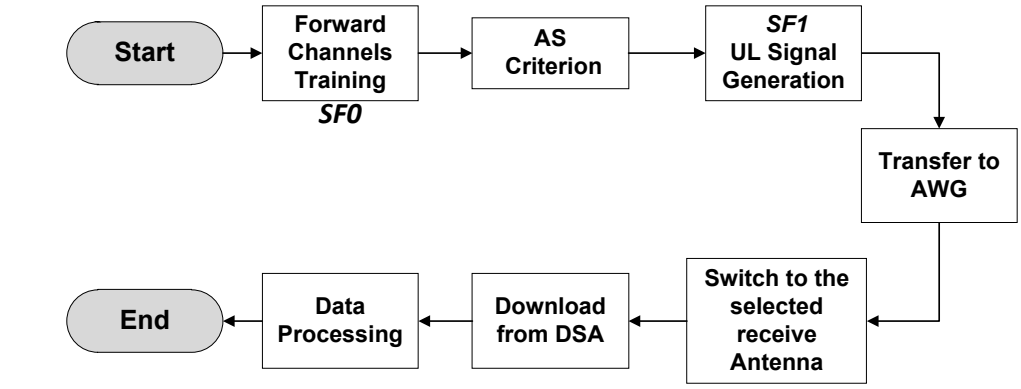

(a)

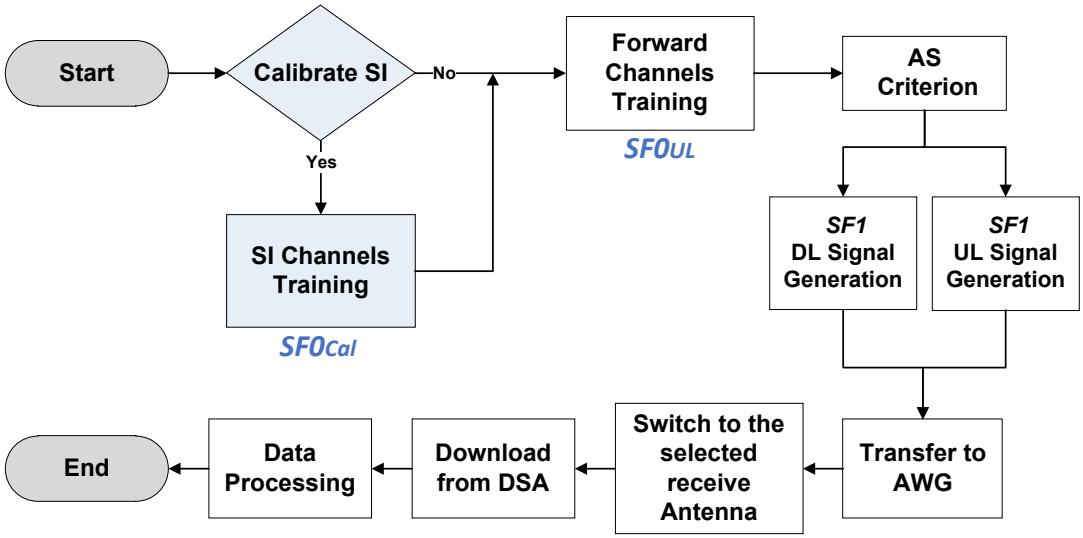

(b)

Figure 6.5: Flowchart of the experiment (a) HD (b) FD with SI channel calibration

6.2.3 Transmission and Reception Workflow

Fig. 6.5a and 6.5b describe the workflow of the HD AS system and the FD AS system in the experiment respectively.

In the HD scenario, the first stage is to train the uplink forward channels. The estimation of the channel and SNR value is done for each receive antenna at the BS. After the AS criterion is deployed, and the best receive antenna is selected, $SF1$ is transmitted and received using the selected antenna and further signal processing on the received data is performed in MATLAB.

In the FD scenario, if the SI channels information has not been estimated yet, or it must be calibrated, the first stage is the training of the SI channels, i.e., the channels between the BS's DL transmitter and each of its receive antennas. This can be done by transmitting and receiving $SF0_{Cal}$, so that the SI channel matrix is estimated and the SI signal power at each receive antenna is measured. Note that the payload in $SF0_{Cal}$ may be omitted, but it is kept here only for the sake of design symmetry. Next, $SF0_{UL}$ is used in order to estimate the forward uplink channel and the signal power at each receive antenna. Afterward, one of the suggested FD AS criteria is deployed, and the best receive antenna is selected. The uplink and downlink $SF1$ signals are transmitted simultaneously, and the UL reception is realized using the selected antenna.

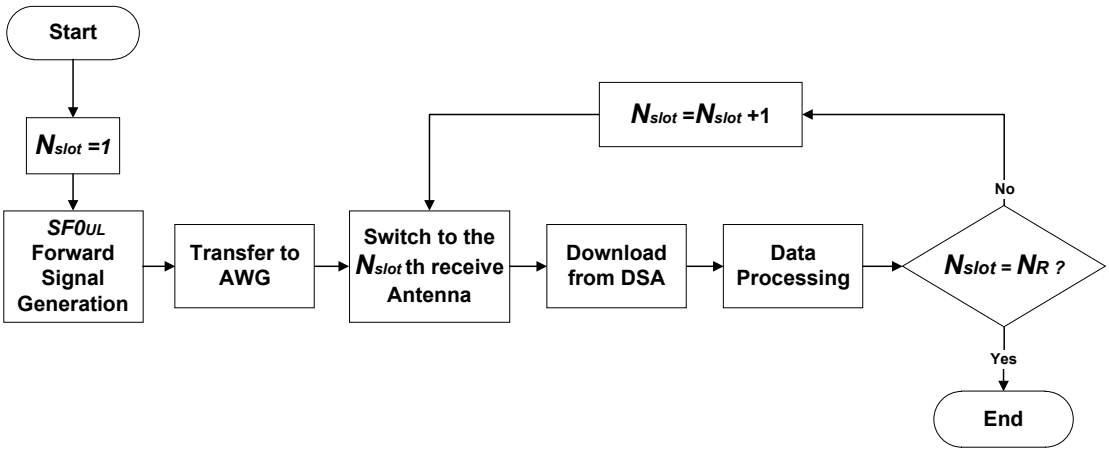

Figure 6.6: Channel estimation flowchart

Fig. 6.6 shows the workflow of the forward channels' training stage. The data of the first slot in $SF0_{UL}$ are generated and then transferred to AWG, where they stored and transmitted repeatedly. The RF switch then operates during the guard period of the slot to switch to the corresponding receive antenna. The DSA then collects the received data and transfers them to the controlling PC to be processed in MATLAB. The cycle of switching-receiving is repeated until N_R slots data are received using the corresponding N_R receive antennas so that all the forward channels are estimated. Note that the channel training has the same stages, whether it is HD or FD operating scenario, and whether the uplink or the SI channels are being estimated, the difference is the training subframe that is being used in the training process.

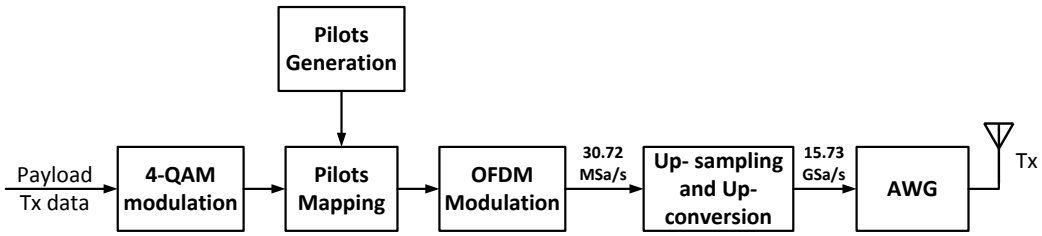

Figure 6.7: Transmission Signal Processing

6.3 Signal Processing in the Testbed

6.3.1 Signal Processing Chain

The sequence of signal processing stages at the transmitter's side of the experiment is presented in Fig. 6.7. The transmit payload data are digitally modulated into 4-QAM with a gray-coded signal constellation, the training pilots are generated and then mapped to the payload symbols. Afterward, the OFDM signal is digitally generated with a sampling rate of 30.72 MSa/s. The OFDM waveform parameters are presented in Table 6.1. The baseband signal is then up-sampled to the AWG's required sampling rate of 15.73 GSa/s, and up-converted to the carrier frequency of 5.2 GHz. The wideband OFDM signal is then transferred to the AWG to be transmitted using the transmit antenna. It must be notified here, that the signal processing stages are similar for the uplink and the downlink signals transmissions, yet the differences are, that each transmission case uses different transmit payload data, and is carried out by using a dedicated AWG channel. It is worth mentioning here, that the OFDM samples in the time domain are Gaussian-like with a high peak to average power ratio (PAPR). In order to use the full dynamic range of the AWG DACs, which means increasing the average transmit power with the fixed full-scale AWG DACs, the PAPR has to be reduced before the AWG DAC. In this experiment, the PAPR reduction is made using the conventional clipping method [150] as explained later.

At the receiver, the wideband OFDM signals are received using one of the receive antennas and then directed to the DSA for analog to digital conversion, where the determined sampling rate for the DSA is 20 GSa/s, the wideband signal is then down-sampled with the baseband OFDM sampling rate of 30.72 MSa/s, and down-converted to the baseband frequency. Afterward, the signal is OFDM demodulated to get the training pilots and payload symbols. The training pilots are used for channel and power estimation, where the payload symbols are 4-QAM demodulated, and the resulting received bitstream is used to calculate the BER of this transmission

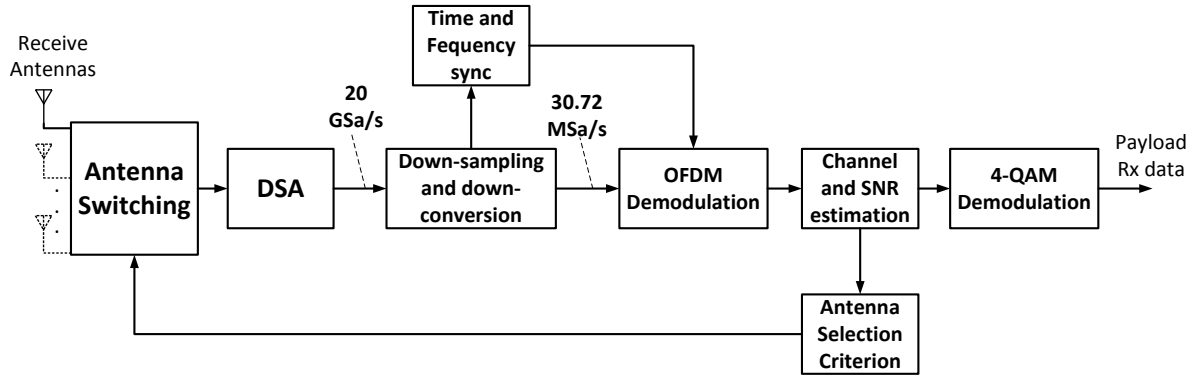

Figure 6.8: Reception Signal Processing

by comparing it to the transmitted payload bitstream. Since no channel coding is implemented in the testbed, the calculated error rate here is uncoded BER.

Table 6.1: Table of OFDM waveform parameters

OFDM Parameter	Value
Carrier Frequency, F_c	5.2 GHz
FFT Size, N_{fft}	2048
Subcarrier Spacing, Δ_f	15 KHz
Number of used Subcarriers, N_{used}	300
Bandwidth, B	4.5 MHz
Sampling Rate, F_s	30.72 MSa/s
Cyclic Prefix Duration, τ_{cp}	8.33 μs
OFDM Symbol Duration, τ_{symb}	75 μs
Modulation Scheme	4-QAM

6.3.2 Signal Processing Modules

After the main functions of the signal processing chain were outlined, the implementation of some key modules will be explained in detail in this subsection.

Pilot generation

The pilots are generated based on LTE standards as shown in [151]. Assuming P_{plt} is the period of pilot REs, the number of pilot symbols for each user is $N_{plt} = N_{used}/P_{plt}$. The pilot symbols for each user are generated using Gold code as

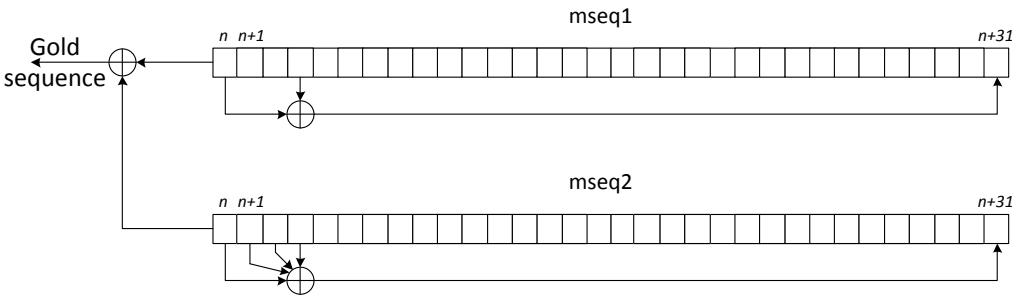

Figure 6.9: Gold code generation using shifting registers

$$x_{plt}(m) = \sqrt{\frac{\delta_{boost}}{2}}(1-2c_{gld}(2m))+j\sqrt{\frac{\delta_{boost}}{2}}(1-2c_{gld}(2m+1)), m = 0, 1, ..., N_{plt}-1, \quad (6.1)$$

where δ_{boost} is the pilot power boosting factor over the payload data REs to improve the performance of channel estimation and synchronization. $c_{gld}(.)$ is a Gold code with order-31, generated by shifting registers shown in Fig. 6.9. The Gold code is derived from the modulo-2 addition of two maximum-length sequences as $c_{gld}(n) = (x_{mseq1}(n + N_{shft}) + x_{mseq2}(n + N_{shft}) mod 2$, where N_{shft} is fast-forward value used to reduce the correlation between sequences, and the two maximum-length sequences are calculated, as shown in the figure, by

$$\begin{aligned} x_{mseq1}(n + 31) &= (x_{mseq1}(n + 3) + x_{mseq1}(n)) mod 2, \\ x_{mseq2}(n + 31) &= (x_{mseq2}(n + 3) + x_{mseq2}(n + 2) + x_{mseq2}(n + 1) + x_{mseq2}(n)) mod 2. \end{aligned} \quad (6.2)$$

OFDM modulation/demodulation with CP

The diagram of OFDM modulation [152] is shown in Fig. 6.10 . First, a serial to parallel convertor is used to rearrange the constellation modulated symbols. The key function of OFDM modulation is the Inverse Fast Fourier transform (IFFT). IFFT block transforms the frequency domain constellation $x_{fd}(u, k)$ to the time domain date $x_{td}(u, n)$, where $x_{fd}(u, k)$ denotes the constellation symbol of the u_{th} user and k_{th} subcarrier in the frequency domain. This process

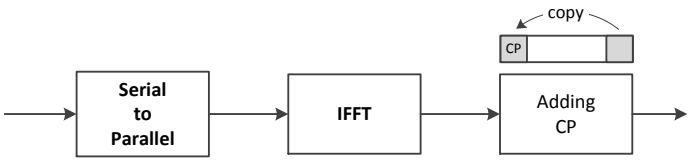

Figure 6.10: OFDM modulation block in details

can be expressed as

$$x_{td}(u,n) = \frac{1}{N_{fft}} \sum_{k \in \mathcal{U}} x_{fd}(u,k) e^{\frac{j2\pi kn}{N_{fft}}}, n = 0, 1, ..., N_{fft} - 1, \tag{6.3}$$

where $\mathcal{U}$ is the set of the active subcarriers in one OFDM symbol. After IFFT, the end part of the time-domain samples is copied to the beginning of the OFDM symbol to produce the Cyclic Prefix (CP). CP aims to protect against the inter-symbol interference (ISI) caused by multipath channels. Besides, the redundancy included by CP can also be utilized by the following signal processing, e.g., timing synchronization. The OFDM demodulation is just the reverse of OFDM modulation, which means removing the CP, FFT, and parallel to serial conversion.

Digital up/down-sampling/conversion

An antialiasing FIR lowpass filter with N_{fir} order is used to make the digital up/down-sampling. Towards the AWG, the up-sampling of the OFDM modulation output is done with a ratio $F_{s,awg}/F_s$, meanwhile, the down-sampling is done from the DSA with a ratio $F_s/F_{s,dsa}$.

In the transmitter, after the up-sampling, the signal is up-converted from the baseband to the RF-band. For the nth sample of the uth up-sampled sequence $x_{upsam}(u,n)$, where $u = 1, 2, ..., N_U$, the up-converted sequence $x_{upcon}(u,n)$ can be obtained, by frequency shifting, as

$$x_{upcon}(u,n) = x_{upsam}(u,n) e^{j2\pi F_c n T_{s,awg}}. \tag{6.4}$$

Meanwhile, the down-conversion is the reversed process as

$$x_{downcon}(l,n) = x_{dsa}(l,n) e^{-j2\pi F_c n T_{s,dsa}}, \tag{6.5}$$

where $x_{dsa}(l, n)$ is the nth sample of the lth DSA output data stream, $l = 1, 2, ..., L$.

PAPR reduction

OFDM signals can have high peak values in the time domain since many subcarrier components are added via the IFFT operation. Thus, OFDM systems are known to have a high PAPR when compared to single-carrier systems. The high PAPR is one of the most harmful features in an OFDM system as it decreases the signal-to-quantization noise ratio (SQNR) of ADC and DAC. The reduction of PAPR allows using the full dynamic range of the convertors. In this experiment, the PAPR reduction is based on the conventional clipping method that clips the samples that exceed the threshold [150].

Assuming that the maximum magnitude of the transmitted sequence $\mathbf{x}_{upcon}(u, n)$ is $\mathbf{x}_{max,u}$, then the threshold can be defined by $\eta_u = \alpha \mathbf{x}_{max,u}$, where α is a fixed factor, set to 0.8 in the experiment. The clipped signal can be written as

$$\mathbf{x}_{clip}(u, n) = \begin{cases} x_{upcon}(u, n), & |x_{upcon}(u, n)| \leq \eta_u, \\ \frac{x_{upcon}(u,n)}{|x_{upcon}(u,n)|}\eta_u, & |x_{upcon}(u, n)| > \eta_u. \end{cases} \tag{6.6}$$

Synchronization

Both parts of the synchronization, time and frequency synchronization, are crucial to the receiver.

The time synchronization aims to find the first sample of the OFDM symbols for the OFDM demodulation. The frequency synchronization is to compensate the residual frequency offset between the AWG and DSA Although the AWG and DSA share the same reference clock, the measured residual frequency offset in the experiment is about 100 Hz.

The time synchronization is done as in [153], where the CP auto-correlation method with Maximum Likelihood (ML) estimation is used. The method employs the redundant information introduced by the CP in OFDM symbols. First, the observation interval of DSA should be defined. Since the transmit data is sent slot-by-slot, the observation interval in general should be at least twice of the slot duration to guarantee that a complete slot will be observed. However, in this experiment, the AWG uses a "continuous" configuration mode. That means that the AWG repeats the slot data continuously, which allows the cyclic auto-correlation to be used. In this case, the observation interval is only one slot, which is enough to find the start sample, and

finally performs a cyclic shift to get the required slot data. The cyclic auto-correlation can be calculated by

$$r(n) = \sum_{n=m}^{N_{samslot}-1} x_{downcon}(n) x^*_{downcon}((n + N_{fft}) \text{mod}\, N_{samslot}), \tag{6.7}$$

where $N_{samslot}$ is the number of samples in one slot. Since there are multiple OFDM symbols in one slot, multiple peaks can be expected in $|r(n)|$, which causes ambiguity to decide the start sample index of the slot. However, if the power boosting factor δ_{boost} is enough to guarantee large pilot, then the start sample index can be determined by the maximum peak of $r(n)$

$$n_0 = \arg\min_n |r(n)|. \tag{6.8}$$

Then based on the ML method in [153], the frequency offset can be estimated as

$$\Delta f_{off} = -\frac{1}{2\pi} \angle r(n_0). \tag{6.9}$$

In case that $n_0 + N_{fft} + N_{cp} > N_{samslot}$, the former smaller peak, i.e., with the index of $n_0 - N_{fft} - N_{cp}$, are used to estimate the frequency offset, which guarantees the constant N_{fft} samples offset between CP samples and the OFDM tail samples in the sequential time.

Channel estimation

For the antenna selection system, the multi-antenna channels are estimated from the transmit antennas to the receive antennas based on the time-domain Least Square (LS) based method in [154]. The same estimation method is used for both forward UL channels, and SI channels. For the uth user and the lth receive antenna, the observations on the pilot subcarriers (REs) in the frequency domain are

$$[\mathbf{y}_l]_{\mathcal{P}_u} = [\mathbf{h}_{lu}]_{\mathcal{P}_u} \odot [\mathbf{x}_u]_{\mathcal{P}_u} + [\mathbf{w}_l]_{\mathcal{P}_u}, \tag{6.10}$$

where $\mathbf{x}_l$, $\mathbf{y}_l$ and $\mathbf{w}_l$ are the uth transmit vector, lth receive vector and lth noise vector, respectively; $\mathbf{h}_{lu}$ is the channel response vector of the uth user and lth receive antenna in the frequency domain; $\mathcal{P}_u$ is the pilot index set of the uth user. The Hadamard multiplication form in (6.10)

can also be expressed as a matrix multiplication

$$[\mathbf{y}_l]_{\mathcal{P}_u} = [\mathbf{X}_u]_{\mathcal{P}_u,\mathcal{P}_u}[\mathbf{h}_{lu}]_{\mathcal{P}_u} + [\mathbf{w}_l]_{\mathcal{P}_u}, \tag{6.11}$$

where $\mathbf{X}_u$ is a diagonal matrix with the elements in $\mathbf{x}_u$ as diagonal entries. The channel response $\mathbf{h}_{lu}$ in the frequency domain is the Fourier transform of the channel impulse response in the time domain. In OFDM modulation, the Fourier transform is approximated by Discrete Fourier Transform (DFT)

$$\mathbf{h}_{lu} = \mathbf{F}\mathbf{g}_{lu}, \tag{6.12}$$

where $\mathbf{F}$ is the $N_{fft} \times N_{fft}$ DFT matrix; $\mathbf{g}_{lu} \in \mathbb{C}^{N_{fft} \times 1}$ is the discrete time-domain channel impulse response. Thus, (6.11) can be rewritten as

$$[\mathbf{y}_l]_{\mathcal{P}_u} = [\mathbf{X}_u]_{\mathcal{P}_u,\mathcal{P}_u}[\mathbf{F}]_{\mathcal{P}_u}\mathbf{g}_{lu} + [\mathbf{w}_l]_{\mathcal{P}_u}. \tag{6.13}$$

In this equation, there are more variables (N_{fft} which is the length of $\mathbf{g}_{lu}$) than the number of equations (N_{plt} which is the number of pilots). This makes (6.13) is underdetermined to estimate $\mathbf{g}_{lu}$. However, as the channel path power only concentrates in the first multiple taps, supposing K_g taps, in $\mathbf{g}_{lu}$, accurate LS estimation of the channel can be obtained if $K_g \ll N_{plt}$, which is expressed by

$$[\hat{\mathbf{g}_{ul}}]_{\mathcal{Q}} = ([\mathbf{F}]^H_{\mathcal{P}_u,\mathcal{Q}}[\mathbf{F}]_{\mathcal{P}_u,\mathcal{Q}})^{-1}[\mathbf{F}]^H_{\mathcal{P}_u,\mathcal{Q}}[\mathbf{X_u}]^{-1}_{\mathcal{P}_u,\mathcal{P}_u}[\mathbf{y_l}]_{\mathcal{P}_u}, \tag{6.14}$$

where the set $\mathcal{Q} = \{1, 2, \cdots, K_g\}$. Note that if $K_g > \mathbf{N}_{plt}$, the matrix $([\mathbf{F}]^H_{\mathcal{P}_u,\mathcal{Q}}[\mathbf{F}]_{\mathcal{P}_u,\mathcal{Q}})^{-1}$ in (6.14) is non-invertible, which can be addressed by a regularization factor δ_{reg}, resulting in

$$[\hat{\mathbf{g}_{ul}}]_{\mathcal{Q}} = ([\mathbf{F}]^H_{\mathcal{P}_u,\mathcal{Q}}[\mathbf{F}]_{\mathcal{P}_u,\mathcal{Q}} + \delta_{reg}\mathbf{I}_{K_g})^{-1}[\mathbf{F}]^H_{\mathcal{P}_u,\mathcal{Q}}[\mathbf{X_u}]^{-1}_{\mathcal{P}_u,\mathcal{P}_u}[\mathbf{y_l}]_{\mathcal{P}_u}, \tag{6.15}$$

In this experiment, the regularization factor $\delta_{reg} = 0.01$ is validated to be able to achieve stable channel estimation results. Finally, DFT is applied to the estimated channel impulse response $\hat{\mathbf{g}}_{lu}$ to obtain the channel response on all of the used subcarriers

$$\hat{\mathbf{h}}_{lu} = [\mathbf{F}]_{\mathcal{U},\mathcal{Q}}[\hat{\mathbf{g}}_{lu}]_{\mathcal{Q}}, \tag{6.16}$$

SNR and SSINR estimation

At first, the signal power and the noise power should be estimated. Then the SNR is estimated by the ratio of the estimated signal power and noise power. For signal power estimation with the linear system model in the frequency domain, the observation vector on the kth subcarrier is

$$\mathbf{y}_k = \hat{\mathbf{H}}_k \mathbf{x}_k + \tilde{\mathbf{w}}_k, \tag{6.17}$$

where $\hat{\mathbf{H}}_k \in \mathbb{C}^{N_R \times N_U}$ is the estimated channel matrix; $\tilde{\mathbf{w}}_k$ is the noise plus channel estimation error. The total signal power by N_R receive antennas can be estimated by

$$\begin{aligned} P_{\text{sig}} &= \mathbb{E}\{\text{tr}\{\hat{\mathbf{H}}_k \mathbf{x}_k \mathbf{x}_k^H \hat{\mathbf{H}}_k^H\}\} \\ &= \text{tr}\{\hat{\mathbf{H}}_k \mathbb{E}\{\mathbf{x}_k \mathbf{x}_k^H\} \hat{\mathbf{H}}_k^H\}. \end{aligned} \tag{6.18}$$

Note that $\mathbb{E}\{\mathbf{x}_k \mathbf{x}_k^H\} = \mathbf{I}_{N_U}$ assumed in the system model. Thus, the total signal power is

$$\begin{aligned} P_{\text{sig}} &= \text{tr}\{\hat{\mathbf{H}}_k \hat{\mathbf{H}}_k^H\} \\ &= ||\hat{\mathbf{H}}_k||_{\text{F}}^2. \end{aligned} \tag{6.19}$$

Based on that, the average signal power per subcarrier and per receive antenna is

$$\bar{P}_{\text{sig}} = \frac{1}{N_R N_{used}} \sum_{k=1}^{N_{used}} ||\hat{\mathbf{H}}_k||_{\text{F}}^2. \tag{6.20}$$

By neglecting the channel estimation error compared to the signal and the noise power, the noise power can be approximately calculated by

$$\bar{P}_{\text{noise}} = \bar{P}_{\mathbf{y}} - \bar{P}_{\text{sig}}, \tag{6.21}$$

where $\bar{P}_{\mathbf{y}}$ is the average total receive power per subcarrier and per receive antenna. Clearly, the accuracy of the noise power estimation, in this case, depends on the accuracy of channel estimation. When the error of the channel estimation is high, the noise power estimation will be dominated by the channel estimation error. The dominance of the channel estimation error is significant especially when SNR is high (18 dB observed in the experiment). Thus, the noise

power should be estimated independently to the signal power. Instead, the time domain CP data is used to estimate the noise power as in [155]. As mentioned earlier, considering the maximum channel delay is K_g taps, where $K_g < N_{cp}$, the CP samples with indices $\mathcal{P}_1 = \{K_g + 1, K_g + 2, \cdots, N_{cp}\}$ in one OFDM symbol are free of inter-symbol-interference. Hence, the noise power can be estimated in the time domain

$$\bar{P}_{\text{noise,td}} = \frac{1}{N_U(N_{cp} - K_g)} \sum_{l=1}^{N_R} \sum_{n \in \mathcal{P}_1} |x_{downcon}(l, n) - x_{downcon}(l, n + N_{fft})|^2. \tag{6.22}$$

Then, the noise power per subcarrier in the frequency domain can be directly obtained by

$$\bar{P}_{\text{noise}} = \bar{P}_{\text{noise,td}} \frac{||\mathbf{F}||_{\text{F}}^2}{N_{fft}}. \tag{6.23}$$

When the DFT matrix $\mathbf{F}$ is normalized, then $\bar{P}_{\text{noise}} = \bar{P}_{\text{noise,td}}$. Finally, the average SNR on each subcarrier is obtained by

$$\rho_{\text{est}} = \frac{\bar{P}_{\text{sig}}}{\bar{P}_{\text{noise}}}. \tag{6.24}$$

Note that the SNR of the system should be defined at the receive antenna side, rather than in the digital baseband. Therefore, the above estimated SNR in the digital baseband should be calibrated by taking the insertion loss of the RF switches into account

$$\rho_{\text{est,as,dB}} = \rho_{\text{est,dB}} + \beta_{\text{IL,switch}}, \tag{6.25}$$

where $\rho_{\text{est,dB}} = 10 \log_{10}(\rho_{\text{est}})$; $\beta_{\text{IL,switch}}$ is the insertion loss of the RF switches in decibel. Through measurement, it is $\beta_{\text{IL,switch}} = 3$ dB.

For the estimation of SSINR, the SI power has to be estimated. The estimation is done as the presented scheme for signal power estimation, where the SI power is the signal power which is transmitted through the SI channels during the calibration subframe.

Antenna selection in wideband systems

After the estimation of SNR, SSINR, and forward/SI channels, the antenna selection is performed using the three criteria which were explained in Section 5.3.

6.4 Testbed Integration and Measurement Environment

As explained in the previous sections, the testbed consists of several hardware entities and complicated digital signal processing modules. Hence, to develop the final FD testbed, a careful and appropriate integration strategy is necessary, as a failure of a single module fails the whole testbed. The integration strategy used in the development of this testbed is shown in Fig. 6.11. The strategy is to start from a basic setup to more complicated configurations to reach the final setup. The integration procedure is divided into five steps.

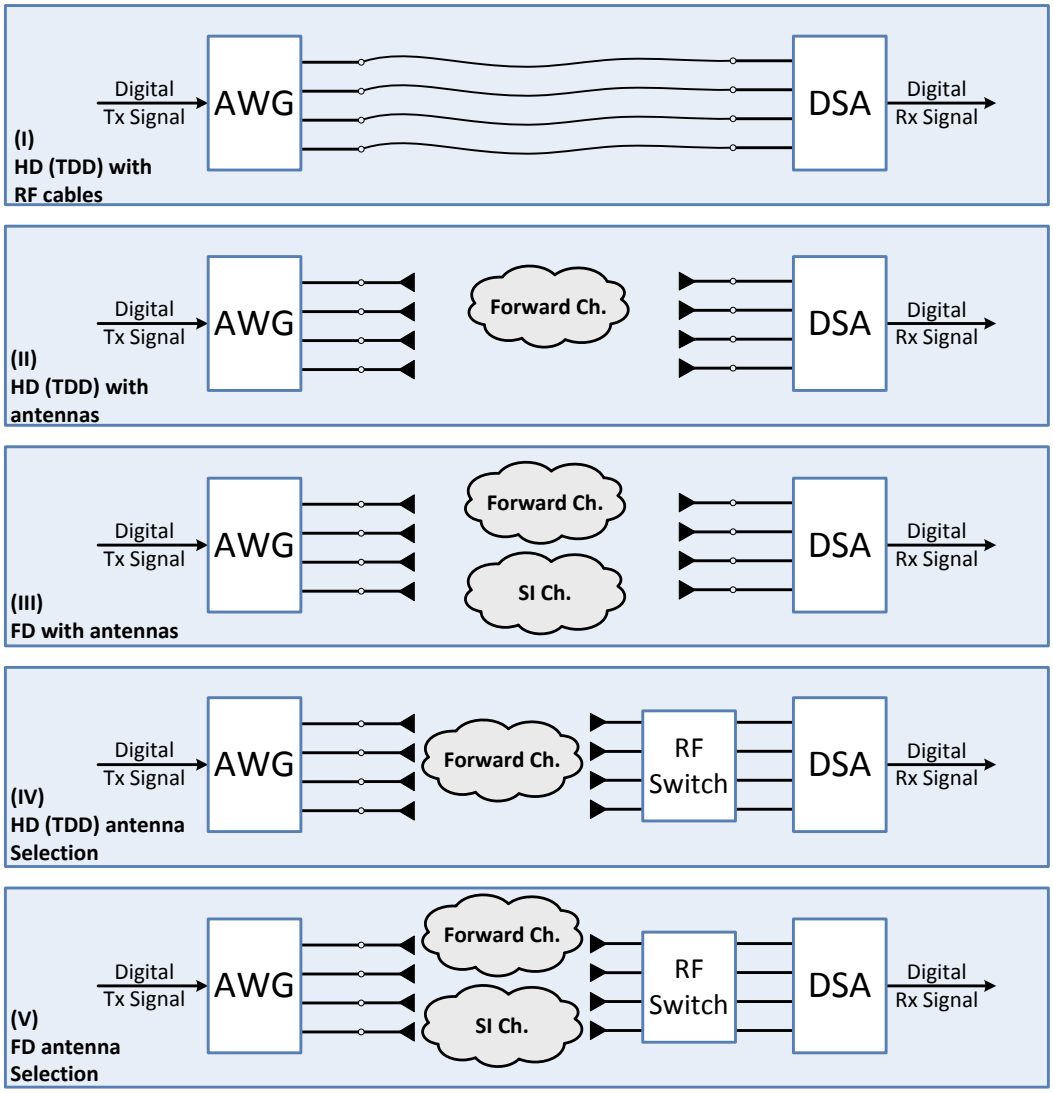

Figure 6.11: FD testbed development strategy

In step (I), the RF cables are used to directly connect the transmitter and the receiver. For each port, a SISO HD (with TDD) system with a single RF cable is set up, which aims to enable the communication-data and device-control links between the PC and AWG/DSA. Another aim is to implement and verify many digital signal processing modules described earlier, e.g., pilot generation, OFDM (de)modulation, synchronization. In a certain time slot, only one transmission port is activated in AWG. In step (II), the RF cables are replaced with antennas in order to test the signal processing models with real wireless channels. The transmission ports are activated consecutively as in Time Division Multiple Access (TDMA). The involved digital signal processing modules are verified to ensure their robustness over multipath-fading channels. The next two steps are done separately, where one of them aims to achieve FD transmission, and the other is to enable and verify AS in the HD transmission mode. The FD transmission is considered in step (III), where the transmission is activated on all the AWG ports at the same time. The BS receiver, in this step, suffers from the high power of DL SI signal. In step (IV), the RF switch is added at the receive side to employ the antenna selection system in HD transmission mode. The associated control functionality from PC to the RF switch via the Arduino board is executed and verified. Finally, in step (V), the FD transmission is activated with AS to finalize the testbed setup and verify the system performance. Fig. 6.12 shows the implemented testbed in the lab.

Different SNR values at the receiver's side are achieved in the measurements. Ten output voltage values of the AWG's output for the uplink signal transmission are used, which correspond to ten transmission power values as denoted in Table 6.2. The AWG's output level for the DL SI transmission signal is always set to the maximum possible output value of (1 [V]), which corresponds to about 0 dBm transmission power. The UL signal transmission is conducted at different UE-BS separation distances between 1m and 4m and considering the line of sight communication scenario. These separation distances correspond to path loss from 45 to 60 dB. Consequently, the received power levels at the femto BS receiver are between -45 and -80 dBm. The distance between the Tx antenna and the closest Rx antenna is about 26cm, which equals to 9 times of the half wavelength. This distance provides far-field propagation and achieves about 35 dB of SI isolation. In order to increase the accuracy of the measurement results, the experiment is repeated for at least twenty times for each transmission power value, and the average results are then considered. When the experiment operates in the presence of the SI signal in the FD scenario, the SI channels are calibrated once for every ten trials of the experiment, considering

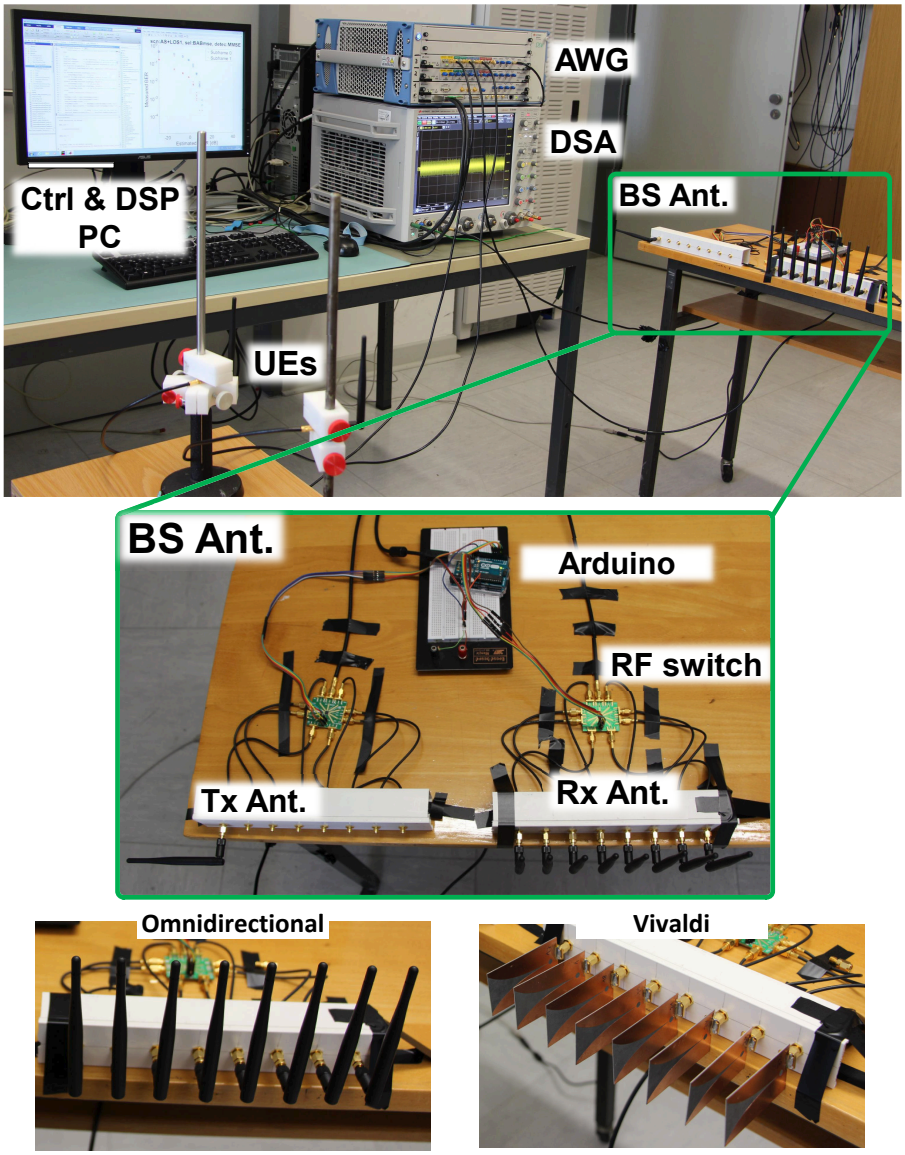

Figure 6.12: The implemented FD antenna selection testbed

that, the SI channels have much fewer channel variations than the forward channels.

Finally, the measurement configuration parameters are shown in Table 6.3, and the layout of the measurement room is shown in Fig. 6.13.

6.5 Testbed Measurement Results

6.5.1 HD Antenna Selection

The measurement results of the HD MSNR AS criterion are presented in Fig. 6.14. It shows the BER performance with and without applying the HD AS criterion at two different UE-BS

Table 6.2: Measured uplink transmission power levels

AWG's output volatge [V]	0.1	0.2	0.3	0.4	0.5	0.6	0.7	0.8	0.9	1
UL transmit power [dBm]	-19	-13.4	-10.1	-7.8	-6.1	-4.8	-3.6	-2.5	-1.6	-0.7

Table 6.3: Testbed configuration parameters

Parameter	Value	Description
F_c	5.2 [GHz]	Carrier frequency
F_s	30.72 [MSa/s]	Sampling rate in baseband
$F_{s,awg}$	15, 73 [GSa/s]	Sampling rate of AWG
$F_{s,dsa}$	20 [GSa/s]	Sampling rate of DSA
N_{fft}	2048	FFT size of OFDM
N_{used}	300	The number of active subcarriers
Δ_F	15 [KHz]	Subcarrier spacing
B	4.5 [MHz]	Bandwidth
N_{cp}	256	The number of samples in CP
K_g	128	The number of channel delay taps
P_{plt}	4	Pilot period in frequency domain for each user
τ_{sym}	75 [μs]	Time duration of one OFDM symbol
τ_{cp}	8.33 [μs]	Time duration of one CP
N_R	8	The number of receive antennas
N_U	2	The number of users
$N_D^{(0)}, N_D^{(1)}$	8	The number of payload OFDM symbols in subframe 0 and 1
$\mathcal{A}$	4	Alphabet size of constellation mapping, 4-QAM

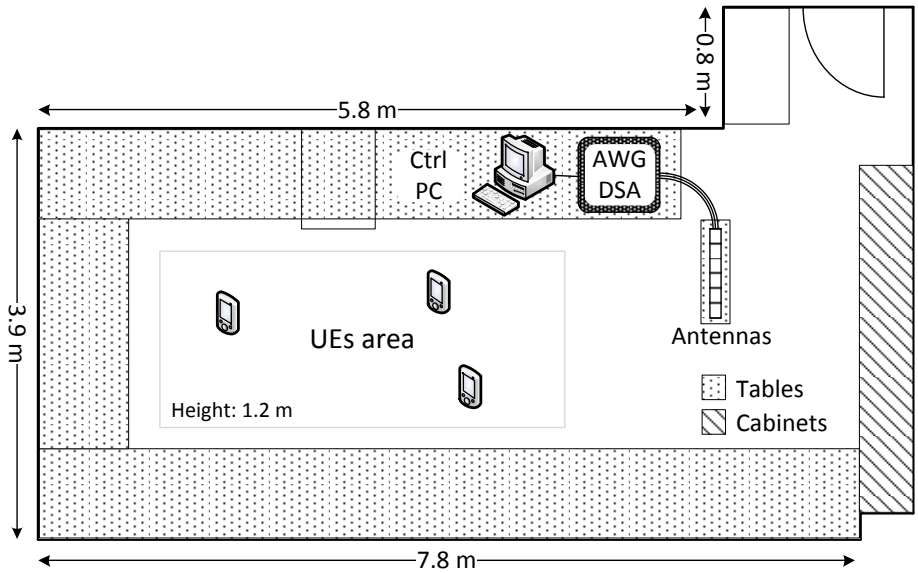

Figure 6.13: The layout of the indoor environment

separation values (1m, 2m). It is evident that applying HD AS criterion overcomes the case when no AS is applied, at both UE-BS separation distances with better BER performances. It can be seen as well, that a better BER performance enhancement is achieved by applying the HD AS criterion at (2m) UE-BS separation, than at (1m) separation, due to better achieved multi-path diversity at (2m) separation.

The sum-rate for the HD case is presented in Fig. 6.15. It is clear that the channel capacity performance for (2m) separation is better than (1m) separation as the channels in the former case have more diversity.

6.5.2 FD AS with three criteria

The three criteria, that were explained in subsection 5.3, are used in the FD system with 8 receive antennas. The BER performance comparison is shown in Fig. 6.16. The three criteria achieve similar BER performances at low SNR values. This can be justified due to the high noise power which causes considerable errors during forward and SI channels estimation. Whereas at high SNR values, the MSSINR criterion overcomes the other two AS criteria. MSNR criterion performs the worst among the three criteria because it only considers the forward channel for the selection.

Fig. 6.17 compares the sum-rate per user performance for the three criteria. MSSINR

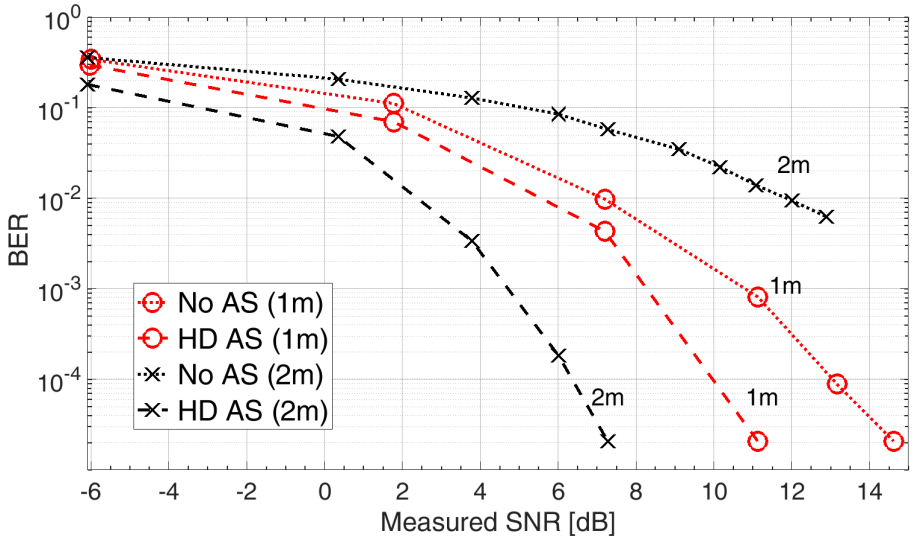

Figure 6.14: HD BER - AS with 8 antennas

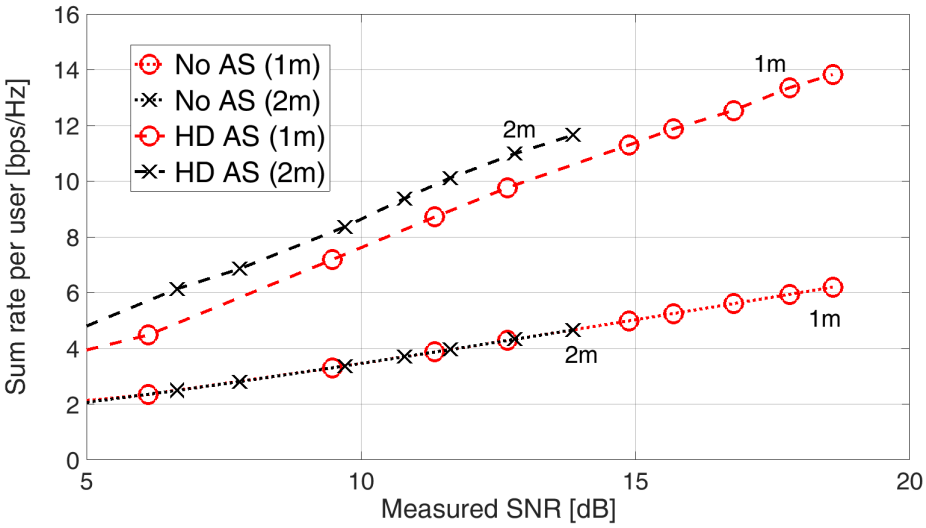

Figure 6.15: HD rate - AS with 8 antennas

achieves slightly better capacity compared to MCGR at low SNRs, meanwhile, they have the same performance when the noise power is much lower than the signal. Such observation can be also seen in Fig. 6.18. The figure shows the enhancement ratio of FD rate over the HD rate. At high SNRs, both MSSINR and MCGR criteria almost reach the theoretical boundary of 2. The residual SI, that can be in some measurements about 3 to 6 dB over the noise, prevents the FD system of exactly doubling the sum rate. Moreover, the PAPR of the OFDM signal and the channels estimation errors cause slight performance degradation. MSNR performance is quite lower compared to the two FD criteria, achieving around 1.45 in best case. Measurements show that SI channel path loss guarantees about 30 to 35 dB of isolation. Besides the digital SIC, which is $\beta = -20$ dB, the AS and cross-polarization provide each about 10 to 15 dB of cancellation. The amount of SIC in propagation and analog domain is α = 55 to 65 dB. The total amount of the achieved SIC is 75 to 85 dB, making SI almost reach the devices measured noise floor which is around -80 dBm.

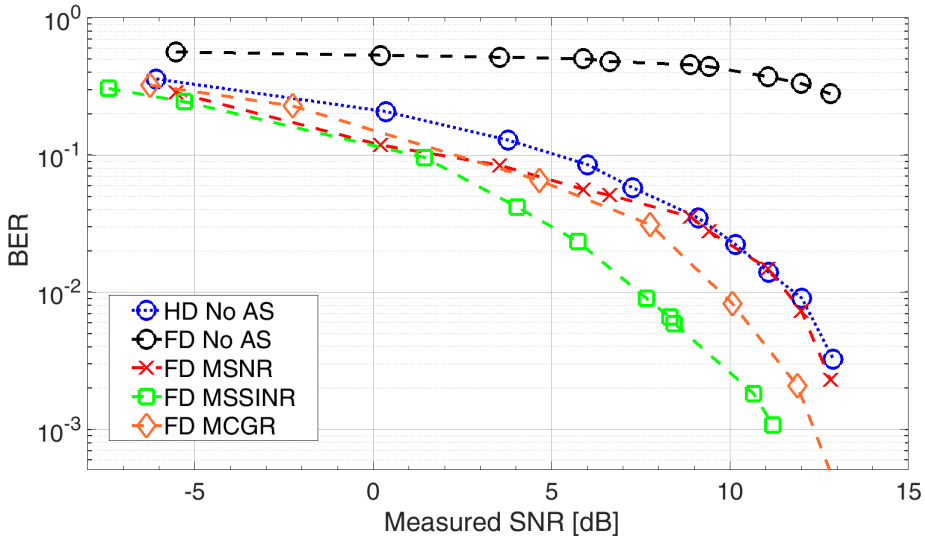

Figure 6.16: FD BER - AS with 8 antennas

The results of the testbed, compared to simulation results, are presented in Fig. 6.19. A slight degradation in the performance is noticed, especially in low SNR range. The reason of that is the channel estimation error which the testbed suffers from, unlike the simulation which assumes a perfect knowledge of the channels.

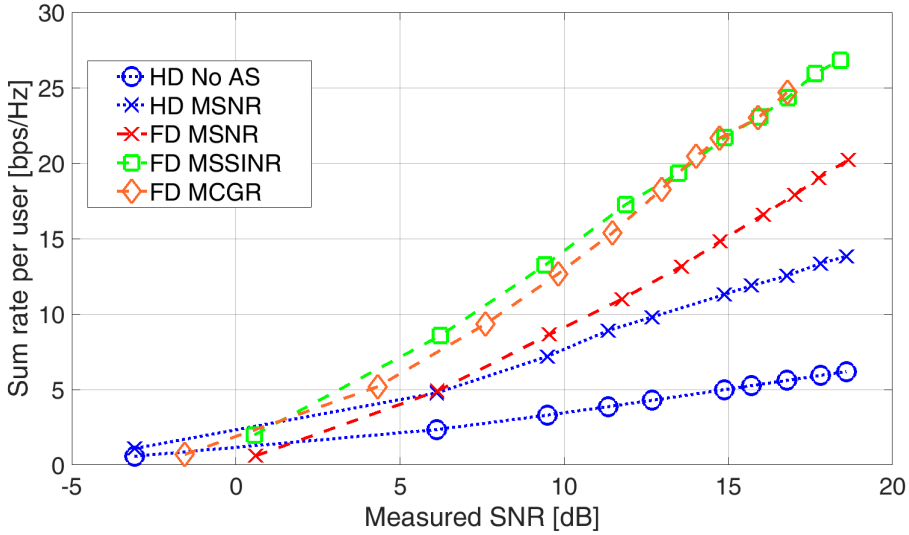

Figure 6.17: FD sum rate - AS with 8 antennas

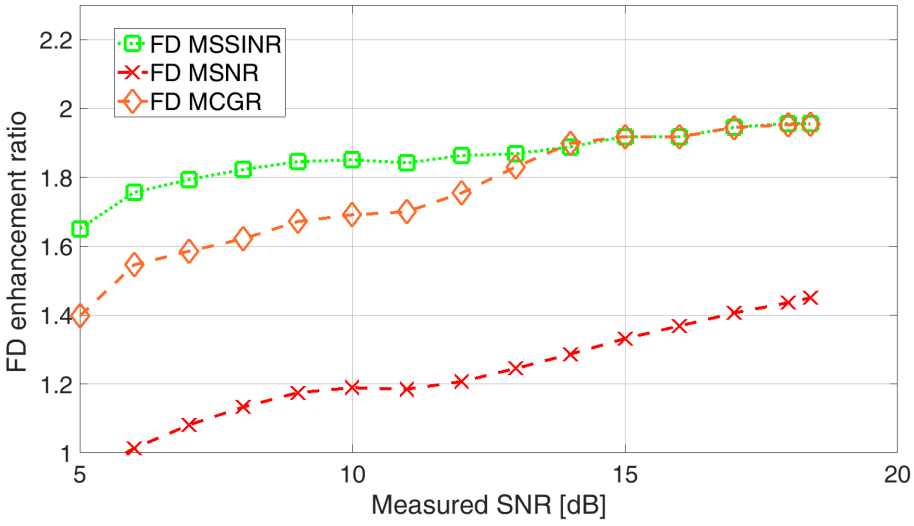

Figure 6.18: FD/HD ratio - AS with 8 antennas

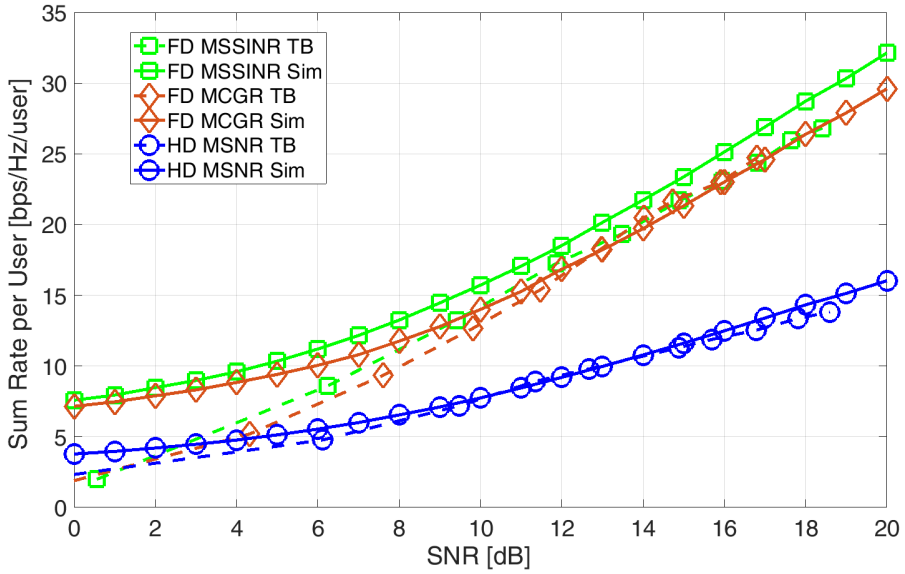

Figure 6.19: Tesbed vs. simulation FD sum rate - AS with 8 antennas

6.5.3 Number of Antennas

The aim here is to measure the effect of the number of receive antennas in the base-station, three cases are considered $N_r \in \{2, 4, 8\}$. In order to compare the performance of the three cases fairly, the residual SI over the noise is measured before applying any digital SIC. This reflects the SI mitigation that can be achieved in the analog domain for each case. RSI can be extracted by subtracting the maximum attainable SSINR, in case of FD, from the maximum attainable SNR of the HD system. Fig. 6.20 shows the measured RSI with the two AS criteria, MSSINR and MCGR. It is clear that for 8 antennas the RSI is below 25 dB, which means less complicated digital SIC is required compared to the case of 2 and 4 receive antennas.

6.5.4 Directional Antennas

Using directional antennas in the base-station provides better SI isolation. Thus, Vivaldi antennas are used with the radiation pattern as in Fig. 6.21. The advantages of Vivaldi antennas are their broadband characteristics and the easy manufacturing using printed circuit board. The 3-dB beamwidth of the used antennas is about 50 degree, this guarantees a better isolation between the transmit and receive antennas in the base-station, and therefore a better FD performance. The UEs antennas, on the other hand, remain omnidirectional in both cases, so only the BS antennas are changed. Fig. 6.22 shows the residual SI in both cases for 8 antennas with two AS criteria,

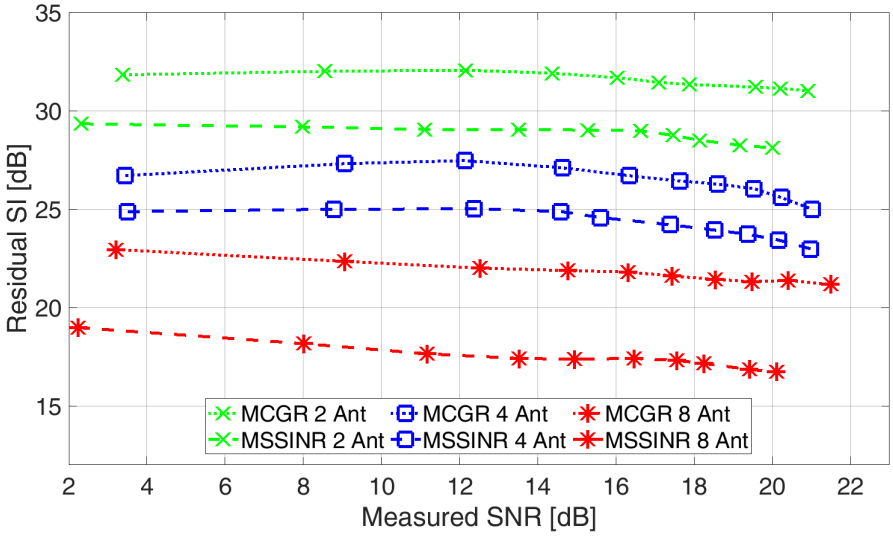

Figure 6.20: RSI in case of different number of antennas

MSSINR and MCGR. It is obvious that the RSI in case of directional antennas is about 7 to 9 dB lower than the omnidirectional antenna. Fig. 6.23 and Fig. 6.24 show the performance enhancement in terms of BER and capacity. Although the benefit of using directional antennas is clear regarding SI isolation, it may cause limitations on BS coverage in some scenarios.

6.5.5 Horizontal and Vertical Antenna Separation

Better isolation can be achieved by changing the type of separation structure between receive and transmit antennas as shown in Fig. 6.25.

By keeping the cross-polarization, and positioning the receive antennas within the axis of transmit dipole antennas, the setup can provide further SI mitigation. Such setup is called ”vertical structure separation” instead of the ”horizontal structure separation” that is used in the previous measurements. However, the geometry of separation is related to the number of antennas which has an impact on the form factor of the designed base-station. Fig. 6.26, Fig. 6.27, and Fig. 6.28 show the performance evaluation of the two separation types in terms of RSI, BER, and capacity.

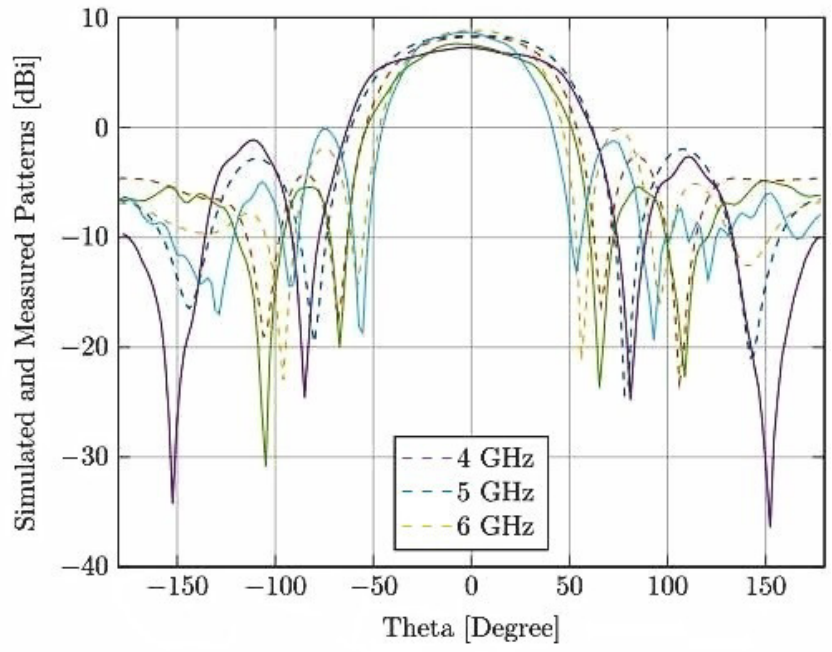

Figure 6.21: Vivaldi directional antenna pattern

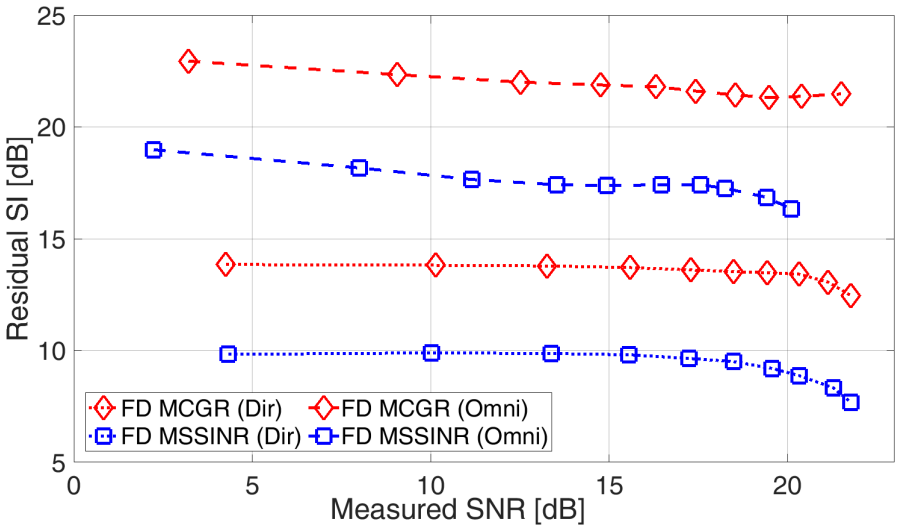

Figure 6.22: RSI with directional antennas

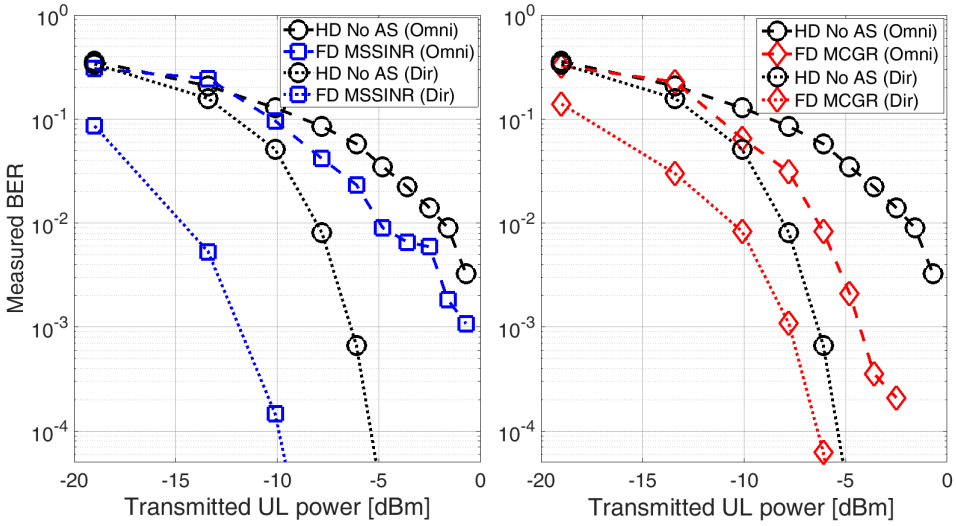

Figure 6.23: BER with directional antennas

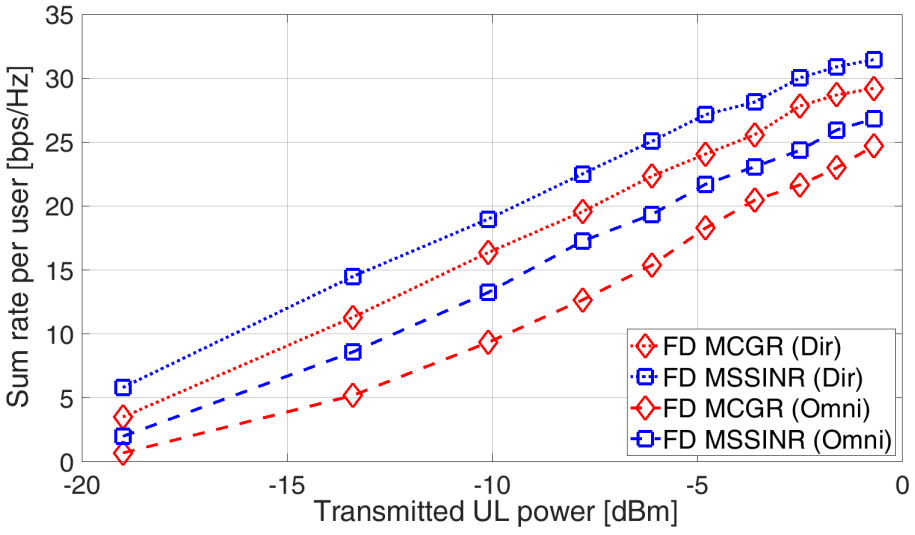

Figure 6.24: Sum rate with directional antennas

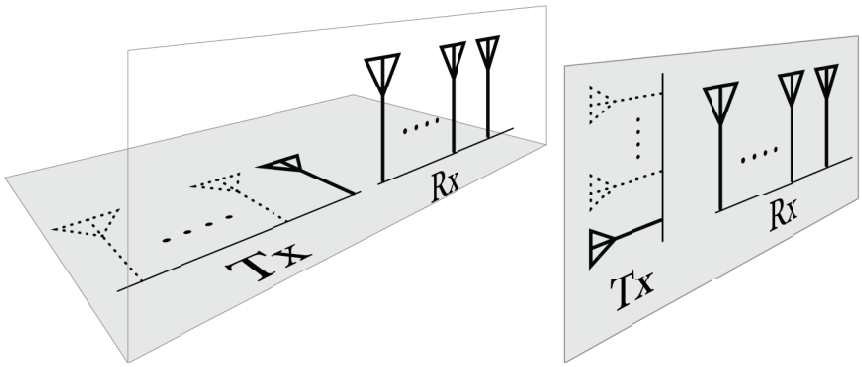

(a) (b)

Figure 6.25: An illustration of two separation structures (a) horizontal structure (b) vertical structure

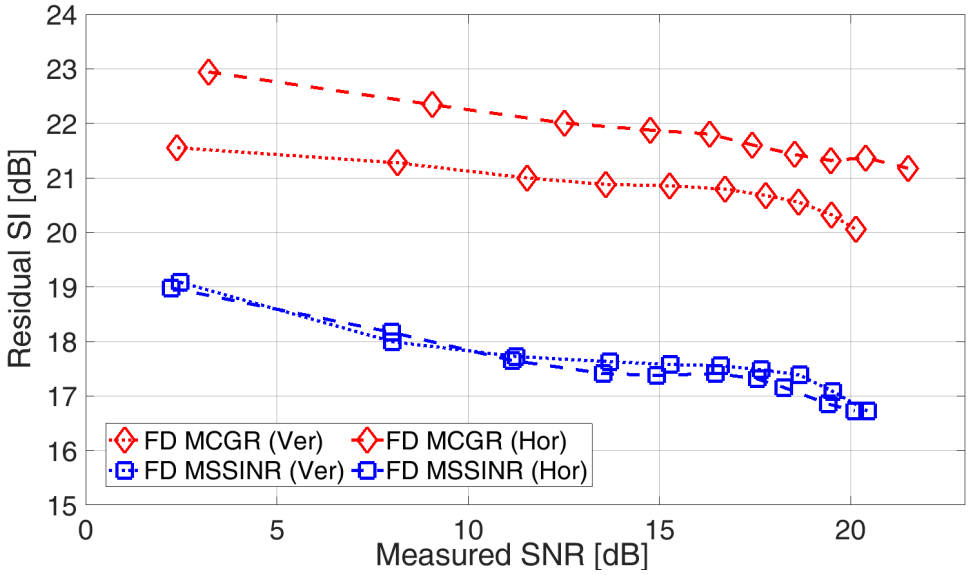

Figure 6.26: Vertical vs horizontal isolation RSI

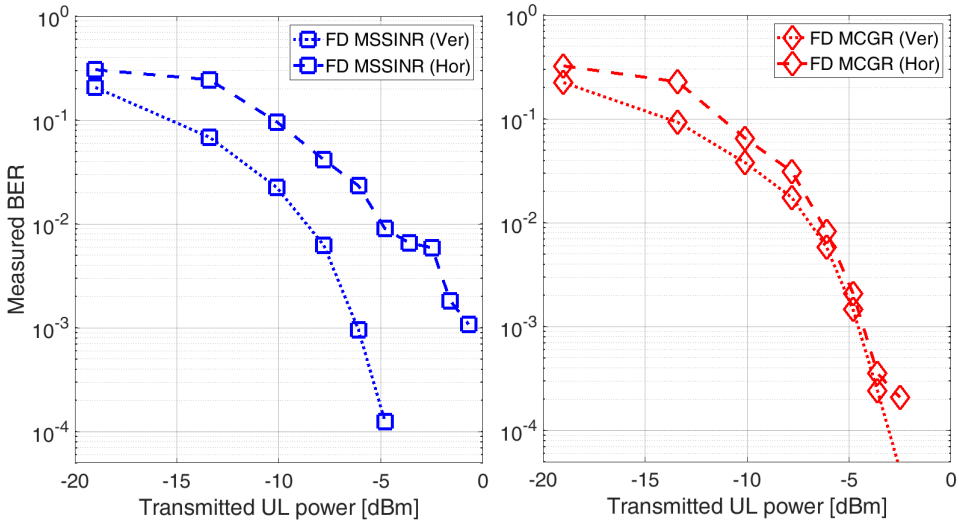

Figure 6.27: Vertical vs horizontal isolation BER

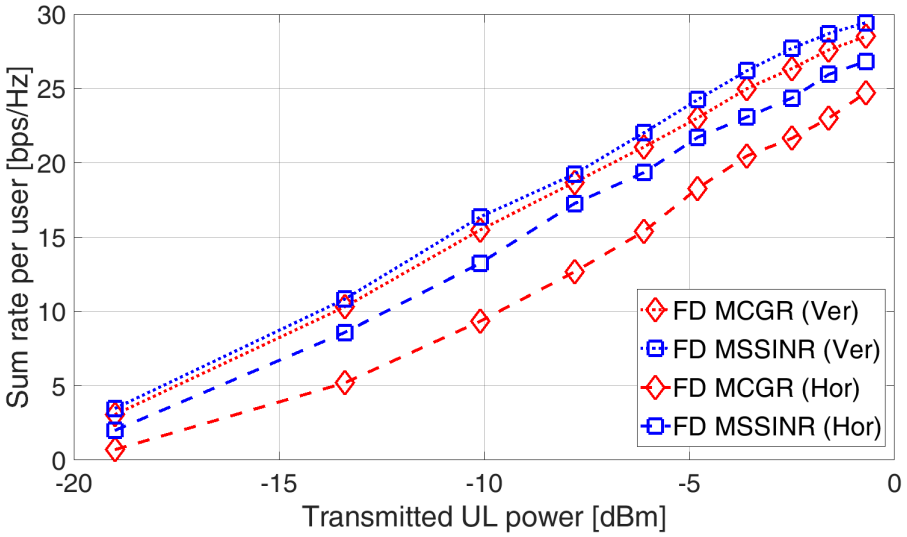

Figure 6.28: Vertical vs horizontal isolation sum rate

6.6 Conclusion

In this chapter, the testbed implementation of an FD base-station with antenna selection is described in details. Measurements are performed with wideband signals at 5 GHz in an indoor environment. Measurement results show that the implemented setup has slight degradation in the system performance compared to simulation, specially in low SNR values. This is due to channel estimation errors that affect the criteria of antenna selection. However, the FD/HD enhancement ratio is between 1.65 and 1.98 for MSSINR algorithm, whereas it is between 1.4 and 1.98 for the less complicated algorithm MCGR. Both criteria show similar performance in high SNR values, meanwhile MCGR shows worse performance by low SNR values. The reason is that MCGR criterion doesn't consider the noise, which is the dominant limitation in low SNR values, rather than the SI. Nevertheless, the results, in general, are encouraging, and they show that FD base-station with AS is a promising approach for enhancing the performance of next generations of cellular system. In general, limited number of users are included in the applied scenarios, thus further work with the proposed schemes in the dissertation would be an interesting topic for future investigations. Furthermore, bulk AS criteria are used in the wideband system, so per-tone AS algorithms would enhance the overall performance. Also, hybrid FD-HD users scenario is an important topic for further research.

Chapter 7

Conclusions and Outlook

The main scope of this thesis is to employ different multi-antenna techniques to enable full-duplex transmission in a base-station. The motivation is to avoid the traditional approaches of self-interference cancellation which depend on copying the transmitted signal by an auxiliary chain, and feeding it back to the receiver in order to be subtracted from the total received signal. We demonstrate, with an example, that these approaches are highly sensitive to hardware impairments of the transceiver analog components. Before that, a literature review is done to describe SIC requirements in FD BS and different SIC schemes in an FD transceiver. Next, IQ imbalance in FD node is studied as an example of the effect of hardware impairments on SIC performance. We show that with relatively small mismatches between I and Q chains, the performance of SIC drops from $70-75$ dB to $35-40$ dB. Then calibration methods are proposed to compensate this performance drop, using either a replicator unit or distributed compensation units. Two types of IQ imbalance are investigated, frequency-independent and frequency-selective mismatches. With these types and methods, we show that the original SIC performance is partially or entirely restored. However, the complexity of compensating IQ imbalance, not to mention other types of impairments (such as non-linearity, phase noise, etc.) raises questions about the effectiveness of using the SI feedback/auxiliary chain approach at the first place. More questions are raised in the case of multi-antenna/MIMO systems where many transceivers are used. We show in this thesis that this approach can be avoided with three multi-antenna technologies.

The first multi-antenna technology is reflect-arrays. We propose the use of reflect-array in FD mobile systems. Dual-polarized reflect-arrays are designed to be used in a full-duplex LTE base-station. We analyze the different self-interference components in indoor and outdoor

environments. Evaluation of the system performance is done considering the BER and the sum rate of the base-station in a simple case of two HD users, and three values of angular separation ($\pm 20°, \pm 30°, \pm 40°$). The results show that the enhancement FD/HD ratio would reach almost the theoretical boundary of two ($1.87 - 1.98$) in this scenario. However, as the work was confined to a simple scenario, further work can be done, like increasing the number of users and doing the beam-forming to different users' positions. The system performance can be enhanced in this complicated scenario by applying digital cancellation schemes to remove the residual self-interference. Nevertheless, we prove that exploiting RA in an FD BS can provide the required SIC isolation even in rich-scattering environments, and the technology of RA is worth further investigation for FD base-stations as it shows promising results.

Afterward, we focus on the exploitation of receive antenna selection, in an FD indoor wideband femto-BS, in two cases, co-located, and distributed antennas. Antenna selection allows the node to select the forward/SI channels pair that guarantees the maximum achievable gain of the desired signal and the minimum leakage of SI signal. In the case of distributed antennas, the simulation results show that distributing the receive antennas carries many effects on the performance. On the one hand, some of them are positive, like the gained diversity and the SI channel path loss. On the other hand, the SI isolation attained by cross-polarization becomes much less effective in this case due to the rich-scattering environment. In total, DAS slightly outperforms the co-located system in the studied scenario.

Finally, a testbed is built in order to experimentally validate the simulation of FD BS with AS. Receive antenna selection is combined with cross-polarization and antennas conditional placement in order to achieve the required SIC. We explain, in detail, the setup, the signal processing, and the measurement environment. Next, the measurement results are shown considering different scenarios in the testbed, such as changing the number of antennas, the type of isolation (vertical/horizontal), and the type of antennas (Omnidirectional/directional). In fact, till the moment, there aren't many testbeds that could realize FD in base-stations. Most of the previous hardware implementations focused on FD relying. Thus, this testbed is considered the first that implements FD transmission in a base-station with antenna selection.

Compared to simulation, the implemented setup shows a slight degradation in the system performance, especially in low SNR values. This is due to channel estimation errors that affect the criteria of antenna selection. However, the FD/HD enhancement ratio is between 1.65 and 1.98 for the MSSINR algorithm, whereas it is between 1.4 and 1.98 for the less complicated algorithm MCGR. Both criteria show similar performance in high SNR values; meanwhile,

MCGR shows worse performance by low SNR values. The reason is that the MCGR criterion doesn't consider the noise, which is the dominant limitation in low SNR values, rather than the SI. Nevertheless, the results, in general, are encouraging, and they show that FD base-station with AS is a promising approach for enhancing the performance of the next generations of cellular systems. This also applies to all the addressed multi-antenna technologies. In general, a limited number of users is included in the applied scenarios; thus, further work with the proposed schemes in the dissertation would be an interesting topic for future investigations. Also, a hybrid FD-HD users scenario is an important topic for further research. The AS and DAS work can be extended to include the transmit antennas in the selection process. Moreover, since bulk AS criteria are used for the OFDM system, further work can be done with per-tone selection. Furthermore, the problem of channel estimation error can be evaluated and analyzed, in details, within the proposed scenarios, especially in the presence of strong noise.

Nonetheless, ever since publishing the quote

'It is generally not possible for radios to receive and transmit on the same frequency band because of the interference that results' [1];

researches have been trying to prove the opposite. Expectations say that within a few years, we shall see a mature full-duplex technology that will have a tremendous impact on future wireless systems. It is a matter of when, rather than if, full-duplex will become fully dependable. Because this is what science is all about, removing *'not'* from the quote above to turn *'It is not possible'* into *'It is possible'*.

List of Publications

Book Chapters

- T. Kaiser and **N. Zarifeh**, ”General principles and basic algorithms for full-duplex transmission,” in Signal Processing for 5G: algorithms and implementations, F.-Long Luo and C. Zhang (eds.), Wiley, Chichester, 2016 (Chapter 16, pp.372-401).

Journal Papers

1. **N. Zarifeh**, Y. Zantah, Y. Gao and T. Kaiser, ”Full-Duplex Femto Base-Station With Antenna Selection: Experimental Validation,” in IEEE Access, vol. 7, pp. 108781-108794, 2019.

2. F. Sheikh, **N. Zarifeh**, T. Kaiser, ”Terahertz Band: Channel Modelling for Short-Range Wireless Communications in the Spectral Windows”, IET Microwaves, Antennas and Propagation, 2016.

Conference Papers

1. **N. Zarifeh**, M. Alissa, T. Kreul and T. Kaiser, ”Antenna Selection Performance of Distributed Antenna Systems in Full-Duplex Indoor Base Station,” 2019 12th German Microwave Conference (GeMiC), Stuttgart, 2019.

2. **N. Zarifeh**, M. Alissa, T. Kreul and T. Kaiser, ”Enabling full-duplex in a wideband indoor base-station using low-complex antenna selection,” 2018 The Loughborough Antennas and Propagation Conference (LAPC), Loughborough, UK.

3. **N. Zarifeh**, M. Alissa, M. Khaliel and T. Kaiser, ”Self-interference mitigation in full-

duplex base-station using dual polarized reflect-array," 2018 11th German Microwave Conference (GeMiC), Freiburg, 2018, pp. 180-183.

4. D. Peethala, **N. Zarifeh**, T. Kaiser, "Probability of coverage based analysis of distributed antenna system and its implementation on LTE based real-time-testbed", 9th Int. Congress on Ultra Modern Telecommunications and Control Systems, Munich, Germany, 6-8 Nov. 2017.

5. R. Steinert, **N. Zarifeh**, C.Y. Chang, A. Anttonen, A. Cipriano, D. Panaitopol, "Toward unifying abstractions for heterogeneous radio infrastructures," Poster in European Conference on Networks and Communications (EuCNC2017), Oulu, Finland, June 12-15, 2017.

6. A. Jendeya, M. El-Absi, **N. Zarifeh**, S. S. Ikki, T. Kaiser, "Interference Alignment and Free-Space Optics Based Backhaul Networks," 11th Int. ITG Conf. Systems, Communications and Coding 2017, Hamburg, Germany, Feb. 6-9, 2017.

7. **N. Zarifeh**, A. Kabbani, M. El-Absi, T. Kreul and T. Kaiser, "Massive MIMO exploitation to reduce HARQ delay in wireless communication system," 2016 IEEE Middle East Conference on Antennas and Propagation (MECAP), Beirut, Lebanon, 2016, pp. 1-5.

8. R. Askar, **N. Zarifeh**, B. Schubert, W. Keusgen, and T. Kaiser, "I/Q Imbalance Calibration for Higher Self-Interference Cancellation Levels in Full-Duplex Wireless Transceivers," 1st Int. Conf. on 5G for Ubiquitous Connectivity, Levi, Finland, 26-27 Nov. 2014.

Projects Deliverables

1. **N. Zarifeh** et al., "Final report on physical and MAC layer modelling and abstraction," COHERENT project deliverable D3.2, EU H2020 5G-PPP, September 2017.

2. A. Anttonen et al., "First report on physical and MAC layer modelling and abstraction," COHERENT project deliverable D3.1, EU H2020 5G-PPP, July 2016.

3. George Agapiou et al., "Exploitation and Techno-economic Model," COHERENT project deliverable D7.4, EU H2020 5G-PPP, May 2018.

4. Theo Kreul et al., "Spectrum Sensing and Cognitive Engine for cognitive LTE," kogLTE (BMBF) Project, September 2015

Bibliography

[1] A. Goldsmith, *Wireless Communications*, Cambridge University Press, 2005.

[2] Cisco, "Cisco visual networking index: Global mobile data traffic forecast update, 2017-2022," White paper, 2019.

[3] GSMA Intelligence, "The mobile economy 2019," White paper, GSMA, 2019.

[4] Sam Barker, "5G market strategies: Consumer & enterprise opportunities & forecasts 2018-2025," White paper, Juniper, 2018.

[5] GSA, "Spectrum for terrestrial 5G networks: Licensing developments worldwide," Technical report, GSA Global mobile Suppliers Association, December 2018.

[6] Huawei, "5G spectrum public policy position," Tech. Rep., Huawei, type = White Paper,, 2017.

[7] N. Zarifeh et al., "Final report on physical and MAC layer modelling and abstraction," COHERENT project deliverable D3.2, EU H2020 5G-PPP, September 2017.

[8] J. Mitola and G. Q. Maguire, "Cognitive radio: making software radios more personal," *IEEE Personal Communications*, vol. 6, no. 4, pp. 13–18, Aug 1999.

[9] S. Sasipriya and R. Vigneshram, "An overview of cognitive radio in 5G wireless communications," in *2016 IEEE International Conference on Computational Intelligence and Computing Research (ICCIC)*, Dec 2016, pp. 1–5.

[10] T. L. Marzetta, "Noncooperative cellular wireless with unlimited numbers of base station antennas," *IEEE Transactions on Wireless Communications*, vol. 9, no. 11, pp. 3590–3600, November 2010.

[11] J. Liu, M. Sheng, L. Liu, and J. Li, "Network densification in 5G: From the short-range communications perspective," *IEEE Communications Magazine*, vol. 55, no. 12, pp. 96–102, Dec 2017.

[12] P. Banelli, S. Buzzi, G. Colavolpe, A. Modenini, F. Rusek, and A. Ugolini, "Modulation formats and waveforms for 5G networks: Who will be the heir of OFDM?: An overview of alternative modulation schemes for improved spectral efficiency," *IEEE Signal Processing Magazine*, vol. 31, no. 6, pp. 80–93, Nov 2014.

[13] D. J. Costello and G. D. Forney, "Channel coding: The road to channel capacity," *Proceedings of the IEEE*, vol. 95, no. 6, pp. 1150–1177, June 2007.

[14] G. D. Forney and G. Ungerboeck, "Modulation and coding for linear gaussian channels," *IEEE Transactions on Information Theory*, vol. 44, no. 6, pp. 2384–2415, Oct 1998.

[15] R. Irmer, H. Droste, P. Marsch, M. Grieger, G. Fettweis, S. Brueck, H. Mayer, L. Thiele, and V. Jungnickel, "Coordinated multipoint: Concepts, performance, and field trial results," *IEEE Communications Magazine*, vol. 49, no. 2, pp. 102–111, February 2011.

[16] N. Zarifeh, A. Kabbani, M. El-Absi, T. Kreul, and T. Kaiser, "Massive MIMO exploitation to reduce HARQ delay in wireless communication system," in *2016 IEEE Middle East Conference on Antennas and Propagation (MECAP)*, Sep. 2016, pp. 1–5.

[17] J. Ala-Laurinaho, J. Aurinsalo, A. Karttunen, M. Kaunisto, A. Lamminen, J. Nurmiharju, A. V. Raisanen, J. Saily, and P. Wainio, "2-d beam-steerable integrated lens antenna system for 5G E-band access and backhaul," *IEEE Transactions on Microwave Theory and Techniques*, vol. 64, no. 7, pp. 2244–2255, July 2016.

[18] 3GPP, "Study on integrated access and backhaul," Tech. Rep. TR 38.874 V16.0.0, 3GPP-NR, Dec. 2018.

[19] S. Hong, J. Brand, Jung Choi, M. Jain, J. Mehlman, S. Katti, and P. Levis, "Applications of self-interference cancellation in 5G and beyond," *Communications Magazine, IEEE*, vol. 52, no. 2, pp. 114–121, February 2014.

[20] Zhongshan Zhang, Xiaomeng Chai, Keping Long, A.V. Vasilakos, and L. Hanzo, "Full duplex techniques for 5G networks: self-interference cancellation, protocol design, and

relay selection," *Communications Magazine, IEEE*, vol. 53, no. 5, pp. 128–137, May 2015.

[21] Yun Liao, Lingyang Song, Zhu Han, and Yonghui Li, "Full duplex cognitive radio: a new design paradigm for enhancing spectrum usage," *Communications Magazine, IEEE*, vol. 53, no. 5, pp. 138–145, May 2015.

[22] Li Wang, Fei Tian, T. Svensson, Daquan Feng, Mei Song, and Shaoqian Li, "Exploiting full duplex for device-to-device communications in heterogeneous networks," *Communications Magazine, IEEE*, vol. 53, no. 5, pp. 146–152, May 2015.

[23] T. Kaiser and N. Zarifeh, "General principles and basic algorithms for full-duplex transmission," in *Signal Processing for 5G: algorithms and implementations*, F.-Long Luo and C. Zhang, Eds., chapter 16, pp. 372–401. Wiley-IEEE Press, 2016.

[24] Yuan Gao, *Low RF-Complexity Massive MIMO Systems: Antenna Selection and Hybrid Analog-Digital Beamforming*, Ph.D. thesis, Duisburg-Essen University, 2017.

[25] E. Everett, C. Shepard, L. Zhong, and A. Sabharwal, "Softnull: Many-antenna full-duplex wireless via digital beamforming," *IEEE Transactions on Wireless Communications*, vol. 15, no. 12, pp. 8077–8092, Dec 2016.

[26] A. Sabharwal, P. Schniter, Dongning Guo, D.W. Bliss, S. Rangarajan, and R. Wichman, "In-Band Full-Duplex Wireless: Challenges and Opportunities," *Selected Areas in Communications, IEEE Journal on*, vol. 32, no. 9, pp. 1637–1652, Sept 2014.

[27] D. Korpi, L. Anttila, and M. Valkama, "Feasibility of in-band full-duplex radio transceivers with imperfect RF components: Analysis and enhanced cancellation algorithms," in *Cognitive Radio Oriented Wireless Networks and Communications (CROWNCOM), 2014 9th International Conference on*, June 2014, pp. 532–538.

[28] E. Ahmed and A.M. Eltawil, "All-Digital Self-Interference Cancellation Technique for Full-Duplex Systems," *Wireless Communications, IEEE Transactions on*, vol. 14, no. 7, pp. 3519–3532, July 2015.

[29] Dinesh Bharadia, Emily McMilin, and Sachin Katti, "Full duplex radios," in *Proceedings of the ACM SIGCOMM 2013 conference on SIGCOMM*, 2013, SIGCOMM '13, pp. 375–386.

[30] T.H. Lee, "The design of CMOS radio-frequency integrated circuits, 2nd edition," *Communications Engineer*, vol. 2, no. 4, pp. 47–47, Aug 2004.

[31] D. Korpi, T. Riihonen, V. Syrjala, L. Anttila, M. Valkama, and R. Wichman, "Full-duplex transceiver system calculations: Analysis of ADC and linearity challenges," *Wireless Communications, IEEE Transactions on*, vol. PP, no. 99, pp. 1–1, 2014.

[32] Mayank Jain, Jung Il Choi, Taemin Kim, Dinesh Bharadia, Siddharth Seth, Kannan Srinivasan, Philip Levis, Sachin Katti, and Prasun Sinha, "Practical, Real-time, Full Duplex Wireless," in *Proceedings of the 17th Annual International Conference on Mobile Computing and Networking*, New York, NY, USA, 2011, MobiCom '11, pp. 301–312, ACM.

[33] R. Askar, T. Kaiser, B. Schubert, T. Haustein, and W. Keusgen, "Active self-interference cancellation mechanism for full-duplex wireless transceivers," in *2014 9th International Conference on Cognitive Radio Oriented Wireless Networks and Communications (CROWNCOM)*, June 2014, pp. 539–544.

[34] Yee Kit Chan, Voon Chet Koo, Boon-Kuan Chung, and Hean-Teik Chuah, "A cancellation network for full-duplex front end circuit," *Progress In Electromagnetics Research Letters*, vol. 7, pp. 139–148, 2009.

[35] M.E. Knox, "Single antenna full duplex communications using a common carrier," in *Wireless and Microwave Technology Conference (WAMICON), 2012 IEEE 13th Annual*, April 2012, pp. 1–6.

[36] T. Miyoshi and Shinichi Miyauchi, "The Design of Planar Circulators for Wide-Band Operation," *Microwave Theory and Techniques, IEEE Transactions on*, vol. 28, no. 3, pp. 210–214, Mar 1980.

[37] Ernst Schloemann, "Miniature circulators," *Magnetics, IEEE Transactions on*, vol. 25, no. 5, pp. 3236–3241, Sep 1989.

[38] H. Katoh, "Temperature-Stabilized 1.7-GHz Broad-Band Lumped-Element Circulator," *Microwave Theory and Techniques, IEEE Transactions on*, vol. 23, no. 8, pp. 689–696, Aug 1975.

[39] M. Duarte and A. Sabharwal, "Full-duplex wireless communications using off-the-shelf radios: Feasibility and first results," in *2010 Conference Record of the Forty Fourth Asilomar Conference on Signals, Systems and Computers*, Nov 2010, pp. 1558–1562.

[40] C. R. Anderson, S. Krishnamoorthy, C. G. Ranson, T. J. Lemon, W. G. Newhall, T. Kummetz, and J. H. Reed, "Antenna isolation, wideband multipath propagation measurements, and interference mitigation for on-frequency repeaters," in *IEEE SoutheastCon, 2004. Proceedings.*, March 2004, pp. 110–114.

[41] Mohammad A. Khojastepour, Karthik Sundaresan, Sampath Rangarajan, Xinyu Zhang, and Sanaz Barghi, "The Case for Antenna Cancellation for Scalable Full-duplex Wireless Communications," in *Proceedings of the 10th ACM Workshop on Hot Topics in Networks*, New York, NY, USA, 2011, HotNets-X, pp. 17:1–17:6, ACM.

[42] Achaleshwar Sahai, Gaurav Patel, and Ashutosh Sabharwal, "Pushing the limits of Full-duplex: Design and Real-time Implementation," *CoRR*, vol. abs/1107.0607, 2011.

[43] Jung Il Choi, Mayank Jain, Kannan Srinivasan, Phil Levis, and Sachin Katti, "Achieving Single Channel, Full Duplex Wireless Communication," in *Proceedings of the Sixteenth Annual International Conference on Mobile Computing and Networking*, New York, NY, USA, 2010, MobiCom '10, pp. 1–12, ACM.

[44] Ehsan Aryafar, Mohammad Amir Khojastepour, Karthikeyan Sundaresan, Sampath Rangarajan, and Mung Chiang, "MIDU: Enabling MIMO Full Duplex," in *Proceedings of the 18th Annual International Conference on Mobile Computing and Networking*, New York, NY, USA, 2012, Mobicom '12, pp. 257–268, ACM.

[45] J. I. Choi, S. Hong, M. Jain, S. Katti, P. Levis, and J. Mehlman, "Beyond full duplex wireless," in *2012 Conference Record of the Forty Sixth Asilomar Conference on Signals, Systems and Computers (ASILOMAR)*, Nov 2012, pp. 40–44.

[46] E. Everett, A. Sahai, and A. Sabharwal, "Passive self-interference suppression for full-duplex infrastructure nodes," *IEEE Transactions on Wireless Communications*, vol. 13, no. 2, pp. 680–694, February 2014.

[47] M. Duarte, A. Sabharwal, V. Aggarwal, R. Jana, K. K. Ramakrishnan, C. W. Rice, and N. K. Shankaranarayanan, "Design and characterization of a full-duplex multiantenna

system for wifi networks," *IEEE Transactions on Vehicular Technology*, vol. 63, no. 3, pp. 1160–1177, March 2014.

[48] A. K. Khandani, "Methods for spatial multiplexing of wireless two-way channels," 2010, US Patent 11581427.

[49] B. Radunovic, D. Gunawardena, P. Key, A. Proutiere, N. Singh, V. Balan, and G. Dejean, "Rethinking Indoor Wireless Mesh Design: Low Power, Low Frequency, Full-Duplex," in *Wireless Mesh Networks (WIMESH 2010), 2010 Fifth IEEE Workshop on*, June 2010, pp. 1–6.

[50] E. Ahmed, AM. Eltawil, and A Sabharwal, "Self-interference cancellation with nonlinear distortion suppression for full-duplex systems," in *Signals, Systems and Computers, 2013 Asilomar Conference on*, Nov 2013, pp. 1199–1203.

[51] L. Anttila, D. Korpi, V. Syrjala, and M. Valkama, "Cancellation of power amplifier induced nonlinear self-interference in full-duplex transceivers," in *Signals, Systems and Computers, 2013 Asilomar Conference on*, Nov 2013, pp. 1193–1198.

[52] Shyamnath Gollakota and Dina Katabi, "Zigzag Decoding: Combating Hidden Terminals in Wireless Networks," *SIGCOMM Comput. Commun. Rev.*, vol. 38, no. 4, pp. 159–170, Aug. 2008.

[53] Daniel Halperin, Thomas Anderson, and David Wetherall, "Taking the Sting out of Carrier Sense: Interference Cancellation for Wireless LANs," in *Proceedings of the 14th ACM International Conference on Mobile Computing and Networking*, New York, NY, USA, 2008, MobiCom '08, pp. 339–350, ACM.

[54] Sachin Katti, Shyamnath Gollakota, and Dina Katabi, "Embracing Wireless Interference: Analog Network Coding," *SIGCOMM Comput. Commun. Rev.*, vol. 37, no. 4, pp. 397–408, Aug. 2007.

[55] Stephen Boyd and Lieven Vandenberghe, *Convex Optimization*, Cambridge University Press, New York, NY, USA, 2004.

[56] M. Duarte, C. Dick, and A. Sabharwal, "Experiment-Driven Characterization of Full-Duplex Wireless Systems," *Wireless Communications, IEEE Transactions on*, vol. 11, no. 12, pp. 4296–4307, December 2012.

[57] R. Askar, N. Zarifeh, B. Schubert, W. Keusgen, and T. Kaiser, "I/Q imbalance calibration for higher self-interference cancellation levels in Full-Duplex wireless transceivers," in *5G for Ubiquitous Connectivity (5GU), 2014 1st International Conference on*, Nov 2014, pp. 92–97.

[58] T. Schenk, *RF Imperfections in High-rate Wireless Systems: Impact and Digital Compensation*, Springer Netherlands, 2008.

[59] Behzad Razavi, *Design of Analog CMOS Integrated Circuits*, McGraw-Hill, Inc., New York, NY, USA, 1 edition, 2001.

[60] D. Korpi, L. Anttila, V. Syrjala, and M. Valkama, "Widely Linear Digital Self-Interference Cancellation in Direct-Conversion Full-Duplex Transceiver," *Selected Areas in Communications, IEEE Journal on*, vol. 32, no. 9, pp. 1674–1687, Sept 2014.

[61] L. Anttila, D. Korpi, E. Antonio-Rodriguez, R. Wichman, and M. Valkama, "Modeling and efficient cancellation of nonlinear self-interference in MIMO full-duplex transceivers," in *Globecom Workshops (GC Wkshps), 2014*, Dec 2014, pp. 777–783.

[62] Shenghong Li and R.D. Murch, "Full-Duplex Wireless Communication Using Transmitter Output Based Echo Cancellation," in *Global Telecommunications Conference (GLOBECOM 2011), 2011 IEEE*, Dec 2011, pp. 1–5.

[63] E. Ahmed and A.M. Eltawil, "On Phase Noise Suppression in Full-Duplex Systems," *Wireless Communications, IEEE Transactions on*, vol. 14, no. 3, pp. 1237–1251, March 2015.

[64] E. Ahmed, A.M. Eltawil, and A. Sabharwal, "Self-interference cancellation with phase noise induced ICI suppression for full-duplex systems," in *Global Communications Conference (GLOBECOM), 2013 IEEE*, Dec 2013, pp. 3384–3388.

[65] E. Ahmed, A.M. Eltawil, and A. Sabharwal, "Rate Gain Region and Design Tradeoffs for Full-Duplex Wireless Communications," *Wireless Communications, IEEE Transactions on*, vol. 12, no. 7, pp. 3556–3565, July 2013.

[66] A. Sahai, G. Patel, C. Dick, and A. Sabharwal, "On the Impact of Phase Noise on Active Cancelation in Wireless Full-Duplex," *Vehicular Technology, IEEE Transactions on*, vol. 62, no. 9, pp. 4494–4510, Nov 2013.

[67] V. Syrjala, M. Valkama, L. Anttila, T. Riihonen, and D. Korpi, "Analysis of Oscillator Phase-Noise Effects on Self-Interference Cancellation in Full-Duplex OFDM Radio Transceivers," *Wireless Communications, IEEE Transactions on*, vol. 13, no. 6, pp. 2977–2990, June 2014.

[68] A. Sahai, G. Patel, C. Dick, and A. Sabharwal, "Understanding the impact of phase noise on active cancellation in wireless full-duplex," in *Signals, Systems and Computers (ASILOMAR), 2012 Conference Record of the Forty Sixth Asilomar Conference on*, Nov 2012, pp. 29–33.

[69] D. Petrovic, W. Rave, and G. Fettweis, "Effects of Phase Noise on OFDM Systems With and Without PLL: Characterization and Compensation," *Communications, IEEE Transactions on*, vol. 55, no. 8, pp. 1607–1616, Aug 2007.

[70] S. Wu, P. Liu, and Y. Bar-Ness, "Phase Noise Estimation and Mitigation for OFDM Systems," *Wireless Communications, IEEE Transactions on*, vol. 5, no. 12, pp. 3616–3625, December 2006.

[71] S. Bittner, W. Rave, and G. Fettweis, "Joint Iterative Transmitter and Receiver Phase Noise Correction using Soft Information," in *Communications, 2007. ICC '07. IEEE International Conference on*, June 2007, pp. 2847–2852.

[72] V. Syrjala and M. Valkama, "Receiver DSP for OFDM Systems Impaired by Transmitter and Receiver Phase Noise," in *Communications (ICC), 2011 IEEE International Conference on*, June 2011, pp. 1–6.

[73] Ville Syrjala and Mikko Valkama, "Iterative Receiver Signal Processing for Joint Mitigation of Transmitter and Receiver Phase Noise in OFDM-Based Cognitive Radio Link," 7 2012, IEEE.

[74] D. Kim, H. Lee, and D. Hong, "A survey of in-band full-duplex transmission: From the perspective of phy and mac layers," *IEEE Communications Surveys Tutorials*, vol. 17, no. 4, pp. 2017–2046, Fourthquarter 2015.

[75] T. Riihonen and R. Wichman, "Analog and digital self-interference cancellation in full-duplex MIMO-OFDM transceivers with limited resolution in A/D conversion," in *2012 Conference Record of the Forty Sixth Asilomar Conference on Signals, Systems and Computers (ASILOMAR)*, Nov 2012, pp. 45–49.

[76] Pham Thanh Hiep and Ryuji Kohno, "Water-filling for full-duplex multiple-hop MIMO relay system," *EURASIP Journal on Wireless Communications and Networking*, vol. 2014, no. 1, pp. 174, Oct 2014.

[77] J. Sangiamwong, T. Asai, J. Hagiwara, Y. Okumura, and T. Ohya, "Joint Multi-Filter Design for Full-Duplex MU-MIMO Relaying," in *Vehicular Technology Conference, 2009. VTC Spring 2009. IEEE 69th*, April 2009, pp. 1–5.

[78] T. Riihonen, S. Werner, and R. Wichman, "Spatial loop interference suppression in full-duplex MIMO relays," in *Signals, Systems and Computers, 2009 Conference Record of the Forty-Third Asilomar Conference on*, Nov 2009, pp. 1508–1512.

[79] T. Riihonen, S. Werner, and R. Wichman, "Residual self-interference in full-duplex MIMO relays after null-space projection and cancellation," in *Signals, Systems and Computers (ASILOMAR), 2010 Conference Record of the Forty Fourth Asilomar Conference on*, Nov 2010, pp. 653–657.

[80] P. Lioliou, M. Viberg, M. Coldrey, and F. Athley, "Self-interference suppression in full-duplex MIMO relays," in *Signals, Systems and Computers (ASILOMAR), 2010 Conference Record of the Forty Fourth Asilomar Conference on*, Nov 2010, pp. 658–662.

[81] T. Riihonen, A. Balakrishnan, K. Haneda, S. Wyne, S. Werner, and R. Wichman, "Optimal eigenbeamforming for suppressing self-interference in full-duplex MIMO relays," in *Information Sciences and Systems (CISS), 2011 45th Annual Conference on*, March 2011, pp. 1–6.

[82] Yingbo Hua, Ping Liang, Yiming Ma, A.C. Cirik, and Qian Gao, "A Method for Broadband Full-Duplex MIMO Radio," *Signal Processing Letters, IEEE*, vol. 19, no. 12, pp. 793–796, Dec 2012.

[83] B.P. Day, A.R. Margetts, D.W. Bliss, and P. Schniter, "Full-Duplex Bidirectional MIMO: Achievable Rates Under Limited Dynamic Range," *Signal Processing, IEEE Transactions on*, vol. 60, no. 7, pp. 3702–3713, July 2012.

[84] T. Riihonen, M. Vehkapera, and R. Wichman, "Large-system analysis of rate regions in bidirectional full-duplex MIMO link: Suppression versus cancellation," in *Information Sciences and Systems (CISS), 2013 47th Annual Conference on*, March 2013, pp. 1–6.

[85] Jong-Ho Lee, "Self-Interference Cancelation Using Phase Rotation in Full-Duplex Wireless," *Vehicular Technology, IEEE Transactions on*, vol. 62, no. 9, pp. 4421–4429, Nov 2013.

[86] Dinesh Bharadia and Sachin Katti, "Full Duplex MIMO Radios," in *Proceedings of the 11th USENIX Conference on Networked Systems Design and Implementation*, Berkeley, CA, USA, 2014, NSDI'14, pp. 359–372, USENIX Association.

[87] D. Lee and B. Min, "2 x 2 MIMO In-band Full-Duplex Radio Front-End with 50 dB Self-Interference Cancellation in 90 MHz Bandwidth," in *2017 IEEE MTT-S International Microwave Symposium (IMS)*, June 2017, pp. 670–672.

[88] R. Askar, F. Baum, W. Keusgen, and T. Haustein, "Decoupling-Based Self-Interference Cancellation in MIMO Full-Duplex Wireless Transceivers," in *2018 IEEE International Conference on Communications Workshops (ICC Workshops)*, May 2018, pp. 1–6.

[89] R. Askar, A. Hamdan, W. Keusgen, and T. Haustein, "Analysis of utilizing lossless networks for self-interference cancellation purpose," in *2018 IEEE Wireless Communications and Networking Conference (WCNC)*, April 2018, pp. 1–6.

[90] R. Sultan, L. Song, K. G. Seddik, and Z. Han, "Full Duplex in Massive MIMO Systems: Analysis and Feasibility," in *2016 IEEE Globecom Workshops (GC Wkshps)*, Dec 2016, pp. 1–6.

[91] A. Shojaeifard, K. Wong, M. Di Renzo, G. Zheng, K. A. Hamdi, and J. Tang, "Massive MIMO-Enabled Full-Duplex Cellular Networks," *IEEE Transactions on Communications*, vol. 65, no. 11, pp. 4734–4750, Nov 2017.

[92] P.J. Schreier and L.L. Scharf, *Statistical Signal Processing of Complex-Valued Data: The Theory of Improper and Noncircular Signals*, Cambridge University Press, 2010.

[93] B. Picinbono and P. Chevalier, "Widely linear estimation with complex data," *Signal Processing, IEEE Transactions on*, vol. 43, no. 8, pp. 2030–2033, Aug 1995.

[94] Lauri Anttila, *Digital front-end signal processing with widely-linear signal models in radio devices*, Ph.D. thesis, Tampere University of Technology, 2011.

[95] "Evolved Universal Terrestrial Radio Access (E-UTRA); user equipment (UE) radio transmission and reception," Tech. Rep. TS 36.101, 3GPP.

[96] M. Sakai, Hai Lin, and K. Yamashita, "Adaptive cancellation of self-interference in full-duplex wireless with transmitter IQ imbalance," in *Global Communications Conference (GLOBECOM), 2014 IEEE*, Dec 2014, pp. 3220–3224.

[97] P. Rykaczewski, J. Brakensiek, and F.K. Jondral, "Towards an analytical model of I/Q imbalance in OFDM based direct conversion receivers," in *Vehicular Technology Conference, 2004. VTC 2004-Spring. 2004 IEEE 59th*, May 2004, vol. 4, pp. 1831–1835 Vol.4.

[98] Jian Luo, A. Kortke, and W. Keusgen, "Efficient Channel Estimation Schemes for MIMO OFDM Systems with NULL Subcarriers," in *Vehicular Technology Conference, 2008. VTC 2008-Fall. IEEE 68th*, pp. 1–5.

[99] D. Chu, "Polyphase codes with good periodic correlation properties (corresp.)," *IEEE Transactions on Information Theory*, vol. 18, no. 4, pp. 531–532, 1972.

[100] Sanjit Mitra, *Digital signal processing : a computer-based approach*, McGraw-Hill/Irwin, Boston, 2001.

[101] T. Hollis and R. Weir., "The Theory of Digital Down Conversion," Tech. report v1.2, Hunt Engineering, 2003.

[102] M. H. Dahri, M. H. Jamaluddin, M. I. Abbasi, and M. R. Kamarudin, "A Review of Wideband Reflectarray Antennas for 5G Communication Systems," *IEEE Access*, vol. 5, pp. 17803–17815, 2017.

[103] N. Zarifeh, M. Alissa, M. Khaliel, and T. Kaiser, "Self-interference mitigation in full-duplex base-station using dual polarized reflect-array," in *2018 11th German Microwave Conference (GeMiC)*, March 2018, pp. 180–183.

[104] J. Shaker, M. R. Chaharmir, M. Cuhaci, and A. Ittipiboon, "Reflectarray research at the communications research centre canada," *IEEE Antennas and Propagation Magazine*, vol. 50, no. 4, pp. 31–52, Aug 2008.

[105] John Huang and Jose Antonio Encinar, *Reflectarray Antennas*, Wiley-IEEE Press, October 2007.

[106] M. R. Chaharmir, J. Shaker, N. Gagnon, and D. Lee, "Design of broadband, single layer dual-band large reflectarray using multi open loop elements," *IEEE Transactions on Antennas and Propagation*, vol. 58, no. 9, pp. 2875–2883, Sep. 2010.

[107] D. M. Pozar, S. D. Targonski, and R. Pokuls, "A shaped-beam microstrip patch reflectarray," *IEEE Transactions on Antennas and Propagation*, vol. 47, no. 7, pp. 1167–1173, July 1999.

[108] R.J. Mailloux, *Phased Array Antenna Handbook*, Artech House antenna library. Artech House, 1994.

[109] J. Shaker, M.R. Chaharmir, and J. Ethier, *Reflectarray Antennas: Analysis, Design, Fabrication, and Measurement*, Antennas and Propagation. Artech House, 2013.

[110] P. Nayeri, F. Yang, and A. Z. Elsherbeni, "Bifocal design and aperture phase optimizations of reflectarray antennas for wide-angle beam scanning performance," *IEEE Transactions on Antennas and Propagation*, vol. 61, no. 9, pp. 4588–4597, Sep. 2013.

[111] Maher Ahmed, *Realistic Frequency Coded Chipless RFID: Physically Modulated Tags and Refectarray Readers*, Ph.D. thesis, Duisburg-Essen University, 2017.

[112] J. Huang, "Bandwidth study of microstrip reflectarray and a novel phased reflectarray concept," in *IEEE Antennas and Propagation Society International Symposium. 1995 Digest*, June 1995, vol. 1, pp. 582–585 vol.1.

[113] M. Khaliel, A. Fawky, M. El-Hadidy, and T. Kaiser, "Uwb reflectarray antenna for chipless rfid applications," in *2014 31st National Radio Science Conference (NRSC)*, April 2014, pp. 17–20.

[114] M. Abd-Elhady., S. H. Zainud-Deen, A. A. Mitkees, and A. A. Kishk, "Wideband rectangular dielectric resonator elements reflectarray," in *The 2nd Middle East Conference on Antennas and Propagation*, Dec 2012, pp. 1–5.

[115] E. Carrasco, J. A. Encinar, and M. Barba, "Bandwidth improvement in large reflectarrays by using true-time delay," *IEEE Transactions on Antennas and Propagation*, vol. 56, no. 8, pp. 2496–2503, Aug 2008.

[116] D. M. Pozar, "Bandwidth of reflectarrays," *Electronics Letters*, vol. 39, no. 21, pp. 1490–1491, Oct 2003.

[117] D. F. Sievenpiper, J. H. Schaffner, H. J. Song, R. Y. Loo, and G. Tangonan, "Two-dimensional beam steering using an electrically tunable impedance surface," *IEEE Transactions on Antennas and Propagation*, vol. 51, no. 10, pp. 2713–2722, Oct 2003.

[118] M. Y. Ismail and R. Cahill, "Beam steering reflectarrays using liquid crystal substrate," in *High Frequency Postgraduate Student Colloquium, 2005*, Sep. 2005, pp. 62–65.

[119] L. Boccia, F. Venneri, G. Amendola, and G. Di Massa, "Application of varactor diodes for reflectarray phase control," in *IEEE Antennas and Propagation Society International Symposium (IEEE Cat. No.02CH37313)*, June 2002, vol. 3, pp. 132–.

[120] A. Ludwig, "The definition of cross polarization," *IEEE Transactions on Antennas and Propagation*, vol. 21, no. 1, pp. 116–119, January 1973.

[121] M. Zhou, H. Cui, L. Song, and B. Jiao, "Transmit-receive antenna pair selection in full duplex systems," *IEEE Wireless Communications Letters*, vol. 3, no. 1, pp. 34–37, February 2014.

[122] F. M. Maciel-Barboza, J. Sanchez-Garcia, S. Armas-Jimenez, and L. Soriano-Equigua, "Uplink and downlink user and antenna selection for mmwave full duplex multiuser systems," in *2016 2nd International Conference on Frontiers of Signal Processing (ICFSP)*, Oct 2016, pp. 142–146.

[123] M. Zhou, L. Song, and Y. Li, "Joint transmit and receive antennas selection for full duplex MIMO systems," in *2014 IEEE Global Communications Conference*, Dec 2014, pp. 3838–3843.

[124] S. Jang, M. Ahn, H. Lee, and I. Lee, "Antenna Selection Schemes in Bidirectional Full-Duplex MIMO Systems," *IEEE Transactions on Vehicular Technology*, vol. 65, no. 12, pp. 10097–10100, Dec 2016.

[125] D. G. Wilson-Nunn, A. Chaaban, A. Sezgin, and M. Alouini, "Antenna Selection for Full-Duplex MIMO Two-Way Communication Systems," *IEEE Communications Letters*, vol. 21, no. 6, pp. 1373–1376, June 2017.

[126] G. Chen, Y. Gong, P. Xiao, and R. Tafazolli, "Dual antenna selection in self-backhauling multiple small cell networks," *IEEE Communications Letters*, vol. 20, no. 8, pp. 1611–1614, Aug 2016.

[127] N. Zarifeh, M. Alissa, T. Kreul, and T. Kaiser, "Enabling full-duplex in a wideband indoor base-station using low-complex antenna selection," in *The Loughborough Antennas Propagation Conference (LAPC 2018)*, Nov 2018, pp. 1–5.

[128] N. Zarifeh, M. Alissa, T. Kreul, and T. Kaiser, "Antenna selection performance of distributed antenna systems in full-duplex indoor base station," in *2019 12th German Microwave Conference (GeMiC)*, March 2019, pp. 32–35.

[129] A. Gorokhov, D. A. Gore, and A. J. Paulraj, "Receive antenna selection for MIMO spatial multiplexing: theory and algorithms," *IEEE Transactions on Signal Processing*, vol. 51, no. 11, pp. 2796–2807, Nov 2003.

[130] A. F. Molisch and M. Z. Win, "Mimo systems with antenna selection," *IEEE Microwave Magazine*, vol. 5, no. 1, pp. 46–56, March 2004.

[131] A. A. M. Saleh, A. Rustako, and R. Roman, "Distributed antennas for indoor radio communications," *IEEE Transactions on Communications*, vol. 35, no. 12, pp. 1245–1251, December 1987.

[132] K. Morita and H. Ohtsuka, "The new generation of wireless communications based on fiber-radio technologies," *IEICE Transactions on Communications*, vol. E76-B, no. 9, pp. 1061–1068, September 1993.

[133] J. Wang and L. B. Milstein, "CDMA overlay situations for microcellular mobile communications," *IEEE Transactions on Communications*, vol. 43, no. 2/3/4, pp. 603–614, Feb 1995.

[134] S. V. Hanly, "Capacity and power control in spread spectrum macrodiversity radio networks," *IEEE Transactions on Communications*, vol. 44, no. 2, pp. 247–256, Feb 1996.

[135] K. J. Kerpez and S. Ariyavisitakul, "A radio access system with distributed antennas," in *1994 IEEE GLOBECOM. Communications: The Global Bridge*, Nov 1994, vol. 3, pp. 1696–1700 vol.3.

[136] H. H. Xia, A. B. Herrera, S. Kim, and F. S. Rico, "A CDMA-distributed antenna system for in-building personal communications services," *IEEE Journal on Selected Areas in Communications*, vol. 14, no. 4, pp. 644–650, May 1996.

[137] G.-H. Chen, C.-M. Yu, and C.-C. Huang, "A simulation study of a distributed antenna-based CDMA system," in *Proceedings of PIMRC '96 - 7th International Symposium on Personal, Indoor, and Mobile Communications*, Oct 1996, vol. 2, pp. 517–521 vol.2.

[138] A. Obaid and H. Yanikomeroglu, "Reverse-link power control in CDMA distributed antenna systems," in *2000 IEEE Wireless Communications and Networking Conference. Conference Record (Cat. No.00TH8540)*, Sept 2000, vol. 2, pp. 608–612 vol.2.

[139] M. V. Clark, T. M. Willis, L. J. Greenstein, A. J. Rustako, V. Erceg, and R. S. Roman, "Distributed versus centralized antenna arrays in broadband wireless networks," in *IEEE VTS 53rd Vehicular Technology Conference, Spring 2001. Proceedings (Cat. No.01CH37202)*, May 2001, vol. 1, pp. 33–37 vol.1.

[140] R. Hasegawa, M. Shirakabe, R. Esmailzadeh, and M. Nakagawa, "Downlink performance of a CDMA system with distributed base station," in *2003 IEEE 58th Vehicular Technology Conference. VTC 2003-Fall (IEEE Cat. No.03CH37484)*, Oct 2003, vol. 2, pp. 882–886 Vol.2.

[141] L. Dai, S. Zhou, and Y. Yao, "Capacity analysis in CDMA distributed antenna systems," *IEEE Transactions on Wireless Communications*, vol. 4, no. 6, pp. 2613–2620, Nov 2005.

[142] 3GPP, "Further advancements for E-UTRA physical layer aspects," Tech. Rep. TR36.814 V9.0.0, 3GPP-LTE, Mar. 2010.

[143] J. Wang and L. Dai, "Downlink rate analysis for virtual-cell based large-scale distributed antenna systems," *IEEE Transactions on Wireless Communications*, vol. 15, no. 3, pp. 1998–2011, March 2016.

[144] H. Jin and V. C. M. Leung, "Full-duplex transmissions in fiber-connected distributed relay antenna systems," in *2012 IEEE Global Communications Conference (GLOBECOM)*, Dec 2012, pp. 4284–4289.

[145] G. Liu, F. R. Yu, H. Ji, and V. C. M. Leung, "Energy-efficient resource allocation in cellular networks with shared full-duplex relaying," *IEEE Transactions on Vehicular Technology*, vol. 64, no. 8, pp. 3711–3724, Aug 2015.

[146] Y. Dong, H. Zhang, M. J. Hossain, J. Cheng, and V. C. M. Leung, "Energy Efficient Resource Allocation for OFDMA Full Duplex Distributed Antenna Systems with Energy

Recycling," in *2015 IEEE Global Communications Conference (GLOBECOM)*, Dec 2015, pp. 1–6.

[147] D. W. K. Ng, Y. Wu, and R. Schober, "Power efficient resource allocation for full-duplex radio distributed antenna networks," *IEEE Transactions on Wireless Communications*, vol. 15, no. 4, pp. 2896–2911, April 2016.

[148] Z. Wei, S. Sun, X. Zhu, Y. Huang, and J. Wang, "Energy-efficient hybrid duplexing strategy for bidirectional distributed antenna systems," *IEEE Transactions on Vehicular Technology*, vol. 67, no. 6, pp. 5096–5110, June 2018.

[149] N. Zarifeh, Y. Zantah, Y. Gao, and T. Kaiser, "Full-duplex femto base-station with antenna selection: Experimental validation," *IEEE Access*, vol. 7, pp. 108781–108794, 2019.

[150] R. O'Neill and L. B. Lopes, "Envelope variations and spectral splatter in clipped multi-carrier signals," in *Proceedings of 6th International Symposium on Personal, Indoor and Mobile Radio Communications*, Sep. 1995, vol. 1, pp. 71–75 vol.1.

[151] S. Sesia, I. Toufik, and M. Baker, *LTE - The UMTS Long Term Evolution: From Theory to Practice*, Wiley, 2nd edition edition, July 2011.

[152] S. B. Weinstein, "The history of orthogonal frequency-division multiplexing [history of communications]," *IEEE Communications Magazine*, vol. 47, no. 11, pp. 26–35, November 2009.

[153] J. J. van de Beek, M. Sandell, and P. O. Borjesson, "ML estimation of time and frequency offset in OFDM systems," *IEEE Transactions on Signal Processing*, vol. 45, no. 7, pp. 1800–1805, July 1997.

[154] L. Deneire, P. Vandenameele, L. van der Perre, B. Gyselinckx, and M. Engels, "A low-complexity ML channel estimator for OFDM," *IEEE Transactions on Communications*, vol. 51, no. 2, pp. 135–140, Feb 2003.

[155] F. Socheleau, A. Aissa-El-Bey, and S. Houcke, "Non data-aided SNR estimation of OFDM signals," *IEEE Communications Letters*, vol. 12, no. 11, pp. 813–815, November 2008.